Targeting Colonic Macrophages as a Potential Therapeutic Option in Metabolic Disease

Inauguraldissertation

zur

Erlangung der Würde eines Doktors der Philosophie

vorgelegt der

Philosophisch-Naturwissenschaftlichen Fakultät

der Universität Basel

von

Theresa Rohm

aus Deutschland

Basel, 2020

Genehmigt von der Philosophisch-Naturwissenschaftlichen Fakultät

auf Antrag von

Prof. Dr. Christoph Hess
Fakultätsverantwortlicher

Prof. Dr. Gerhard M. Christofori
Korreferent

PD Dr. Claudia Cavelti-Weder
Dissertationsleiterin

Basel, den 18.Februar 2020

Prof. Dr. Martin Spiess

Dekan der Philosophisch-Naturwissenschaftlichen Fakultät

Table of Contents

Abstract

Obesity is characterized by chronic low-grade inflammation. However, the initiating mechanisms remain poorly understood. Here, we characterized intestinal macrophage subpopulations and their role in high-fat diet (HFD)-induced obesity in mice and humans. Pro-inflammatory/monocyte-derived intestinal macrophages transiently increased upon food intake and became chronically elevated upon HFD, suggesting a link between macrophage numbers and glycemia. Indeed, pharmacological dose-dependent or genetic ablation of macrophages improved glucose homeostasis. In particular, colon-specific macrophage depletion improved glycemic control and ameliorated β-cell function. Intestinal macrophage activation upon HFD was characterized by a strong interferon signature and metabolic shift, potentially via mTOR activation. Accordingly, colon-specific mTOR-inhibition enhanced insulin and GLP-1 secretion. In obese humans, pro-inflammatory intestinal macrophages were also increased, potentially by enhanced monocyte recruitment. Taken together, these data reveal that intestinal innate immunity contributes to glycemic dysfunction in obesity. Therefore, specifically targeting colonic macrophages or their activation might be a novel therapeutic avenue to improve glycemic control.

List of Abbreviations

ADP	Adenosine diphosphate
ATMs	Adipose tissue macrophages
ATP	Adenosine triphosphate
Ca^{2+}	Calcium
CCR	Chemokine receptor
CD	Cluster of differentiation
CRP	C-reactive protein
CSF1R	Colony stimulating factor 1 receptor
DN	Double negative
DP	Double positive
EDTA	Ethylenediaminetetraaceticacid
FFA	Free fatty acid
FBS	Fetal bovine serum
GF	Germ-free
GIP	Glucose-dependent insulinotropic polypeptide
GLP-1	Glucagon like peptide 1
GLUT	Glucose transporter
gMFI	Geometric mean fluorescence intensity
GSIS	Glucose stimulated insulin secretion
GTT	Glucose tolerance test
HBSS	Hank's Balanced Salt Solution
HEPES	4-(2-hydroxyethyl)-1-piperazineethanesulfonic acid
HFD	High-fat diet
iDCs	Intestinal dendritic cells
IFN	Interferon
IL	Interleukin
ILC	Innate lymphoid cell
iMacs	Intestinal macrophages
i.p.	Intraperitoneal
IPGTT	Intraperitoneal glucose tolerance test
ITT	Insulin tolerance test
K^{+}	Potassium

LPM	Large peritoneal macrophages
LPS	Lipopolysaccharide
mAb	Monoclonal Antibody
MAIT	Mucosal associated invariant T cell
MHC	Major Histocompatibility Complex
OGTT	Oral glucose tolerance test
PBS	Phosphate buffered saline
PCA	Principle Component Analysis
PCR	Polymerase chain reaction
PM	Peritoneal macrophages
PP	Pancreatic polypeptide
P/S	Penicillin Streptomycin
pS473	Phosphorylated Akt (Serine 473)
pS6	Phospho-S6 Ribosomal Protein (Serine 235/236)
RNA	Ribonucleic acid
RPM	Cell culture medium (established at the Roswell Park Memorial Institute)
SPM	Small peritoneal macrophages
TCA	Tricarboxylic acid cycle
TLR	Toll-like receptor
TNF	Tumor necrosis factor
T1D	Type 1 diabetes
T2D	Type 2 diabetes
β-cell	Pancreatic beta-cell

1 Introduction

1.1 Overview

Obesity has become a global health problem of epidemic proportions[1,2]. Among its many detrimental consequences, it is also a major risk factor for the development of type 2 diabetes (T2D)[3]. So far, chronic low-grade inflammation triggering insulin resistance is thought to be a key component of metabolic disease[4]. This metabolic inflammatory state – also called "meta-inflammation" – is governed by immune cells in response to excess of nutrients and energy[4]. Especially, macrophages in the adipose tissue have been established as the major players of the inflammatory processes in the development of metabolic disease[5]. However, it is difficult to point out the exact starting point of chronic low-grade inflammation in metabolic disease and its underlying molecular mechanisms.

As the gut is the primary organ exposed to food antigens, the gastrointestinal tract might play a major role in mediating chronic low-grade inflammation and obesity-associated glucose dysregulation. Additionally, since macrophages are key contributors in metabolic disease, they could potentially mount a first-line response in the gastrointestinal tract to dietary and microbial cues and thereby impact glycemic control. The aim of the current study was to elucidate the role of specific intestinal macrophage subpopulations on glucose metabolism in high-fat diet (HFD)-induced metabolic disease and the underlying mechanisms. Understanding the relation between dietary and microbial cues, the host's immune system and its metabolic response is crucial for an in-depth understanding of disease mechanism and the potential development of immune-modulatory treatments in obesity.

1.2 Metabolic Disease

Metabolic disease refers to a combination of central obesity and metabolic dysregulation, including glucose intolerance, insulin resistance, dyslipidemia and hypertension[6–8]. All these factors strongly increase the risk for T2D as well as the risk for cardiovascular disease and also mortality[9].

The World Health Organization (WHO) reported that obesity has nearly tripled since 1975[10]. The WHO estimates that more than 1.9 billion (40 %) of adults are overweight, of whom 650 million (13 %) are considered as clinically obese (WHO, 2016)[10]. Additionally, there is a strong association between obesity and diabetes. The majority (80 %) of individuals with T2D are also obese[3]. The incidence of diabetes has risen from 108 million in 1980 to 422 million people in 2014 with a global estimated prevalence of 8.5 % (WHO, 2014)[11].

Furthermore, diabetes has become one of the leading causes of death worldwide (WHO, 2016). In 2012 ,1.6 million deaths were directly caused by complications of diabetes, whereas another 2.2 million were caused by high blood glucose levels[1].

1.2.1 Obesity and Diabetes Mellitus

Obesity is defined as excessive fat accumulation that increases risk to health[12]. The body mass index (BMI) (weight[kg]/stature[m^2][13]) has been established to classify overweight (BMI > 25 kg/m^2) and obesity (BMI > 30 kg/m^2)[14], however, it does not take into account the fitness level or the percentage of muscles of an individual. Obesity has a strong relationship to increased risk for insulin resistance and T2D[12]. It increases with age, genetic predisposition and an inappropriate lifestyle characterized by an imbalance between calorie intake and energy expenditure due to reduced physical activity[15]. Elevated levels of triglycerides, glycerol, hormones, cytokines and C reactive protein (CRP) are also involved in the development of insulin resistance in obese patients[16].

Additionally, the high amounts of non-esterified fatty acids reduce the use of glucose by the skeletal muscle ("Randle cycle"), stimulate the hepatic production of very low-density lipoproteins (VLDL) as well as glucose, which affects insulin secretion[15]. This in turn causes higher blood glucose levels and can lead to long-term complications, dysfunction or failure of different orangs, especially the eyes, kidney, nerves, heart and blood vessels[17].

1.2.2 Type 1 and Type 2 Diabetes Mellitus

Diabetes mellitus is a chronic metabolic disease and can be classified into different subtypes in terms of diagnostic criteria, etiology and genetics[18]. Diabetes in general is characterized by high blood glucose levels (random glucose $\geq$ 200 mg/dL or $\geq$ 11.1 mmol/L or fasted glucose $\geq$ 126 mg/dL or $\geq$ 7 mmol/L)[17], termed hyperglycemia, resulting from defects in insulin secretion, insulin resistance or a combination of both[19]. In addition, diabetes can be diagnosed using glycated hemoglobin, hemoglobin A1c (HbA1c; $\geq$ 6.5 % or $\geq$ 48 mmol/mol) as an indicator for the average of glycemic control over the past three months[17,19]. In 1997, the American Diabetes Association (ADA)[17] proposed the following classification for the two main diabetes types: Type 1 diabetes (T1D: β-cell destruction leading to insulin deficiency), and Type 2 diabetes (T2D: β-dysfunction with insulin resistance). Although this standard classification is necessary for treatment strategies, the boundaries of diabetes types needs to be seen as flexible, since not every patient, particular young people, will fit into a single type[20].

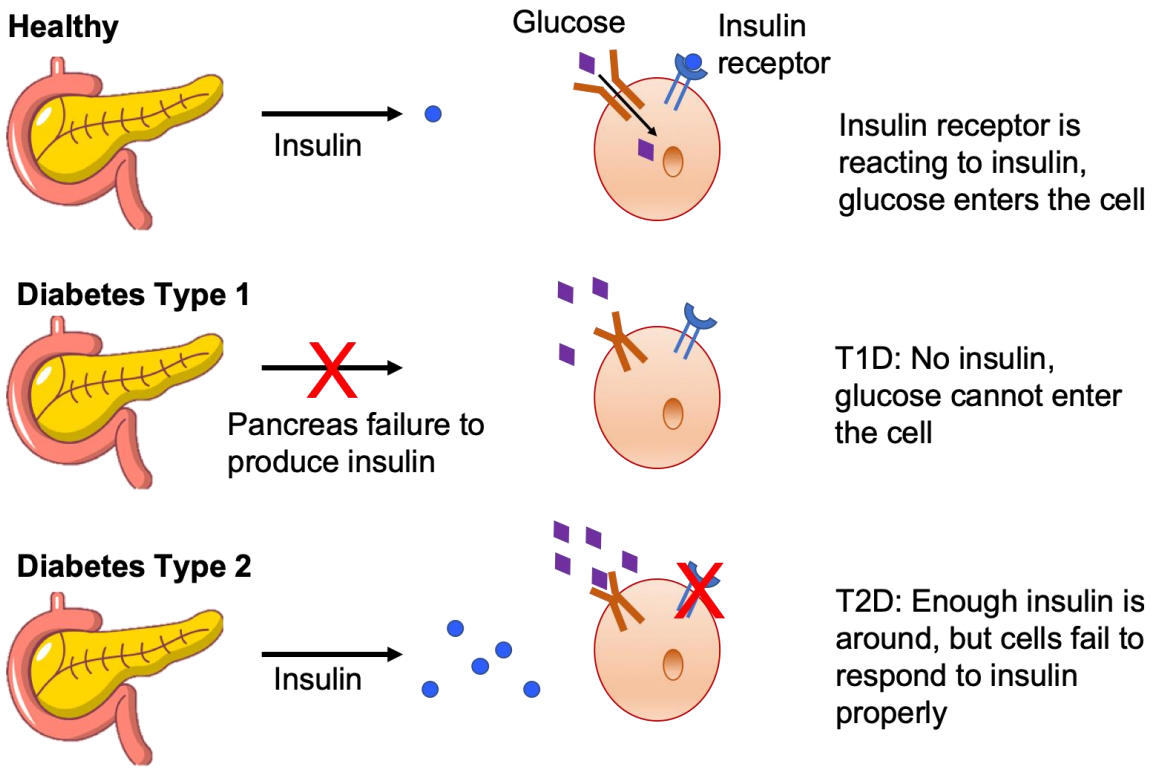

Fig. 1 Pathophysiology of type 1 and type 2 diabetes. Figure was adapted from[21].

Only about 5-10 % of patients diagnosed with diabetes have T1D[22]. This type of diabetes has also been named insulin-dependent diabetes as it results from a cellular-mediated autoimmune destruction of the insulin-producing β-cells of the pancreas (see 1.3.1 The Pancreases)[17]. The autoimmune response involves T-cells (insulitis) as well as B-cells (humoral response)[23]. It has been suggested that environmental factors and a genetic predisposition trigger islet autoantibodies causing the lack of insulin and the development of T1D[24]. T1D typically occurs in childhood (80-90% of patients under the age of < 20 years), but can also occur in adolescence or adulthood[23,25].

The most common form of diabetes is T2D with 90-95% of patients being diagnosed with this type of diabetes. It is also called “non-insulin-dependent diabetes” or “adult-onset diabetes” and is caused by the failure of β-cells to secrete sufficient amounts of insulin (= insulin deficiency) to compensate for insulin resistance[17]. Obesity, as mentioned before, is the major risk factor driving insulin resistance and thereby causing T2D[26]. Interacting genetic, environmental and behavioral risk factors like overnutrition and a sedentary life style thus contribute to T2D[26]. This relative insulin deficiency leads to a decrease in glucose transport to insulin-target tissues such as liver, muscle and fat cells. The resulting high demand for insulin cannot be satisfied and leads to failed adaption causing β-cell dysfunction[27] and reduced pancreatic β-cell mass due to increased apoptosis[28]. Originally, insulin resistance has been seen

as the key driver of T2D. However, insulin resistance has been recently discussed as an adaptive defense mechanism to the insulin-induced metabolic stress overload[29,30]. Therefore, overriding insulin resistance with intense insulin therapy might even be harmful for overweight or obese patients with severe insulin resistance[29]. Therefore, treatments counteracting nutrient-overload to lower glucose are preferable. Furthermore, inflammatory processes (see 1.4 Chronic Inflammation in Metabolic Disease) induced by the immune system, especially macrophages in the adipose tissue are well established to play a key role in the development of obesity-related insulin resistance and hence T2D[5,12].

1.3 Glucose Metabolism

In metabolic disorders, the main focus is on the regulation and metabolism of glucose. Glucose is the main energy source of our body[31]. Nevertheless, when elevated it can lead to the main characteristic of T2D - hyperglycemia - due to dysregulation of glucose hemostasis[17,32]. To better understand the disease pathophysiology of diabetes, it is important to bear in mind the mechanisms regulating glucose homeostasis. Glucose homeostasis describes the balance of glucose entering the circulation (glucose appearance) and its removal from the circulation (glucose disappearance)[33]. Glucose appearance can be caused by intestinal absorption following food intake or hepatic processes such as the breakdown of glycogen by glycogenolysis or the synthesis of glucose by gluconeogenesis as well as renal production by gluconeogenesis and glycogenolysis[33]. Gluconeogenesis is driven by fasting and primarily generated from lactate and amino acids[34].

The anabolic hormone insulin was discovered as a the main regulator of glucose disappearance in the blood stream[35]. The primary action of insulin is to promote glucose uptake into the muscle and adipose tissue, thereby lowering blood glucose levels[36]. In addition, insulin suppresses postprandial glucagon secretion, promotes protein and fat synthesis and the use of glucose as an energy source. The glucose agonist - glucagon - was identified as a major stimulus of hepatic glucose production[37,38]. Glucagon stimulates the breakdown of liver stored glycogen, hepatic gluconeogenesis and ketogenesis, thereby preventing hypoglycemia in the fasted state[39]. Another important β-cell hormone is amylin, which is formed and co-secreted with insulin in response to caloric intake suppressing glucagon release, delaying the rate of gastric emptying and stimulating satiety[35,40]. Also, the gut incretin glucagon-like peptide-1 (GLP-1) has been recognized as a key determinant of glucose maintenance. GLP-1 is secreted from L cells of the gastrointestinal mucosa upon food intake and is known to slow down gastric emptying, enhance insulin secretion and suppress glucagon secretion[41–43]. Other glucose regulatory hormones are glucose-dependent insulinotropic peptide (GIP), epinephrine, cortisol

and growth hormones[33].Thus, glucose homeostasis is based on a multi-hormonal interplay between insulin, glucagon, amylin and incretins.

1.3.1 The Pancreas

To ensure normal body functions, a tight control of changes in blood glucose levels are of upmost importance. To ascertain this, a network of various hormones and neuropeptides secreted from different locations in the body has developed (brain, pancreas, liver, intestine as well as adipose and muscle tissue). The pancreas represents the main key player for glucose homeostasis in this network[44]. The pancreas is both an exocrine (secreting digestive enzymes) and endocrine (releasing hormones into the circulation) organ[45]. Little grape-like cell clusters enriched with digestive enzymes termed acini, located at the terminal ends of the pancreatic ducts, form the exocrine part. The endocrine cells account for 1-2 % of the pancreas and are clustered together in so called islets of Langerhans due to their island-like structure and their discoverer Paul Langerhans (Fig. 2)[36,46]. These islets include five different cell types: glucagon producing α-cells (15-20 %); amylin, C-peptide and insulin secreting β-cells (65-80 %); pancreatic polypeptide (PP) producing PP-cells (3-5 %), somatostatin rich δ-cells (3-10 %) and ghrelin-producing ε-cells (<1 % of total islet cells)[47–50]. These secreted hormones have different functions and roles in maintaining glucose homeostasis. As mentioned above, insulin decreases glucose and glucagon increases blood glucose levels[48]. While somatostatin counteracts glucagon and insulin release[51], PP controls the endocrine and exocrine pancreas secretion activity[49]. To ensure rapid delivery of secreted hormones to the circulation, pancreatic islets are highly vascularized.

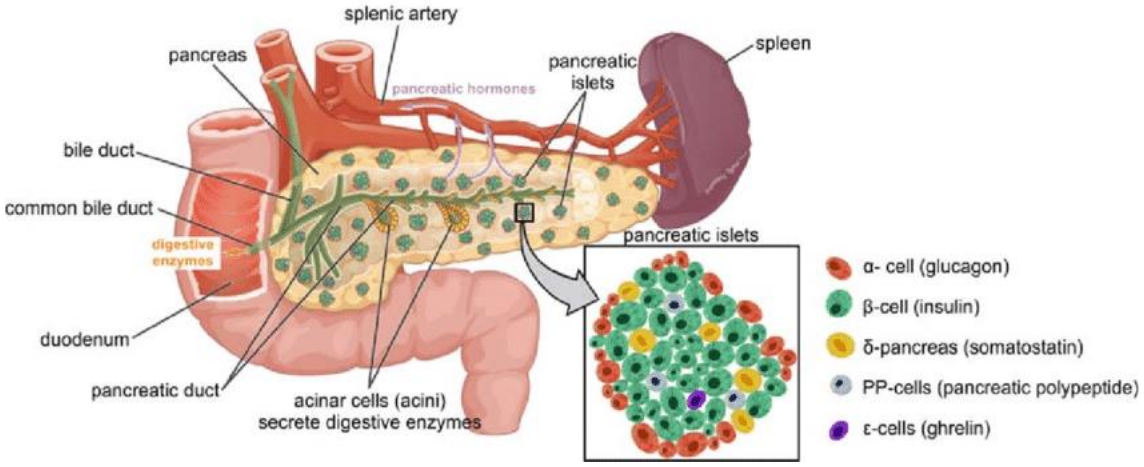

Fig. 2 Overview of pancreas anatomy. The pancreas is composed of an exocrine (acinar cells secreting digestive enzymes) and endocrine part (islets of Langerhans) consisting of five different hormones producing cell types: α-cells, β-cells, PP-cells, δ-cells and ε-cells. Figure was taken and adapted from[52,53].

1.3.2 Insulin Secretion

In response to caloric intake, insulin is secreted by the β-cells of the pancreas. This process is called glucose-stimulated insulin secretion (GSIS) (Fig. 3) which is the main feature of adult β-cells[54]. In the pathogenesis of T2D this function is dysregulated or even completely lost[36,55].

Elevated blood glucose levels are rapidly detected by the β-cells after glucose enters the cytoplasm via glucose transporter 2 (GLUT2) proteins located at the cell surface. After entry into the cell, glucose is first processed via glycolysis into pyruvate. Thereafter, adenosine triphosphate (ATP) is generated by mitochondrial pyruvate oxidation through the tricarboxylic acid cycle (TCA), resulting in a higher ATP/ADP ratio. This process closes ATP-sensitive potassium (K^+_{ATP}) channels and thereby induces membrane depolarization[56], which in turn opens voltage-dependent Calcium (Ca^{2+}) channels, leading to a cytosolic increase of Ca^{2+}. Higher intracellular Ca^{2+} facilitates membrane fusion of insulin containing granules and finally exocytosis of insulin.[36,44,57,58]

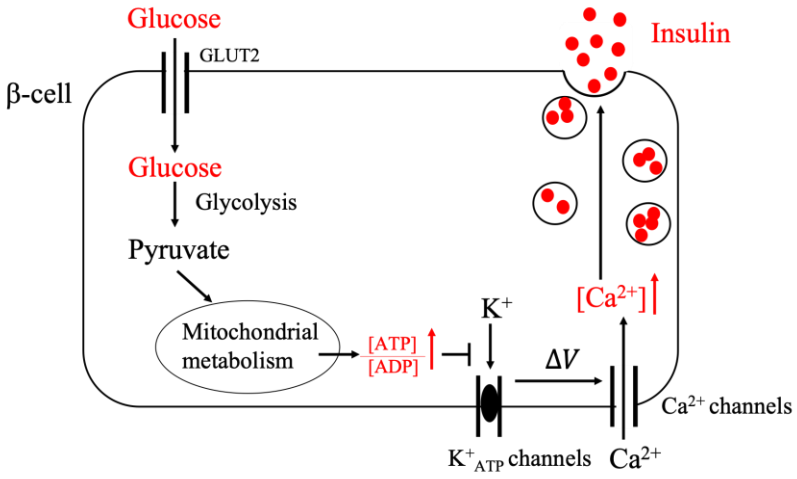

Fig. 3 Glucose-stimulated insulin secretion in pancreatic β-cells. After glucose entry, glucose is converted to pyruvate during glycolysis, later generated to ATP by mitochondrial oxidative phosphorylation. The increased ratio of ATP/ADP levels leads to closed K^+_{ATP} channels causing polarization of the cell membrane. Ca^{2+} channels are voltage dependent and thus open upon polarization. This results in a higher Ca^{2+} influx. Subsequently, vesicles containing insulin will be secreted by exocytosis. Figure was adapted from[57].

1.4 Chronic Inflammation in Metabolic Disease

Besides the classical disease manifestations of glucose intolerance, insulin resistance, dyslipidemia and hypertension[59,60], chronic low-grade inflammation has emerged as a key feature of metabolic disease[4,61,62]. This inflammation is characterized by abnormal cytokine production, activation of inflammatory signaling pathways and especially the infiltration of macrophages into different tissues. For instance, adipose tissue inflammation, where macrophages accumulate in adipose tissue, is a main attribute of obesity[63,64]. In addition,

systemic inflammation plays a central role in obesity and insulin resistance as seen by increased inflammation markers, such as tumor necrosis factor (TNF)[65], Interleukin-1β (IL-1β)[66], IL-6[67] or CRP[68,69]. Overstimulation with glucose or free fatty acids cause intracellular stress, such as endoplasmic reticulum (ER) stress or excess of ROS production by mitochondria, inducing inflammatory pathways associated with insulin resistance[70–73]. To date, however, the origin of this inflammatory process is unclear.

1.5 Macrophages

In chronic diseases such as metabolic disease, macrophages have been identified as crucial contributors to the inflammatory processes mediating glucose dysregulation[74,75]. Macrophages belong to the innate immunity, which is the first line response of our immune system upon infection[76,77]. The innate immune system recognizes pathogen-associated molecular patterns (PAMPs) and reacts rapidly but in a non-specific manner[77]. Macrophages have been discovered by Metchnikoff and were termed after their phagocytic activity (*makrós= big, phagein= eat)*[78]. The progenitors of these phagocytic cells have the ability to self-renew, or rise from yolk sac, fetal liver as well as from bone marrow-derived blood monocytes[79–84]. Their major lineage regulator is the colony stimulating factor 1 receptor (CSF1R)[85]. CSF1R is a transmembrane tyrosine kinase receptor that is mostly expressed on all mononuclear phagocytes and important for their development und functional activity[86,87]. Under physiological conditions macrophages maintain tissue homeostasis by clearing dead cells or damaged tissue[88]. However, dysregulated conditions triggered by physical, chemical or metabolic stimuli induce inflammation, as seen by secreted proinflammatory mediators by injured cells[89]. Constant metabolic stimuli overload the system and cause a chronic low-grade inflammation. This inflammation mostly is governed by an infiltration and accumulation of macrophages, in T2D especially in adipose tissue[90,91]. Furthermore, researchers have demonstrated a high plasticity and functional diversity at particular tissue locations[92,93]. According to their activation status, macrophages can be classified into quiescent (M0), activated (pro-inflammatory "M1" by LPS/IFN-γ) and alternatively activated (anti-inflammatory "M2" by IL-4/IL-13/IL-10) macrophages[94,95]. M1 macrophages are highly inflammatory and linked to inflammatory diseases[91,96,97]. Being activated, they change their phenotype and release inflammatory mediators, such as proinflammatory cytokines initiating inflammatory cascades. Macrophage polarization can be metabolically reprogramed and alter the regulation of glucose metabolism[98]. In diabetes the classical secreted proinflammatory cytokine is IL-1β, which has been shown to block insulin signaling and induce insulin resistance[99,100]. However, it has also been shown that macrophage-

derived IL-1β secretion can also play a physiological role such as supporting postprandial insulin secretion[101].

1.6 Gastrointestinal Changes in Metabolic Disease

The gastrointestinal tract's immune system could be a potential starting point of inflammation in metabolic disease as the gut is the primary site exposed to food antigens. Indeed, evidence points to the gastrointestinal tract as a site of inflammation in obesity as evidenced by changes in the microbiota (see 1.6.1 Gut Microbiota) and the intestinal immune system (see 1.6.2 Intestinal Immunity).

1.6.1 Gut Microbiota

In terms of metabolic disease, the main focus of the role of the gastrointestinal tract up to now concerned the gut microbiome. Changes in the gut flora, termed as "dysbiosis", are believed to contribute to chronic low-grade inflammation by increased permeability and thereby leaking of bacterial products such as lipopolysaccharides into the systemic circulation upon HFD[102,103]. The leakage of those endotoxins across the epithelial gut barrier is termed endotoxemia and potentiates systemic inflammation[104,105]. Researchers have tried to understand how the gut microbiota contribute to metabolic disease, especially insulin resistance. So far, it was reported that the microbiota composition and function can fluctuates depending on quantity and dietary composition[106,107]. In a healthy gut, microbiota *Bacteroidetes* and *Firmicutes* dominate with 90 % of the bacterial phylotypes besides other phyla such as *Actinobacteria*, *Verrucomicrobia,* and *Fuscobacteria*[108]. In obesity, a less diverse genomic repertoire of gut microbiota was identified[109,110]. Dietary intervention was able to restore gut microbial richness and improve inflammation[109]. In addition, a microbial shift characterized by an altered *Bacteroidetes*/*Firmicutes* ratio with an increase of *Firmicutes* bas been described in ob/ob mice[109]. However, human studies could not confirm the link between higher ratios of *Firmicutes* to *Bacteroidetes* in obese subjects[111–113].

A first connection between gut microbiota and glucose homeostasis was made with germ-free (GF-) mouse experiments. Hereby, GF-mice were protected from obesity and insulin resistance upon HFD which was reversed after fecal transplant[114]. Additionally, microbiota-targeted therapies in humans have been shown to improve glucose metabolism[115–117]. Fecal transplants from obese or diabetic patients can partly reproduce an obese metabolic phenotype in GF-mice[118]. Other studies have linked molecular markers to dysregulated glucose homoestasis[110,119,120]. However, also controversial data exist, for instance a recent study showing that short-term HFD induced microbial changes are not causally linked to insulin

resistance[121]. However, it was shown that gut microbiota can influence glucose homeostasis via the regulation of bile acids, for instance triggering the activation of farnesoid X receptor (FXR) or G protein-coupled bile acid receptor TGR5[122,123]. Other suggested mechanisms include the modulation of incretin secretion such as GLP-1 and GIP[124–126] and short fatty acid production[127]. However, the underlying mechanism how the gut microbiota impact on glucose metabolism is not fully understood.

1.6.2 Intestinal Immunity

The gastrointestinal tract hosts a large variety of immune cells that potentially respond to microbial or dietary cues by mounting an inflammatory response and influencing thereby glycemic control. So far, increased TNF-expression, activation of NFκB or TLR4-immunoreactivity or IL-1β and IL-12p40 have been described locally in the gut wall after HFD[102,128,129]. These inflammatory changes suggest that intestinal immune cells play a crucial role in mediating inflammatory as well as metabolic alterations upon HFD. However, how high caloric diets act on intestinal immune cell populations and whether such changes contribute to glucose dysregulation remains elusive.

The literature has suggested a possible link between changes in the adaptive intestinal immunity and obesity and insulin restiance[130–132]. Here, studies revealed a pro-inflammatory shift with reduced Foxp3$^+$ regulatory T cells, increased Th1, CD8$^+$ and IL-17-producing γδT cells upon HFD[130]. Furthermore, the gut anti-inflammatory agent, 5-aminosalicylic acid, reversed bowel inflammation and metabolic parameters[130]. In addition, mucosa-associated invariant T (MAIT) cells, known as innate-like T cells, were shown to decrease in obese or T2D patients causing an activated phenotype associated with elevated Th1 and Th17 cytokine production. However, detailed characterization of MAIT cells as well as their contribution to inflammation in T2D has not yet been done. In terms of innate immunity, IL-22, which is produced by innate lymphoid cells (ILC), might be involved in maintaining mucosal immunity during obesity[133]. However, IL-22-/- mice do not show any changes in metabolic parameters under HFD, whereas recombinant IL-22 was able to reduce bodyweight und metabolic complications[133]. Other studies showed that eosinophil depletion upon HFD correlated with increased intestinal permeability and HFD intake[133].

So far, not much is known about the contribution of intestinal macrophages and dendritic cell (DC) and their subpopulations. One study shows that DCs remain unchanged in numbers under HFD[134]. An increased inflammatory tone in intestinal macrophages has been reported to precede adipose tissue inflammation during obesity[135]. However, the characterization of

specific intestinal macrophage subpopulations, as well as a causal link between changes in their function and metabolic disease, has as of yet not been assessed.

1.7 Intestinal Macrophages

Evidence has pointed to intestinal macrophages as a "remote control" for adipose tissue inflammation and insulin resistance[135,136]. Intestinal macrophages are a heterogeneous cell population. Based on surface marker expression, like Ly6C-MHCII, they have been classified into five subpopulations P1-P5 that follow along a common differentiation trajectory (Fig. 4)[137–139]. All subpopulations originate from bone marrow-derived Ly6C^{high} monocyte precursors[140], which first differentiate into CCR2^{+} macrophages that can be further subdivided into pro-inflammatory ("M1"-like) subpopulations P1, P2 and an intermediate stage P3[138]. These short-lived transitional cells gradually lose their pro-inflammatory phenotype to become CCR2^{-} anti-inflammatory/resident ("M2"-like) macrophages, which include subpopulations P4 and P5[137,139]. Early in life, yolk-sac-derived macrophages were still present in the intestine. However, in adult mice, resident macrophages seem to mainly originate from circulating monocytes [135,139].

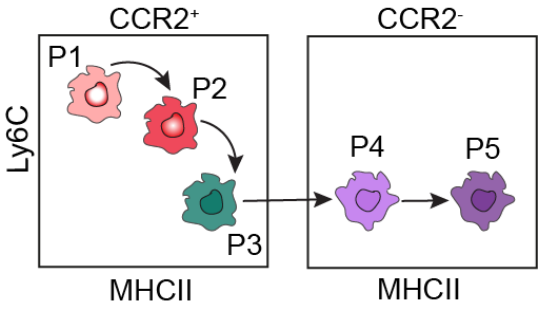

Fig. 4 Monocyte-waterfall of intestinal macrophages. Intestinal macrophages can be subdivided into CCR2^{+} pro-inflammatory ("M1"-like) P1, P2 subpopulations and an intermediate subpopulation P3 as well as in CCR2^{-} ("M2"-like) anti-inflammatory/resident subpopulations P4, P5. Figure was adapted from[235]

In normal health, the anti-inflammatory/resident intestinal macrophages predominate. They display a remarkable anergy towards pro-inflammatory stimuli such as bacteria or TLR-ligands despite their phagocytic activity[138,141]. However, in intestinal inflammation, such as Crohn's disease or colitis, intestinal macrophages retain an inflammatory phenotype and are developmentally disturbed at subpopulation P2. This differentiation stop results in the accumulation of pro-inflammatory/monocyte-derived macrophages[137,138,142–145]. However, whether obesity affects these intestinal macrophage subpopulations and what role they play in glucose metabolism is currently unknown

2 Aim of the Thesis

As macrophages are key players of chronic low-grade inflammation in metabolic disease, they could potentially mount a first-line response in the gastrointestinal tract to dietary or microbial cues and thereby affect glycemic control. So far, the phenotypic and functional profile of intestinal macrophage subpopulations and their contribution to glycemic control is still unknown.

The aim of the current study was to elucidate the role of intestinal macrophage subpopulations in glucose metabolism and the molecular mechanisms involved. Intricately understanding the relation between dietary and microbial cues, the host's immune system and its metabolic response is crucial for an in-depth understanding of the disease mechanism in obesity. This might open up new possibilities in the development of immune-modulatory treatments for metabolic disease.

3 Material and Methods

3.1 Experimental Model and Subject Details

Mice

Male C57BL/6N (B6) mice and CCR2$^{-/-}$ mice (in-house-bred: Department of Biomedicine, University Hospital Basel, Switzerland or ordered from Charles River, Wilmington, US) were maintained in our SPF-facility at room temperature of 22°C on a 12h light/12h dark cycle. Germ-free B6J mice were bred and maintained in flexible-film isolators or in individually ventilated cages (IVC) at the Clean Mouse Facility, University of Bern, Switzerland. For most of the HFD studies 5-8 week-old weight-matched mice were fed either a HFD or chow diet for up to 3 months.

Physiology: To assess the physiology of intestinal macrophages, B6 mice on chow diet and coconut-based HFD (60% fat; #D12331 Research Diets, New Brunswick, US) were sacrificed at three different timepoints: 4 pm ,12 pm, and 8 am. Fed mice were compared to fasted controls.

Fasting/Refeeding: Mice were fasted overnight with free access to water. Refeeding with coconut-based HFD was done in the morning for 30 min up to 4 h.

Chronic HFD feeding: In our chronic HFD-induced obesity mouse model mice were fed a high-fat diet ad libitum; either coconut-based (Surwit with sucrose HFD; 60 % fat; #D12331 Research Diets or Sniff, Soest, Germany) or a lard-based purified HFD (60 %; #D12492i; Research Diets) for up to three months. Control groups were fed either a chow diet (#3436, Kliba nafag, Kaiseraugst, CH) or a purified control diet with nearly no fibers (Starch: 10 % kcal % fat; D#12450Ji; Research Diets). See diet details in Table 1.

Table 1. Diet composition of control diets and HFD

Diet	Fat	Protein	Carbohydrates	Fibers
Chow diet	4.5 % Crude fat	18.5 %	35 % Starch	4.5 %
Coconut HFD	58 % Coconut fat (Soybean and Coconut Oil)	16.4 %	25.5 % (Maltodextrin 10, Sucrose)	0.5 %
Starch	10 % Lard fat (Soybean Oil and Lard)	20 %	70 % Starch (Maltodextrin 10, Sucrose)	0 %
Lard HFD	60 % Lard fat (Soybean Oil and Lard)	20 %	20 % (Maltodextrin 10, Sucrose)	0 %

Units in kcal%.

Human subjects

Colon biopsies were collected from both male and female obese (BMI > 32 kg/m^2, n=8) and lean (BM < 27 kg/m^2, n=13) individuals with an average age of 60±14.89 years. Gastroscopy biopsies of lean (n=12) and obese (n=12) patients were also collected from both genders with an average age of 48.83±16.72 years. In addition, blood was obtained from male and female obese (n=15) and lean (n=21) patients with an average age of 52±17.36 years. Exclusion Criteria: Inability to provide informed consent, intake of corticosteroids, anti-inflammatory/ immunosuppressive drugs potentially altering immune cells, clinical signs of current infection, known anemia (e.g. hemoglobin < 110 g/L for males, < 100 g/L for females) or neutropenia (e.g. leukocyte count < 1.5 × 10^9/L or ANC < 0.5 × 10^9/L), known immunodeficiency (e.g. HIV), vasculitis or collagenosis, inflammatory bowel disease, adrenal insufficiency and/or substitution with glucocorticoids, known clinically significant kidney or liver disease (e.g. creatinine > 1.5 mg/dL, AST/ALT > 2 × ULN, alkaline phosphatase > 2 × ULN, or total bilirubin [tBili] > 1.5 × ULN, liver cirrhosis Child B or C), risky daily alcohol consumption (> 24g/d for males, > 12g for females), known uncontrolled congestive heart failure, known uncontrolled malignant disease or currently pregnant or breastfeeding. Subjects were referred by the Department of Gastroenterology at the University Hospital Basel/Clarunis, University Center for Gastrointestinal and Liver Diseases Basel or the doctor's office MagenDarm Basel for a diagnostic colonoscopy on the basis of symptoms suggestive for irritable bowel syndrome or for colorectal cancer screening (recommended in Switzerland after the age of 50 years). Researchers were blinded during sample-processing and data acquisition. For the statistical analysis between obese and lean patient, researchers were unblinded.

Study Approval

All animal procedures were approved by the local Animal Care and Use Committee and performed in accordance with Swiss Federal regulations. The human material was collected and used with informed consent. Permission for the human study (ID: 2018-00712; full title "Characterization of human intestinal macrophages in metabolic disease- iMAC study" ClinicalTrails.gov) was obtained by the Ethical commission in Basel (Ethikkommission Nordwest- und Zentralschweiz).

3.2 Macrophage Depletion and mTOR Inhibition Models

Systemic Depletion by CSF1R inhibitor BLZ945: For dose-dependent depletion of macrophages, HFD-fed mice were treated by oral gavage with 50, 100 or 200 µg/g CSF1R inhibitor (BLZ945; MTA Novartis, Basel, Switzerland) or its vehicle (20 % Captisol; Ligand, San Diego, US) for up to ten weeks (5 times/week). Treatment started 1 week before HFD feeding.

Intrarectal and Intraperitoneal Application of Clodronate Liposomes: To specifically deplete colonic macrophages, mice were anesthetized with isoflurane and clodronate liposomes were injected intrarectally with a flexible gavage needle coated with lubricant. This colon-specific depletion model was compared to systemic depletion by intraperitoneal (i.p.) application of clodronate liposomes. In both strategies either clodronate liposomes (#C-005) or control PBS liposomes (#P-005, Liposoma B.V.[146]) were injected every other day (100 µL/500 µg/injection) starting from day -4 until day 6 after start of HFD feeding. Application rhythm was assigned similar to the intrarectal inoculation with clodronate liposomes in Qualls et al, 2006[147].

Intrarectal and Intraperitoneal Application of Rapamycin: To inhibit mammalian target of rapamycin (mTOR), mice were treated intrarectally or i.p. with 3 mg rapamycin/kg/every other day (Cat#HY-10219, MedChemExpress), according the application of clodronate liposomes.

3.3 Isolation of Intestinal Macrophages

Colon: Intestinal lamina propria lymphocytes were isolated from the colon of mice or from human biopsies. For mouse colon, the length was measured, fat was removed and the tissue was first cut open longitudinally, then cut into 1 cm pieces and washed in ice-cold DPBS or HBSS (without Mg/Ca). To remove the epithelial layer, tissue pieces and biopsies were washed twice in HBSS/2 mM EDTA shaking 20 min at 37 °C. EDTA was removed by washing in HBSS only and transferred into a gentle MACS C-tube (#130-096-334, Miltenyi Biotec) containing 3 mL Complete IMDM Medium (1x IMDM, 10 % FBS, P/S, Glutamax). Next 3 mL of 2x Collagenase VIII (#C2139, Sigma-Aldrich) digestion mix (Complete IMDM, 2mg/mL Collagenase VIII, 25 µg/mL DNase I) was added to start enzymatic digestion shaking at 37 °C (mouse colon: 25-30 min, human biopsies: 35-40 min). Digested tissue was homogenized using the gentleMACS Octo Dissociator (Militenyi Biotec; program: ms_intestine-01) and digestion was stopped by adding 60 µL/ 6 mL 0.5M EDTA. For leukocyte enrichment a percoll gradient (40 %/70 %, #GE17-0891-01, GE Healthcare) was performed (600 g, 20 min, 22 °C, brake and acceleration 0 or 1). The lymphocyte ring was collected from the interphase, and washed (550 g, 5 min, 22 °C) with FACS Buffer (1xDPBS, 0.5% BSA, 5 mM EDTA). The pellet was

resuspended in 200 µL FACS Buffer containing Fc Blocking and filtered through a 35 µM strainer FACS tube (#352235, Corning).

3.4 Isolation of Macrophages from other Tissues

Adipose and Liver Tissue: Adipose and liver tissue were minced with scissors and rinsed with 1x HBSS (adipose tissue: 4 mL; liver lope: 1 mL). Digestion was started by adding 4 or 1 mL, respectively of 2x Collagenase IV (#C2139, Worthington) digestion mix (1x HBSS, 20 mM HEPES, 3 mg/mL Collagenase IV and 16.5 µg/mL DNAse I) and shaking for 20-30 min at 37 °C; 400 rpm. After 15 min liver samples were pipetted up and down. Digestion was quenched by adding FACS buffer and the suspension was filtered through a cotton gauze. Erythrocytes were removed using Red Cell Lysis Buffer (154 mM NH4Cl, 10 mM KHCO3, 0.1 mM EDTA). Liver lymphocytes were enriched using a 70 %/40 % percoll gradient. Later cells were washed and filtered for FACS staining.

Peritoneum: To isolate peritoneal macrophages the abdominal skin was peeled off. Peritoneum was perfused with 10 mL FACS buffer and the mouse carefully shaken and pierced over a glass funnel into a 50 mL reaction tube. The isolated cells were filtered through a 70 µm strainer (#431751, Corning) and pelleted (550 g, 5 min, 4 °C). Cells were lysed using Red Cell Lysis Buffer, washed and filtered for FACS staining.

Brain: To isolate microglia whole-brains were excised from the skull and mechanically dissociated in FACS buffer using a Dounce-homogenizer (#D9938-1SET, Merck). Cells were then passed through a 70 µm cell strainer, washed with FACS buffer and enriched by performing a 70 % 37 % percoll gradient (30 min, 750 g, minimal brake). The microglia-containing interphase was subsequently collected and filtered, washed and used for FACS analysis.

3.4 Antibodies and Flow Cytometry

Flow Cytometry Staining: To reduce unspecific binding, the Fc receptor was blocked using CD16/32 prior to incubation with monoclonal antibodies (mAbs) for 30 min-1 h on ice. All mAbs used for flow cytometry are listed in Table 2. If FACS analysis could not be done at the same day stained cells were fixed by using fixation buffer (#00-5523-00S, Thermo Fisher Scientific, Waltham, US).

MitoTracker Staining: For MitoTracker staining cells were washed with cold FACS Buffer after the surface staining and then stained with MitoTracker probes (Thermo Fisher Scientific) at 37 °C in the dark (10 nM MitoGreen and 5 n MitoRed for 20 min in 10 % FACS Buffer, 1 µM MitoSOX for 10 min in 1x HBSS (no Mg/Ca)).

mTOR Staining: For the assessment of mTOR activation cells were fixed with BD Fix I Buffer (Becton Dickinson Biosciences, Franklin Lakes, US) (10 min, 37 °C) after surface staining. Subsequently, cells were washed and permeabilized by adding BD Perm Buffer II. After 30 min incubation on ice cells were washed twice with FACS Buffer. Cell pellet was then stained for 1 h at RT with anti-pS6 and anti-pS473.

Samples were acquired with a LSRIIFortessa or Aria III (BD Biosciences) and analyzed with FlowJo software 10.6.1 (BD Biosciences).

Table 2. Flow Cytometry Antibodies and Reagents

REAGENT or RESOURCE	SOURCE	IDENTIFIER
Antibodies for Murine Intestinal Macrophages		
Anti-mouse CD16/CD32	Biolegend	Cat#101310; RRID: AB_2103871
Anti-mouse CD3 (145-2C11) APC-Cy7	Biolegend	Cat#100330; RRID: AB_1877170;
Anti-mouse CD19 (6D5) APC-Cy7	Biolegend	Cat#115530; RRID: AB_830707
Anti-mouse NK1.1 (PK136) APC-Cy7	Biolegend	Cat#108723; RRID: AB_830870
Anti-mouse Ly6G (1A8) APC-Cy7	Biolegend	Cat#127624; RRID: AB_10640819
Anti-mouse CD45 (30-F11) PerCP-Cy5.5	Biolegend	Cat#103131; RRID: AB_893344
Anti-mouse CD24 (M1/69) PE-Cy7	Biolegend	Cat#101821; RRID: AB_756047
Anti-mouse CD11b (M1/70) BV421	Biolegend	Cat#101236; RRID: AB_11203704
Anti-mouse CD64 (X54-5/7.1) APC	Biolegend	Cat#139306; RRID: AB_11219391
Anti-mouse Ly6C (HK 1.4) FITC	Biolegend	Cat#128005; RRID: AB_1186134
Anti-mouse I-A/I-E (M5/114.15.2) BV785	Biolegend	Cat#107645; RRID: AB_2565977
Anti-mouse CCR2 (475301) PE	R&D Systems	Cat#FAB5538P-25/100; RRID: AB_10718414
Anti-mouse CD11c (N418) BV650	Biolegend	Cat#117339; RRID: AB_2562414
Anti-mouse CD103 (2E7) PE-Dazzle594	Biolegend	Cat#121430; RRID: AB_2566493
Antibodies for Adipose Tissue Macrophages		
Anti-mouse F4/80 (BM8) PE	Biolegend	Cat#123110; RRID: AB_893486
Anti-mouse CD11c (N418) PE-Cy7	Biolegend	Cat#117318; RRID: AB_493568
Anti-mouse CD206 (C068C2) A647	Biolegend	Cat#141712; RRID: AB_10900420
Anti-mouse Siglec F (E50-2440) BV510	BD Biosciences	Cat#740158; RRID: AB_2739911
Antibodies for other Stainings		
Anti-mouse F4/80 (BM8) e660	Thermo Fisher Scientific	Cat#50-4801-80; PRID:AB_11150065
Anti-mouse CD11b (M1/70) A488	Thermo Fisher Scientific	Cat#53-0112-80; PRID:AB_469900
Anti-mouse CD11b (M1/70) e660	Thermo Fisher Scientific	Cat#50-0112-82; PRID:AB_11218507
Anti-mouse CD45 (30-F11) A700	Biolegend	Cat#103128; RRID: AB_493715
Anti-mouse Ly6C (AL-21) BV605	BD Biosciences	Cat#563011; RRID: AB_2737949
Anti-mouse Akt (pS473) PE	BD Biosciences	Cat#560378; RRID: AB_1645328
Anti-mouse S6 (pS235/pS236) (N7-548) A488	BD Biosciences	Cat#560434; RRID: N/A
Antibodies for Human Intestinal Macrophages		
Anti-human CD19 (HIB19) PE-Cy5	Biolegend	Cat#302209; RRID: AB_314239
Anti-human CD3 (UCHT1) PE-Cy5	Biolegend	Cat#300410; RRID: AB_314064
Anti-human CD56 (5.1H11) PE-Cy5	Biolegend	Cat#362515; RRID: AB_2564088
Anti-human CD20 (2H7) PE-Cy5	Biolegend	Cat#302307; RRID: AB_314255
Anti-human TCRαβ (IP26) PE-Cy5	Biolegend	Cat#306710; RRID: AB_314648
Anti-human CD45 (HI30) PerCP-Cy5.5	Biolegend	Cat#304027; RRID: AB_1236444
Anti-human CD64 (10.1) A647	Biolegend	Cat#305012; RRID: AB_528867

Anti-human HLA-DR (L243) A488	Biolegend	Cat#307619; RRID: AB_493176
Anti-human CD14 (MφP9) BUV395	BD Biosciences	Cat#563562; RRID: AB_2744288
Anti-human CD16 (3G8) BUV496	BD Biosciences	Cat#564654; RRID: AB_2744294
Anti-human CD209 (9E9A) PE	Biolegend	Cat#330105; RRID: AB_1134060
Anti-human CD163 (GH1/61) BV421	Biolegend	Cat#333611; RRID: AB_2562462
Anti-human CCR2 (KO36C2) BV510	Biolegend	Cat#357217; RRID: AB_2566503
Anti-human CD33 (WM53) BV785	Biolegend	Cat#303427; RRID: AB_2650887
CD103 (Ber-ACT8) BV605	Biolegend	Cat#350217 ;RRID: AB_2564282
Chemicals and Reagents		
Fix Buffer I	BD Biosciences	Cat#557870
Perm Buffer III	BD Biosciences	Cat#558050
MitoTracker. Green FM	Thermo Fisher Scientific	Cat# M7514
MitoTracker. Red CMXRos	Thermo Fisher Scientific	Cat#M7512
MitoSOX™ Red mitochondrial superoxide indicator	Thermo Fisher Scientific	Cat# M36008
DAPI	Biolegend	Cat#422801
Zombie Aqua Fixable Viability Kit	Biolegend	Cat#423102
Zombie NIR Fixable Viability Kit	Biolegend	Cat#423105

Flow cytometry Gating Strategies:

Intestinal Macrophages: Intestinal macrophages were characterized as $CCR2^{+}$ (pro-inflammatory/monocyte-derived: P1, P2 and intermediate: P3) and $CCR2^{-}$ (anti-inflammatory/resident: P4, P5) as previously described[137,138,148](see Figure 1A). The following surface markers were used: negative selection for NK1.1, CD3, CD19, Ly-6G (to exclude NK-, T-, B- cells, neutrophils) and positive selection for live cells (DAPI or Zombie Aqua negative), CD45 (pan-leukocyte marker), CD11b, CD24, CD64, Ly-6C and CCR2 (to exclude $CD24^{hi}Ly\text{-}6C^{-}CD64^{-}$ DCs and distinguish $CCR2^{+}$ ($CCR2^{+}CD64^{low\ to\ high}$) and $CCR2^{-}$ ($CCR^{-\ to\ low}CD64^{high}$) subsets), MHCII/Ly-6C (to characterize iMac subpopulations P1-P5)).

Intestinal Dendric Cells: Intestinal Dendritic cells (DC) were assigned within live $CD45^{+}Lin^{-}$ cells after exclusion of $CD64^{+}$ macrophages and gating on $MHCII^{+}CD11c^{+}$ DCs into 4 different DC subpopulations: double negative (DN), $CD11b^{+}CD103^{-}$, $CD11b^{-}CD103^{+}$, $CD11b^{+}CD103^{+}$(DP) (see Figure S1C)[149].

MitoTracker Staining: For mitochondria function assays isolated intestinal macrophages were identified as live($DAPI^{-}$)$CD45^{+}CD11b^{+}Lin^{-}$ and excluding $CD64^{-}Ly6C^{-}$ and characterized as P1-P5 subpopulations by MHCII/Ly6C using following surface markers: CD3/CD19/NK1.1/Ly6G APC-Cy7, CD45 A700, CD11b BV421, Ly6C BV605, MHCII BV785, CD64 APC.

mTOR Staining: For the assessment of mTOR activation anti-pS6 (mTOR) A488 (BD) and anti-pS473 (Akt) PE (BD) were used. Surface staining including e455 or NIR fixable dye, CD3/CD19/NK1.1/Ly6G APC-Cy7, CD45 A700, CD11b BV421, CD64 APC, Ly6C BV605, MHCII BV785 was performed.

Adipose Tissue Macrophages: After excluding eosinophils ($CD45^+F4/80^{low}SiglecF^+$), ATMs ($liveCD45^+CD11b^+F4/80^+$) were classified as double negative (DN), monocyte-derived M1a ($CD11c^+CD206^-$), inflammatory M1b ($CD11c^+CD206^{mid}$) and anti-inflammatory M2 ($CD11c^{-\text{ to low}}CD206^{hi}$) subpopulations[150–153] (see Figure S1G).

Peritoneal Macrophages: Macrophages ($CD45^+CD11c^-$nonDCs) isolated from the peritoneum were identified as small (SPM: $CD11b^+F4/80^{low}$) and large (LPM: $CD11b^+F4/80^{hi}$) peritoneal macrophages[154] (see Figure 3A).

Liver Kupfer Cells: Hepatic macrophages were characterized using different surface markers including CD45, F4/80, Ly6C, CD11b and CD11c. Hereby, we could identify macrophages among hepatic $CD45^+$ leukocytes: monocyte-derived macrophages ($CD11b^+F4/80^{+/-}Ly6C^{+/-}$) and Kupffer cells/resident macrophages ($CD11b^+F4/80^+$)[155–157].

Microglia: Microglia could be detected in extracted brain cells by the expression of CD45 and CD11b (see Figure 3A).

Islet Macrophages: Pancreatic islet macrophages were identified in live $CD45^+$ leucocytes as $CD11b^+F4/80^+$.

Human intestinal macrophages: Human intestinal macrophages were characterized as $CD14^{high}$ (pro-inflammatory/monocyte-derived: P1, P2 and intermediate: P3) and $CD14^{low}$ (anti-inflammatory/resident: P4, P5) (see Figure 7A)[138,158]. The following human surface markers were used: Negative selection for CD19, CD20, CD3, TCRαβ, CD56 (to exclude B cells, T cells, NK cells) and positive selection for live cells (Zombie NIR negative), CD45 (pan-leukocyte marker), CD64 and CD33 (macrophage marker to exclude $CD33^-CD64^-$), HLA-DR and CD14 (excluding $HLA\text{-}DR^-CD14^-$) to distinguish $CD14^{high}$ ($HLA\text{-}DR^{low\text{ to }high}CD14^{high}$) and $CD14^{low}$ ($HLA\text{-}DR^+CD14^{low}$) subsets), CD163 and CD209 (to characterize subpopulations P1-P5))[138,158]. Intestinal dendritic cells (DC) were identified by the expression of CD103. Additional monocytes marker, such as CCR2, CD14 and CD16 were also included in the staining.

Peripheral blood mononuclear cells (PBMCs): PBMCs can be classified into classical ($CD14^{++}$ $CD16^{-}$), intermediate ($CD14^{++}CD16^{+}$) and non-classical ($CD14^{+}CD16^{++}$) human monocyte subpopulations (see Figure 7D)[159]. All antibodies used for the biopsies were used also for staining PBMCs.

3.5 Metabolic Assessments

Metabolic phenotype was assessed by glucose and insulin tolerance tests (GTT/ ITT) performed at 1, 4 and 12 weeks of HFD feeding. For a GTT mice were fasted 6 h. After intraperitoneal (IPGTT) or oral (OGTT) injection of glucose (2 g/ kg bodyweight) blood glucose was monitored from the tail vein after 15, 30, 60, 90 and 120 min using a glucometer (Freestyle, Abbot). For active GLP-1 measurements 25 mg/kg sitagliptin (Cat#sc-364620, Santa Cruz) was injected i.p. 30 min before oral glucose application. To block GLP-1 or parasympathetic action 236 µg/kg Exendin (9-39) (#H-8740, Bachem) or 5 mg/kg atropine (#A0257-5G, Sigma), respectively, were i.p. injected at timepoint -30 min prior glucose application. Blood was sampled in EDTA tubes for further analysis. For measurements of GLP-1 100 µM DPP4 inhibitor Diprotein A was additionally added.

ITT was performed after 3 h of fasting by injecting 1-2 U/kg body weight insulin i.p. (Actrapid HM Penfill, Novo Nordisk), glucose levels were measured at 0, 15, 30, 60,90 and 120 minutes after injection.

Plasma insulin, GLP-1, TNF and IL-6 were quantified by electrochemiluminescence (MESO SECTOR S 600) using kits from Meso Scale Diagnostics (MSD, Rockville, MD, USA), according to the manufacturer`s instructions: Mouse/Rat Insulin Kit (#K152BZC),V-PLEX Plus Proinflammatory Panel 1 Mouse Kit (#K15048G), V-PLEX GLP-1 Active Kit vers. 2 (#K15030D).

3.6 Quantitative Reverse Transcriptase-Polymerase Chain Reaction (RT-PCR)

RNA was extracted from distal colon and epididymal adipose tissue using NucleoSpin RNA kit (#740955.250, Macherey-Nagel) or the RNeasy Plus Universal Mini kit (#73404, QIAGEN) according to manufacturer`s instructions. Reverse transcription was performed with GoScript™ Reverse Transcription Mix (#A2801, Promega). For qPCR GoTaq qPCR Master Mix (#A6002, Promega) was used. Data was acquired on a ViiA7 Real-Time PCR System (Thermo Fisher Scientific). Primer sequences (Microsynth, Balgach, Switzerland) are listed in Table 3. The data presented correspond to the mean of $2^{-\Delta\Delta Ct}$ after being normalized to the housekeeping genes B2m and Ppia.

Table 3. Primers sequences used for quantitative real time-PCR

Gene	Forward Primer	Reverse Primer
Housekeeping genes		
B2m	5′ TTCTGGTGCTTGTCTCACTGA	5′ CAGTATGTTCGGCTTCCCATTC
Ppia	5′ GAGCTGTTTGCAGACAAAGTTC	5′ CCCTGGCACATGAATCCTGG
Inflammation markers		
Tnf	5′ ACTGAACTTCGGGGTGATCG	5′ TGAGGGTCTGGGCCATAGAA
Il6	5′ GGATACCACTCCCAACAGACCT	5′ GCCATTGCACAACTCTTTTCTC
Il1b	5′ GCAACTGTTCCTGAACTCAACT	5′ ATCTTTTGGGGTCCGTCAACT
Kc	5′ CTGGGATTCACCTCAAGAACATC	5′ CAGGGTCAAGGCAAGCCTC
Il10	5′ AGGCGCTGTCATCGATTTCTC	5′ GCCTTGTAGACACCTTGGTCTT
Il18	5′TCTTGCGTCAACTTCAAGGA	5′GTGAAGTCGGCCAAAGTTGT
Il22	5′TTG AGG TGT CCA ACT TCC AGC A	5′AGC CGG ACG TCT GTG TTG TTA
Tgfb1	5′CTCTCCACCTGCAAGACCAT	5′CGAGCCTTAGTTTGGACAGG
Immune cells		
Ly6c	5′ GCAGTGCTACGAGTGCTATGG	5′ ACTGACGGGTCTTTAGTTTCCTT
Cd68	5′ GCAGCACAGTGGACATTCAT	5′ AGAGAAACATGGCCC GAAGT
Adgre1 (Emr1)	5′ GCC CAG GAGTGGAATGTCAA	5′ CAGACACTCATCAACATCTGCG

3.7 Isolation of Pancreatic Islets

To isolate pancreatic mouse islets, collagenase IV (1.4 mg/mL; Worthington) digestion solution was injected into the pancreas via the common bile duct after mouse was euthanized. The perfused pancreas was digested at 37 °C for 30 min, thereafter quenched (1x HBSS, 1 M HEPES, 0.5 % BSA) and filtered. Islets were handpicked under a stereoscopic microscope and cultured in RPMI-1640 (containing 11.1 mM glucose, 10 % FBS, 100 U/mL P/S, 2 mM Glutamax, 50 µg/mL Gentamycin, 10 µg/mL Fungison). For flow cytometry analysis islets were washed at the same day in PBS/ 0.5 mM EDTA, trypsinized and around 100 islets/tube were collected.

3.8 Glucose-Stimulated Insulin Secretion (GSIS) Assay

For GSIS handpicked primary mouse islets were incubated in RPMI-1640 medium overnight. The next day islets were washed and pre-incubated in Krebs-Ringer-bicarbonate buffer (KRB: 115 mM NaCl, 4.7 mM KCl, 2.6 mM $CaCl_2$ $2H_2O$, 1.2 mM KH_2PO_4, 1.2 mM $MgSO_4$ $2H_2O$, 10 mM HEPES, 0.5 % BSA, pH 7.4) containing 2.8 mM glucose. After 1.5 h buffer was replaced to KRB containing low (2.8 mM, basal) or high (16.7 mM, stimulated) glucose and supernatant was collected after 1 h to assess basal and glucose stimulated insulin release. The stimulatory index was defined as the ratio of stimulated insulin secretion at 16.7 mM/h to basal insulin secretion at 2.8 mM/h. To obtain insulin content islets were vortexed in 0.18 mol/l HCl in 70 % ethanol and incubated at least 1 h at -20 °C. Secreted and content insulin were measured by Mouse/Rat Insulin Kit (#K152BZCMeso Scale Discovery).

3.9 Microbiota Analysis

gDNA extraction from stool samples: Contents from small intestine, cecum and colon, or feces were frozen in 2 mL tubes and stored at -80 °C until extraction. To extract genomic DNA (gDNA) from feces QIAamp FAST DNA Stool Mini Kit (#51604 Qiagen, Hilden, Germany) was used following the vendor`s instructions with the following adjustment: homogenization of stool particles was performed with 100 mg baked glass beads (Sigma Aldrich) using a tissue lyser for 3 min, 30 Hz per run (Retsch MM400). DNA concentration was measured by Nanodrop2000 (Thermo Fisher Scientific).

16S amplicon PCR: 100 ng of bacterial DNA were used to amplify the V5/V6 region of the 16S ribosomal gene by PCR using Platinum Taq DNA polymerase (Invitrogen). We used barcoded forward fusion primers 5'- CCATCTCATCCCTGCGTGTCTCCGACTCAG-BARCODE-ATTAGATACCCYGGTAGTCC-3', where core primers have been modified by the addition of a PGM sequencing adaptor, a GT-spacer and unique barcode (see Table 4), that allow pooling of up to 96 different barcodes in combination with the reverse fusion primer 5'-CCTCTCTATGGGCAGTCGGTGATACGAGC-TGACGACARCCATG-3'[160–162]. All primers were used at a 10 µM working concentration. Cycling conditions were following: initial 5 min denaturation at 94 °C , followed by 35 cycles of 1 minute denaturation at 94 °C, 20 s annealing at 46 °C and 30 s extension at 72 °C. The final extension step took place for 7 min at 72 °C. The PCR product (ca 350 bp) was loaded on a 1 % agarose gel, cut out with a scalpel extracted using the QIAqick Gel Extraction Kit protocol (#28706, Qiagen). The resulting dsDNA concentration was measured by Qubit dsDNA HS Assay Kit (#Q32854, Thermo Fisher Scientific).

16S sequencing: Up to 96 libraries were diluted at 26 pM and were pooled. Libraries were prepared with the OT2 HiQ View 400 kit and emulsion PCR performed on the Ion OneTouch 2 (OT2) instrument (ThermoFischer). The template-positive Ion Sphere Particles containing clonally amplified DNA were enriched using the Ion OneTouch ES instruments (ThermoFisher). Sequencing was carried out using the Ion PGM HiQ View Sequencing 400 kit with the Ion Personal Genome Machine System on an Ion 316 Chip v2 (ThermoFisher)[163].

Table 4. Primers sequences used for 16S amplicon PCR

1	CTAAGGTAAC	**33**	TTCTCATTGAAC	**65**	TCCTGGCACATC
2	TAAGGAGAAC	**34**	TCGCATCGTTC	**66**	CCGCAATCATC
3	AAGAGGATTC	**35**	TAAGCCATTGTC	**67**	TTCCTACCAGTC
4	TACCAAGATC	**36**	AAGGAATCGTC	**68**	TCAAGAAGTTC
5	CAGAAGGAAC	**37**	CTTGAGAATGTC	**69**	TTCAATTGGC
6	CTGCAAGTTC	**38**	TGGAGGACGGAC	**70**	CCTACTGGTC
7	TTCGTGATTC	**39**	TAACAATCGGC	**71**	TGAGGCTCCGAC
8	TTCCGATAAC	**40**	CTGACATAATC	**72**	CGAAGGCCACAC
9	TGAGCGGAAC	**41**	TTCCACTTCGC	**73**	TCTGCCTGTC
10	CTGACCGAAC	**42**	AGCACGAATC	**74**	CGATCGGTTC
11	TCCTCGAATC	**43**	CTTGACACCGC	**75**	TCAGGAATAC
12	TAGGTGGTTC	**44**	TTGGAGGCCAGC	**76**	CGGAAGAACCTC
13	TCTAACGGAC	**45**	TGGAGCTTCCTC	**77**	CGAAGCGATTC
14	TTGGAGTGTC	**46**	TCAGTCCGAAC	**78**	CAGCCAATTCTC
15	TCTAGAGGTC	**47**	TAAGGCAACCAC	**79**	CCTGGTTGTC
16	TCTGGATGAC	**48**	TTCTAAGAGAC	**80**	TCGAAGGCAGGC
17	TCTATTCGTC	**49**	TCCTAACATAAC	**81**	CCTGCCATTCGC
18	AGGCAATTGC	**50**	CGGACAATGGC	**82**	TTGGCATCTC
19	TTAGTCGGAC	**51**	TTGAGCCTATTC	**83**	CTAGGACATTC
20	CAGATCCATC	**52**	CCGCATGGAAC	**84**	CTTCCATAAC
21	TCGCAATTAC	**53**	CTGGCAATCCTC	**85**	CCAGCCTCAAC
22	TTCGAGACGC	**54**	CCGGAGAATCGC	**86**	CTTGGTTATTC
23	TGCCACGAAC	**55**	TCCACCTCCTC	**87**	TTGGCTGGAC
24	AACCTCATTC	**56**	CAGCATTAATTC	**88**	CCGAACACTTC
25	CCTGAGATAC	**57**	TCTGGCAACGGC	**89**	TCCTGAATCTC
26	TTACAACCTC	**58**	TCCTAGAACAC	**90**	CTAACCACGGC
27	AACCATCCGC	**59**	TCCTTGATGTTC	**91**	CGGAAGGATGC
28	ATCCGGAATC	**60**	TCTAGCTCTTC	**92**	CTAGGAACCGC
29	TCGACCACTC	**61**	TCACTCGGATC	**93**	CTTGTCCAATC
30	CGAGGTTATC	**62**	TTCCTGCTTCAC	**94**	TCCGACAAGC
31	TCCAAGCTGC	**63**	CCTTAGAGTTC	**95**	CGGACAGATC
32	TCTTACACAC	**64**	CTGAGTTCCGAC	**96**	TTAAGCGGTC

Analysis of 16S data: Samples with less than 1000 reads were excluded from the analysis if not stated otherwise. Data analysis was performed using the QIIME pipeline version 1.8.0[164]. OTUs were picked at a threshold of 97 % similarity using usearch61_ref v.6.1.544[165] followed by rarefaction and taxonomy assignment using Greengenes database.

3.10 RNA-Sequencing

For single-cell RNA-sequencing (scRNA-seq) (liveCD45$^+$Lin$^-$CD11b$^+$CD24$^-$ and CD64$^+$ or Ly6C$^+$) CD11b$^+$nonDCs colonic macrophages (see gating strategy[148] and Figure 1A) were sorted from mice fed 1 week HFD (n=2) or control diet (n=2) using FACS Aria III (BD Biosciences). Cell suspensions were loaded on the wells of a 10X Genomics Chromium Single Cell Controller (one well per mouse replicate). Single cell capture and cDNA and library preparation were performed with a Single Cell 3' v2 Reagent Kit (10X Genomics) according to the manufacturer's instructions. Sequencing was performed on one lane of an Illumina NexSeq 500 machine flow-cell at the ETH Zurich Genomics Facility in Basel, Switzerland.

Data were analyzed by the Bioinformatics Core Facility, Department of Biomedicine, University of Basel, Switzerland. Read quality was assessed with the FastQC tool (version 0.11.5). In brief, sequencing files were processed with Kallisto (version 0.46.0) and BUStools (version 0.39.2) to perform sample and cell demultiplexing, read pseudo-alignment to the mouse transcriptome (Ensembl release 97) and to generate a UMI counts table[166,167]. Further processing of the UMI counts table was performed using R 3.6.0 and Bioconductor 3.10 packages[168], notably DropletUtils (version 1.6.1)[169,170] scran (version 1.14.5) and scater (version 1.14.5)[171], following mostly the steps illustrated in the simpleSingleCell Bioconductor workflow[172].

Based on the distributions observed across cells, cells with library sizes lower than 795, total number of features detected lower than 317, or with a fraction of UMI counts attributed to the mitochondrial genes of 0% or higher than 7% were filtered out[173]. Low-abundance genes with average normalized $\log_2$ counts lower than 0.003 were filtered out. This resulted in a filtered matrix including UMI counts for 11,820 genes and 5,797 cells (3,013 from Chow-fed mice and 2,784 from HFD-fed mice). UMI counts were normalized with size factors estimated from pools of cells to deal with dominance of zeros in the matrix[172,174]. A mean-dependent trend was fitted to the variances of the log expression values of endogenous genes to distinguish between genuine biological variability and technical noise (*trendVar* function of the scran package with loess trend and span of 0.05)[175]. The fitted trend was used to subtract technical noise from the data using the *denoisePCA* function, retaining the 8 first principal components of the PCA for later analysis steps.

The package SingleR (version 1.0.0) was used for reference-based annotation of the cells and identification of likely contaminants in our dataset[176]. We used the Immunological Genome Project (ImmGen) mouse microarray dataset[177] as reference, and eliminated 377 cells not annotated to the broad cell types “macrophages” or “monocytes”.

Clustering of cells was done on normalized log-count values using hierarchical clustering on the Euclidean distances between cells (with Ward’s criterion to minimize the total variance within each cluster; package cluster version 2.1.0). The 6 clusters used for following analyses were identified by applying a dynamic tree cut (package dynamicTreeCut, version 1.63-1).

Differential expression between HFD and chow conditions, stratified by cluster was performed using a “pseudo-bulk” approach[178]: UMI counts of cells from each sample in each cluster were summed. This resulted in 4 samples per cluster, aggregated from 29 to 776 cells. Cluster P2.2 was excluded from the analysis because it contained too few chow cells. For each

cluster, only genes with CPM (normalized counts per million mapped reads) values above than 1 in at least 2 of the 4 pseudo-bulk samples, and detected in at least 5 % of the individual cells were retained.

The package edgeR (version 3.28)[179] was used to perform TMM normalization[180] and to test for differential expression with the Generalized Linear Model (GLM) framework. Genes with a false discovery rate (FDR) lower than 1 % were considered differentially expressed. Gene set enrichment analysis (GSEA) was performed with the function camera[181] using the default parameter value of 0.01 for the correlations of genes within gene sets, on gene sets from the hallmark collection[182] of the Molecular Signature Database (MSigDB, version 7.0)[183], or on DoRothEA v2 regulons[184]: human TOP10score regulons were downloaded from https://github.com/saezlab/DoRothEA and we obtained the corresponding mouse regulons by considering 1-to-many orthologs of the human genes in each regulon (using Ensembl Compara release 97). We considered only sets containing at least 5 genes from the filtered dataset and with a FDR lower than 10 %.

3.11 Human Study

Biopsies: Colon, stomach and duodenum biopsies were collected from lean, healthy controls (BMI < 27 kg/m^2) and obese (BMI > 32 kg/m^2) subjects undergoing screening colonoscopies or gastroscopies. Human intestinal macrophages were isolated by enzymatic digestion (see isolation of intestinal macrophages).

Human blood: Blood was collected in (2x) EDTA containing tubes. After the dilution with 1x DPBS (1 part blood : 3 parts DPBS), a ficoll density gradient by using Lymphoprep density gradient medium (#07851, Stemcell technologies) and Leucosep tubes (#871346, OpoPharma) was performed (25 min, 453 g, 22 °C, brake: 1, acceleration: 4). The Lymphoprep layer was washed with FACS Buffer (300 g, 10 min) and Red Cell Lysis Buffer (154 mM NH4Cl, 10 mM KHCO3, 0.1 mM EDTA) was used to remove residual erythrocytes. The remaining cells were washed with FACS Buffer, resuspended in 800 µL FACS Buffer and around 1 million cells were used for further flow cytometry staining. Flow cytometry data were correlated to clinical parameters documented by the case report forms, such as age, gender, race, weight, BMI, blood pressure, diabetes (including date of diagnosis), and other relevant diagnoses.

3.12 Statistical Analysis

The data are presented as mean ± standard error of the mean (SEM) with the numbers of experiments or mice indicated in the figure legends. To test statistical difference between two groups unpaired Mann-Whitney U test with two tailed distribution was used using Prism8 software (GraphPad Software, San Diego, CA). Two-sided P-values of 0.05 or less were considered to be statistically significant, *p<0.05, **p<0.01, ***p<0.001.

3.13 Data Availability

RNA-seq Data

Transcriptome sequencing data of intestinal macrophages have been deposited in the Gene Expression Omnibus (GEO), with the accession number GSE143351.

Go to https://www.ncbi.nlm.nih.gov/geo/query/acc.cgi?acc=GSE143351 and enter token **unoveyewbnyzpuj** into the box.

4 Manuscript

May 4th, 2020

Targeting Colonic Macrophages Improves

Glycemic Control in High-Fat Diet-induced Obesity

Intestinal Macrophage Subpopulations in Metabolic Disease

Theresa V. Rohm[1,2], Shefaa AlAsfoor[1,2], Angela J.T. Bosch[1,2], Zora Baumann[1,2], Sophia J. Wiedemann[1,2], Josua Wehner[1,2], Elise Dalmas[1,2], Leila Rachid[1,2], Regula Fuchs[1], Julien Roux[2,3], Catherine Mooser[4,5], Stephanie C. Ganal-Vonarburg[4,5], Julia B. Pilz[6], Petr Hruz[7], Daniel T. Meier[1,2], Claudia Cavelti-Weder[1,2*]

[1]Clinic of Endocrinology, Diabetes and Metabolism, University Hospital Basel, 4031 Basel, Switzerland.
[2]Department of Biomedicine (DBM), University of Basel, University Hospital Basel, 4031 Basel, Switzerland.
[3]Swiss Institute of Bioinformatics (SIB), 4031 Basel, Switzerland.
[4]Department of Visceral Surgery und Medicine, Bern University Hospital, University of Bern, 3008 Bern, Switzerland.
[5]Department for BioMedical Research (DBMR), University of Bern, Bern, Switzerland.
[6]Arztpraxis MagenDarm Basel, 3008 Basel, Switzerland.
[7]Clarunis, University Center for Gastrointestinal and Liver Diseases Basel, 4002 Basel, Switzerland.
[*]**Correspondence:** claudia.cavelti-weder@usb.ch

Word count: 34`495 (including spaces)
Number of references: 60
Number of tables and figures: 7 figures

Targeting Colonic Macrophages Improves Glycemic Control in High-Fat Diet-induced Obesity

Graphical Abstract

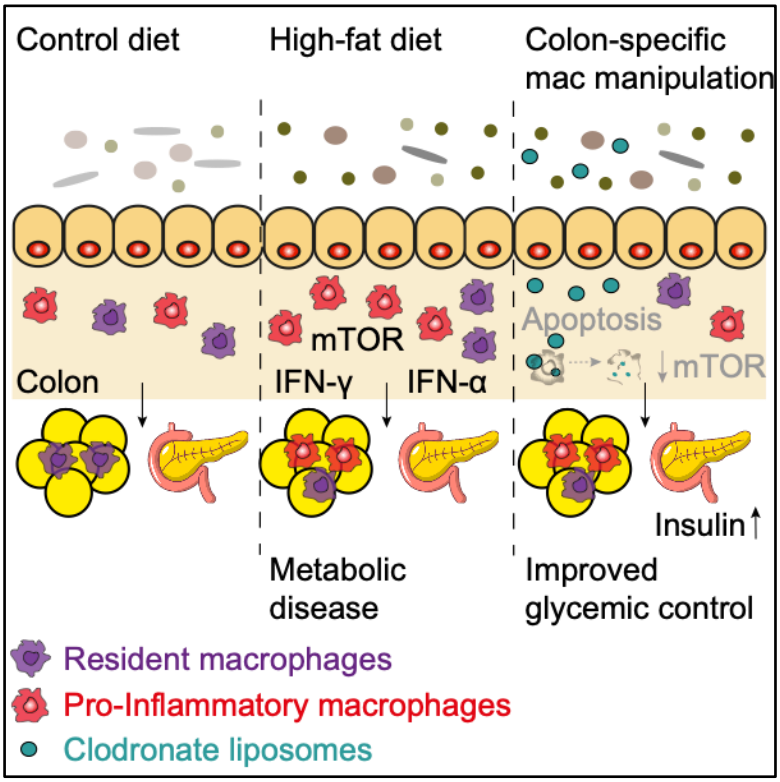

Authors

Theresa V. Rohm, Shefaa AlAsfoor, …, Daniel T. Meier, Claudia Cavelti-Weder

Correspondence

claudia.cavelti-weder@usb.ch (C.C.W.)

In Brief

The interplay between intestinal macrophages and β-cells remains elusive. Rohm et al. reveal that colon-specific macrophage depletion or inhibition of macrophage activation by blocking mTOR-signaling restores glycemic control.

Highlights

- Pro-inflammatory intestinal macrophage subpopulations are increased in obese mice and humans
- Colon-specific macrophage depletion improves β-cell function, glucose tolerance and insulin resistance
- Intestinal inflammation involves an interferon signature and a metabolic shift, potentially via mTOR
- Colon-specific mTOR inhibition of intestinal macrophages restores β-cell dysfunction

SUMMARY

The obesity epidemic continues to rise worldwide. However, the initiating mechanisms of glucose dysregulation in obesity remain poorly understood. We assessed distinct intestinal macrophage subpopulations and the role they play in glucose homeostasis in mice fed a high-fat diet (HFD) and obese humans. Pro-inflammatory/monocyte-derived intestinal macrophages transiently increased upon food intake and became chronically elevated with HFD. This suggested a link between macrophage numbers and glycemia, which we confirmed by genetic and pharmacological dose-dependent ablation of macrophages. In particular, colon-specific macrophage depletion ameliorated glycemic control and β-cell function. Colonic macrophage activation upon HFD feeding was characterized by an interferon signature and metabolic shift, potentially via mTOR activation. Accordingly, colon-specific mTOR inhibition enhanced insulin and GLP-1 secretion. In obese humans, pro-inflammatory intestinal macrophages were also increased. Thus, pharmacological colon-specific targeting of macrophages could be a potential therapeutic approach in obesity to improve glycemic control.

Key words: Metabolic disease; diabetes; obesity; chronic inflammation; intestinal inflammation; innate immunity of the gut; macrophages, mucosal immunity

INTRODUCTION

Glucose dysregulation and chronic low-grade inflammation are key features of metabolic disease. However, little is known about the initiating events that lead to these metabolic disturbances in high-fat diet (HFD)-induced obesity. Since the gut is the primary organ exposed to food antigens and bacteria, the gastrointestinal tract could play a major role in triggering glucose intolerance and inflammation.

So far, altered gut microbiota known as "dysbiosis" has received particular attention in diet-induced obesity. Hereby, dysbiosis is believed to contribute to metabolic dysfunction, inter alia, via bile acid metabolism, production of short chain fatty acids and leakage of bacterial products (Utzschneider et al., 2016). Accordingly, germ-free mice are protected from glucose intolerance and adiposity (Backhed et al., 2004). Gut immunity could be the missing link between dietary and microbial cues and glucose homeostasis as the gut constitutes the largest immune system of the body. Changes in adaptive gut immunity have already been described in mice fed a HFD. These include reduced $Foxp3^+$ T regulatory cells and increased IFN-γ-producing Th1, $CD8^+$ and IL-17-producing γδ T cells (Luck et al., 2015). In terms of innate immunity, TLR4, TNF and NFkB are known to be up-regulated in the gut upon HFD (de La Serre et al., 2010; Ding et al., 2010). Additionally, an increased inflammatory tone in intestinal macrophages has been reported to precede adipose tissue inflammation in obesity (Kawano et al., 2016). This suggests that intestinal innate immunity, in particular macrophages, play a crucial role in metabolic disease.

Macrophages are the most abundant leukocytes in the healthy gut (Mowat and Agace, 2014). However, intestinal macrophages are not a homogenous cell population, but consist of five distinct subpopulations that follow a differentiation trajectory (Tamoutounour et al., 2013; Tamoutounour et al., 2012). They originate from $Ly6C^{high}$ monocyte precursors, which first differentiate into $CCR2^+$ macrophages and can be subdivided into pro-inflammatory subpopulations P1 and P2, and an intermediate stage P3 (Bain et al., 2013). These short-

lived/non-mature transitional cells gradually lose their pro-inflammatory phenotype to become $CCR2^-$ anti-inflammatory/resident macrophages, which include subpopulations P4 and P5 (Tamoutounour et al., 2013; Tamoutounour et al., 2012). In the healthy gut, the majority of intestinal macrophages consists of the resident subpopulation P5, which is characterized by a distinct anergy towards typical pro-inflammatory stimuli, such as bacterial products or TLR-ligands despite avid phagocytic activity (Bain et al., 2013; Smythies et al., 2005). During intestinal inflammation such as colitis, this differentiation trajectory is disrupted at subpopulation P2, resulting in the accumulation of pro-inflammatory macrophages in the gut (Bain et al., 2013; Platt et al., 2010; Tamoutounour et al., 2012). However, it is currently unknown whether obesity affects intestinal macrophage subpopulations or what role they play in regulating glucose homeostasis. Therefore, the aim or our study was to elucidate the role of intestinal macrophage subpopulations in glucose metabolism of obese mice and humans. An in-depth understanding of this relationship might open up new possibilities for immune-modulatory treatments in metabolic disease.

Here, we found that HFD feeding leads to an increase in pro-inflammatory intestinal macrophage subpopulations that involved an interferon signature and metabolic shift, potentially via mTOR activation. Depleting colon-specific macrophages or inhibiting their activation by blocking mTOR-signaling restored glycemic control. These data indicated an interplay between dietary cues, intestinal macrophage subpopulations and insulin-producing β-cells, which regulates glucose homeostasis. Targeting colonic macrophages could thus represent a therapeutic approach to improve glycemic control.

RESULTS

Pro-inflammatory Intestinal Macrophage Subpopulations are Transiently Increased upon Food Intake and Chronically Elevated Following High-Fat Diet Feeding

There is growing evidence that the intestinal immune system is an important contributor to metabolic disease (Winer et al., 2016). However, the role of specific intestinal macrophage subpopulations in metabolic disease remains unknown. To address this, we first analyzed five intestinal macrophage subpopulations in response to distinct nutritional cues. After mice ate regular chow diet, pro-inflammatory intestinal macrophage subpopulation P1 increased compared to fasted controls, suggesting a transient innate immune response upon food intake (Figure 1A,B, middle panel). In contrast, subpopulations P2 to P5 were comparable in both fasted and chow-fed mice (Figure S1A). Similarly, HFD refeeding for up to 4 hours induced an acute response of innate gut immunity, as shown by enhanced expression of Ly6C in pro-inflammatory intestinal macrophage subpopulation P1 (Figure 1B, right panel).

When mice were kept on HFD for a week, gene expression of inflammatory markers *Tnf* and *Ly6c* was increased in colon tissue, while typical markers of resident macrophages *Tgfb1*, *Adgre1* and *Cd68* were reduced (Figure 1C). This points to a shift towards pro-inflammatory colonic macrophage subpopulations upon HFD. Indeed, after 1 week of HFD we found an increase in $CCR2^{+}$ pro-inflammatory colonic macrophages, especially in pro-inflammatory subpopulations P1/P2, which persisted for up to 12 weeks of HFD compared to chow diet (Figure 1A,D). In contrast, in $CCR2^{-}$ anti-inflammatory/resident macrophages mainly subpopulation P4 was reduced (Figure 1D). Additionally, intestinal neutrophils were increased, while dendritic cells did not show a consistent change in mice fed a HFD (Figure S1C-F). Stomach size was reduced after 4 and 12 weeks, while the caecum and colon were already shortened after 1 week of HFD (Figure S1B), consistent with previous literature (Kawano et al., 2016). Adipose tissue inflammation, a hallmark of chronic inflammation in metabolic disease, appeared later at 12 weeks of HFD as shown by pro-inflammatory gene

expression and increased inflammatory adipose tissue macrophage (ATM) subpopulation M1b (Figure 1E,F, Figure S1G). Concomitant with altered innate mucosal immunity from 1 week of HFD feeding onwards, we found increased TNF and IL-6 in the blood, glucose intolerance, and hyperinsulinemia (Figure 1G,H). These data indicated that pro-inflammatory intestinal macrophage subpopulations transiently increased upon food intake and became chronically elevated following HFD feeding. This innate immune response in the gut occurred simultaneously with glucose intolerance and was only later followed by adipose tissue inflammation and obesity.

Gut Microbiota are Essential for the Increase of Pro-inflammatory Intestinal Macrophage Subpopulations upon HFD, while the Fat Source Modulates its Magnitude

We next investigated whether the dietary composition, such as fiber content or the fat source influence the shift towards pro-inflammatory macrophages and glucose intolerance upon HFD feeding. Fiber-rich chow was compared to fiber-deficient starch control diet and coconut- and lard-based HFDs were compared to their respective control diets (diets see Table S1). Such a detailed assessment is crucial as regular chow contains fibers and may differ considerably depending on seasonal harvests, unlike purified/ standardized HFDs. Body weights were comparable within the two control and HFD groups, respectively (Figure 2A). After 3 months, mice fed fiber-deficient diets including starch control, coconut- and lard-based HFDs had decreased caecum and colon sizes compared to fiber-rich chow diet (Figure 2B), potentially due to an increased osmotic load. Fiber content did not affect intestinal macrophage or dendritic cell subpopulations (Figure 2C, Figure S2A). Also, fat pad weights, M1 ATMs and circulating pro-inflammatory cytokines TNF and IL-6 were similar in mice fed chow or starch control diets, whereas M2 ATMs were reduced in the absence of fibers (Figure 2D, Figure S1C). Along with unaltered innate immunity, mice fed fiber-rich and fiber-deficient control diets had comparable glucose tolerance and insulin sensitivity (Figure 2G).

When comparing mice on two different HFDs to those on respective control diets (chow as control for coconut-based HFD; starch as control for lard-based HFD), both HFDs induced an increase in pro-inflammatory $CCR2^+$ intestinal macrophages, especially pro-inflammatory subpopulations P1 and P2 (Figure 2E). However, mice on lard-based HFD had a significantly increased total number of intestinal macrophages, implying a heightened innate immune response. Intestinal dendritic cells did not show a consistent pattern with HFD (Figure S2B). In adipose tissue, both HFDs led to increased M1b ATMs and circulating pro-inflammatory cytokines (Figure 2F, Figure S1C), again with a higher inflammatory response in mice fed a lard-based HFD, as seen by an increase in total ATMs. This enhanced immune response correlated with worsened glucose tolerance and increased insulin resistance in mice fed lard- compared to coconut-based HFD (Figure 2G). These data suggested that the source of dietary fat, but not fiber content, modulated the innate inflammatory response to HFD and glycemic control.

Next, we used 16S ribosomal gene sequencing to assess how the different diets affect gut microbiota as potential mediators of glucose intolerance. At baseline, microbiota composition was similar between all groups. One week of fiber-deficient diets (starch control, coconut- and lard-based HFDs) resulted in similar microbial shifts as shown in the Principle Component Analysis (PCA) and relative phyla (Figure 2H) and genus abundance (Figure S2D). After 13 weeks, however, distinct differences between the two HFDs became apparent: Whereas mice fed a coconut-based HFD had a similar microbiota composition compared to 1 week (reduced *Firmicutes*), lard-based HFD shifted up in the PCA due to changes on the phylum (increased *Firmicutes* and reduced *Bacteroidetes*, Figure 2H) and genus level (Figure S2D). Hence, microbial dysbiosis per se, but not a specific composition, correlated with glucose intolerance.

To test how HFD affects intestinal macrophage subpopulations in the absence of gut microbiota, we used germ-free mice, which are known to be protected from glucose intolerance

and adiposity (Backhed et al., 2004). As previously described, germ-free mice on chow diet had fewer intestinal macrophages compared to colonized mice (Bain et al., 2014), which was most pronounced in mice on fiber-deficient starch control diet (Figure 2C (colonized) vs. Figure S2E (GF)). However, the distribution pattern of intestinal macrophage subpopulations was similar to colonized mice on chow diet (Figure S2F). Of note, germ-free mice showed very low numbers of $CD11b^{+}CD103^{+}$ conventional DCs (Figure S2G), possibly due to lower TLR activation in the absence of microbial entry (Kinnebrew et al., 2012). Upon HFD, germ-free mice showed neither an increase in pro-inflammatory intestinal macrophage subpopulations (P1 and P2), nor changes in dendritic cells or plasma TNF and IL-6 levels (Figure 2I, Figure S2H,I). These data indicated that a lack of gut microbiota prevented the recruitment and hence the increase in pro-inflammatory intestinal macrophages upon HFD in germ-free mice, thereby potentially protecting them from glucose intolerance.

Macrophage Numbers are Linked to Glycemic Control

As the degree of the innate inflammatory response correlated with glycemic control, we next hypothesized that the number of macrophages is directly linked to glucose metabolism. To address this question, we dose-dependently depleted macrophages by treating mice fed a HFD with the colony-stimulating factor 1 receptor (CSF1R)-inhibitor BLZ945 (50, 100, 200 μg/g/d) or vehicle. CSF1R regulates the survival, proliferation, and differentiation of macrophages (Pixley and Stanley, 2004). We found that treatment with BLZ945 reduced $CCR2^{+}$ pro-inflammatory and $CCR2^{-}$ anti-inflammatory/resident intestinal macrophages and their subpopulations P1-P5 with most pronounced effects in the mid and high dose groups (Figure 3A,B, Figure S3A). Additionally, CSF1R-inhibition resulted in a dose-dependent reduction in fat mass, ATMs (after 2 weeks preferentially M2- and after 2 months additionally M1-macrophages), microglia, and large and small peritoneal macrophages (Figure 3C-E, Figure S3B). Glucose metabolism was gradually improved with increasing BLZ945

concentrations as shown by fasting glycemia, glucose tolerance and insulin sensitivity (Figure 3F,G, Figure S3C). Body weights were slightly (not significantly) reduced in the highest dose group after 2 months of CSF1R-inhibition, potentially reflecting lower insulin levels (Figure S3D). Thus, these results suggested a direct link between the number of macrophages and glycemic control.

Next, we aimed to test glucose metabolism in a model with predominantly reduced pro-inflammatory intestinal macrophage subpopulations P1 and P2. To this end, we used CCR2-/- mice that lack CCR2-dependent monocyte recruitment (Bain et al., 2014). CCR2-/- mice had sharply reduced monocyte-derived intestinal macrophage subpopulations P1 and P2 on chow diet (P1 8.08±4.88%, P2 1.12±0.55% of wild-type controls). Unexpectedly, 1 week of HFD resulted in a partial re-appearance of pro-inflammatory Ly6C^{high} intestinal macrophages in CCR2-/- mice, suggesting a CCR2-independent monocyte influx upon short-term HFD feeding (Figure S3E,F). However, CCR2-/- mice exhibited much lower absolute numbers of intestinal macrophages than wild-type mice on HFD (Figure S3G). After three months of HFD, pro-inflammatory intestinal macrophages P1/P2 were hardly present in CCR2-/- mice, while reductions in anti-inflammatory macrophages were less pronounced (P1 9.86±4.50%, P2 4.97±1.50%, P4 66.92±46.89% and P3+P5 75.17±38.88% of wild-type mice; Figure 3H). Additionally, ATMs were reduced in all subpopulations in CCR2-/- mice compared to wildtype mice (Figure 3I). This inability to elevate pro-inflammatory intestinal macrophages and ATMs upon HFD went along with modestly improved glycemic control and increased insulin levels (Figure 3J, Figure S3H). Thus, the number of macrophages, in particular pro-inflammatory subpopulations, could be linked to glycemic control.

Colon-specific Macrophage Depletion Improves Glucose Metabolism

To determine whether there is a causal link between colonic macrophages and glucose homeostasis, we established a colon-specific macrophage ablation model by intrarectally

administrating clodronate or PBS liposomes in mice on HFD (Qualls et al., 2006). With intrarectal clodronate liposomes, we achieved colon-specific macrophage depletion as shown by reduced colonic macrophages, especially the pro-inflammatory subpopulation P1 and P2 (Figure 4A). In contrast, tissue macrophages were not reduced in adipose tissue, liver, pancreatic islets and brain (Figure 4B-C). Pro-inflammatory cytokines were not increased in colon tissue or plasma, excluding local or systemic inflammation due to intrarectal clodronate liposomes (Figure 4D, Figure S4A). Colon-specific depletion of macrophages improved fasting glycemia, glucose tolerance with enhanced insulin secretion, and insulin resistance, while body weights were comparable between the groups (Figures 4E,F). Glucose stimulated insulin secretion of isolated islets from clodronate-treated mice indicated improved β-cell function as shown by lower basal insulin and an enhanced stimulation index (Figure 4G). Mechanistically, improved β-cell function might be partially mediated through glucagon-like peptide-1 (GLP-1) as inhibition of GLP-1 activity with exendin (9-39) prior to glucose stimulation *in vivo* mitigated improved glycemia in macrophage-depleted mice (Figure 4H). In contrast, blocking the parasympathetic activity by atropine prior to glucose tolerance testing did not abolish improved glycemic control in macrophage-depleted mice (Figure S4B), suggesting that muscarinergic neuronal circuits did not mediate this phenotype. Of note, microbial dysbiosis could be ruled out as a possible cause for improved glycemic control since microbiota composition was not altered in mice treated with clodronate (Figure 4I, Figure S4C). Overall, our colon-specific macrophage depletion model demonstrated a causal link between the number of colonic macrophages and improved glycemic control/β-cell function, which might be partially mediated by GLP-1.

To differentiate colon-specific from systemic effects of macrophage depletion by clodronate liposomes, we injected clodronate or PBS liposomes intraperitoneally into mice fed a HFD. Intraperitoneal injections of clodronate liposomes systemically depleted macrophages as shown by reduced macrophages in the colon, adipose tissue, liver and peritoneal cavity, while

islet macrophages and microglia were not reduced (Figure 4J-L). Meanwhile, plasma IL-6 was elevated, potentially due to apoptosis of macrophages (Figure 4M). Systemic clodronate liposomes also improved glucose tolerance, which might be driven by increased insulin sensitivity as indicated by lower insulin levels and reduced adipose tissue inflammation (Figure 4N). Thus, colon-specific macrophage depletion with improved β-cell function was at least as effective as systemic macrophage ablation, which rather acted via an insulin-sensitizing mechanism.

Transcriptional Response upon HFD in Intestinal Macrophages Involves an Interferon-Signature and Metabolic Shift, potentially through mTOR-Signaling

To investigate the underlying mechanism of the intestinal innate immune response upon HFD, we performed single cell RNA-sequencing (scRNA-seq) of colonic macrophages in mice fed coconut-based HFD or chow diet. Hierarchical clustering analysis identified macrophage subpopulations P1-P5 as previously defined by flow cytometry, whereby subpopulations P2 and P5 comprised two related clusters (Figure 5A,C). This classification was consistent with *ab initio* annotation using ImmGen FACS-sorted bulk samples of pure cell types as a reference (Heng et al., 2008) (Figure S5A). Cell clusters positioned along a presumed differentiation trajectory (PC1) and an activation/inflammation axis (PC2) and showed little overlap between chow diet and HFD, which indicated a strong transcriptional response upon HFD (Figure S5B). Consistent with flow cytometry, there was a relative increase in pro-inflammatory and a decrease in anti-inflammatory/resident subpopulations upon HFD (Figure 5B). To compare the transcriptomes of intestinal macrophages between chow diet and HFD, we stratified the analysis into subpopulations (clusters) to correct for differential abundance across conditions. Based on the number of differentially expressed genes, HFD induced most pronounced effects in intestinal macrophage subpopulations P1 and P2 (Figure S5C). Genes up-regulated by HFD involved interferon signaling (*Irf7, Ifitm1, Ifi205, Isg15),* chemokines (*Cxcl9, Ccl5/8*),

guanylate-binding proteins *(Gbp2/5)*, and macrophage activation genes *(Ly6a/c2/i)* (Figure S5C, Figure S6). In addition, analysis of "regulons" (sets of regulatory transcription factors) revealed enhanced *Stat1/2*, *Irf1/8* and *Etv7* under HFD, the latter a component of the mTOR complex mTORC3 (Harwood et al., 2018) (Figure S5D). Gene set enrichment analysis (GSEA) using MSigDB hallmark pathways showed up-regulation of interferon gamma (IFN-γ) and alpha (IFN-α) response, oxidative phosphorylation, and allograft rejection in mice fed a HFD (Figure 5D, Figure S5E).

At the protein level, we confirmed up-regulated IFN-γ in intestinal macrophages of mice fed a HFD (Figure 5E). Also, measures of mitochondrial mass (MitoGreen), membrane potential (MitoRed), and abundance of reactive oxygen species (ROS; MitoSOX) were enhanced in all intestinal macrophage subpopulations of mice fed a HFD, verifying a metabolic shift towards an anabolic state (Figure 5F,G). As mTOR signaling is a common regulator of both interferon signaling and energy metabolism (Cao et al., 2008; Linke et al., 2017; Schmitz et al., 2008), we postulated that mTOR might govern the transcriptional changes in intestinal macrophages upon HFD. Indeed, we found enhanced mTOR activity as shown by increased phosphorylation of S6 (pS6) and Akt (pS473) in all macrophage subpopulations of mice fed a HFD (Figure 5H). Hence, enhanced mTOR signaling could mediate the transcriptional response in macrophages under HFD, involving an interferon signature and metabolic shift towards an anabolic state.

Colonic-Specific mTOR Inhibition Restores Glycemic Control

Next, we assessed whether enhanced mTOR signaling in the gut contributes to HFD-related glucose intolerance. Therefore, we intrarectally administered the mTOR inhibitor rapamycin to mice on HFD and assessed the effect on glucose metabolism *in vivo*. Upon intrarectal rapamycin treatment, pS6 and pS473 decreased in all intestinal macrophage subpopulations (Figure 6A,B), while mTOR activity in ATMs remained largely unaltered (Figure 6D). In

addition, colon-specific mTOR inhibition reduced the superoxide (ROS) indicator MitoSOX in all intestinal macrophages, suggestive for decreased metabolic activity (Figure 6C). Next, we assessed whether colonic mTOR activity is also linked to glucose homeostasis upon HFD. Hereby, we found that intrarectal rapamycin administration led to significantly increased insulin levels, potentially via increased levels of the insulin secretagogue GLP-1 (Figure 6E-F). This was accompanied by lower basal insulin and an increased stimulation index in islets *ex vivo* (Figure 6G), which pointed towards improved β-cell function similar to the colon-specific macrophage depletion model.

In contrast, systemic rapamycin by intraperitoneal injections reduced pS6 and pS473 not only in colonic macrophages, but also in splenic monocytes and ATM subpopulations (Figure 6H-K). Concerning glucose metabolism, systemic rapamycin administration led to impaired glucose tolerance and insulin resistance in mice fed a HFD, as previously reported (Figure 6L,M; (Lamming et al., 2012)). Further, systemic mTOR inhibition was associated with reduced M2 ATMs (not shown). These findings showed that colon-specific inhibition of mTOR restored HFD-induced β-cell dysfunction, while systemic mTOR inhibition induced insulin resistance.

Pro-inflammatory Intestinal Macrophages are also Increased in Human Obese Subjects

To translate our findings to human disease, we characterized intestinal macrophages from colon biopsies of obese (BMI >32 kg/m^2) and lean individuals (BMI <27 kg/m^2). First, we analyzed the human equivalents of intestinal macrophage subpopulations P1-P5 by flow cytometry (Bain et al., 2013) (Figure 7A). Consistent with our findings in mice, we found increased colonic CD14^{high} pro-inflammatory macrophage subpopulation P2 in obese subjects (Figure 7B,C). In addition, pro-inflammatory subpopulations P1 and P2 were also increased in the stomach and duodenum (Figure S7A-C).

Since intestinal macrophages originate from circulating blood monocytes (Bujko et al., 2018), we further assessed monocytes and their subsets in lean and obese subjects. We noted elevated $CD64^{+}CD33^{+}CD14^{+}$ monocytes in obese subjects (Figure 7D). Monocytes were further distinguished based on the differential expression of CD14 and CD16 ($CD14^{++}CD16^{-}$ classical, $CD14^{++}CD16^{+}$ intermediate, and $CD14^{+}CD16^{++}$ non-classical monocytes) (Ziegler-Heitbrock et al., 2010). We found increased intermediate monocytes in obese subjects. Most of these increased $CD14^{++}$ monocytes were HLA-DR+$CD163^{-}$, which corresponds to a pro-inflammatory phenotype similar to macrophage subpopulation P2. Together, these data established a link between human obesity and increased levels of pro-inflammatory intestinal macrophages, most likely via recruitment of $CD14^{++}$ blood monocytes.

DISCUSSION

Our results revealed a direct cross-talk between nutritional cues, intestinal macrophage subpopulations, and insulin-producing β-cells. Pro-inflammatory intestinal macrophage subpopulations transiently increased with food intake and became chronically elevated upon HFD. The acute response of intestinal macrophages upon food intake could potentially constitute a physiological response as postprandial macrophage-derived IL-1β stimulates insulin secretion (Dror et al., 2017). It seems that this innate immune activation in the gut overshoots with excessive fat intake. Interestingly, animal- (lard) as opposed to plant-derived (coconut) fat led to a heightened innate immune response and was associated with worsened glycemic control. We did not identify a characteristic pattern of gut microbiota composition that correlates with HFD-induced glucose intolerance, but rather unspecific dysbiosis. However, monocyte recruitment into the gut wall and hence differentiation into intestinal macrophages seems to depend on the presence of gut microbiota as germ-free mice lacked an inflammatory shift in intestinal macrophages. This suggests that the number of macrophages is directly linked with glycemic control. Indeed, dose-dependent pharmacological macrophage depletion gradually improved glucose tolerance in mice on HFD. Moreover, CCR2-/- mice, which predominantly lack pro-inflammatory macrophage subpopulations, also had improved glucose metabolism. Hence, the number of macrophages, in particular pro-inflammatory subpopulations, seem to be linked to glycemic control.

To substantiate the causal link between intestinal macrophages and glycemic control, we colon-specifically depleted macrophages by intrarectal administrations of clodronate liposomes, which resulted in improved glucose homeostasis. Currently, the vast majority of *in vivo* macrophage ablation models only achieve systemic depletion. While systemic macrophage depletion was mainly driven by improved insulin sensitivity, our colon-specific approach corroborated an islet cell phenotype, establishing a crosstalk between colonic macrophages and β-cells.

To understand the mechanism of intestinal inflammation upon HFD and potentially identify therapeutic targets, we performed single-cell RNA-seq of colonic macrophages. We found an interferon signature and metabolic shift towards oxidative phosphorylation upon HFD, which converge in mTOR signaling as a potential common regulatory pathway (Cao et al., 2008; Schmitz et al., 2008). Thus, we postulated that mTOR might govern the observed HFD-driven transcriptional response in macrophages. We found that mTOR activity was indeed enhanced in all intestinal macrophage subpopulations in mice fed HFD. In line with our results, mTOR activation has been described to occur in response to nutrients, and is exaggerated in a nutrient-overabundant state such as obesity (Um et al., 2004; Zoncu et al., 2011). While systemic mTOR inhibition was associated with insulin resistance as previously shown (Lamming et al., 2012), our data suggest that blocking mTOR specifically in the colon could have beneficial metabolic effects. A previous study indicated that inhibition of mTOR in the upper small intestine by intraluminal instillations improves glucose homeostasis by lowering glucose production (Waise et al., 2019). Our approach with intrarectal administrations of rapamycin has the advantage that it is non-invasive and potentially transferrable to humans. Moreover, colonic macrophages were identified as site of action of rapamycin as mTOR activity was down-regulated in all subpopulations. Similar to our colon-specific macrophage depletion model, local mTOR inhibition resulted in improved β-cell function. Our data thus emphasize the need for tissue- or even cell-specific targets and identified mTOR activation in colonic macrophages as potential treatment target in HFD-induced glucose intolerance. Administrations of mTOR inhibitors in form of suppositories to colon-specifically block mTOR signaling might serve as a promising strategy.

Our findings are of high clinical significance as obese human subjects also exhibited increased pro-inflammatory intestinal macrophages. So far, an increase of pro-inflammatory intestinal macrophages has only been documented in inflammatory bowel disease (Bain et al., 2013; Ogino et al., 2013). The validation of our preclinical data in human obesity is noteworthy

as usually there is considerable heterogeneity among human subjects through different lifestyle modalities. Monocytes as the known precursors of human intestinal macrophages (Bujko et al., 2018) could potentially serve as biomarkers for increased inflammatory macrophages in the gut. We observed a higher $CD14^{++}CD16^{+}$ intermediate monocyte subpopulation, which is characterized by a pro-inflammatory phenotype (Rossol et al., 2012) and known to correlate with adiposity and cardiovascular risk (Poitou et al., 2011; Rogacev et al., 2012). In addition, $CD64^{+}$ expression on monocytes is associated with the production of type I interferons (Li et al., 2010). Thus, monocytes could be activated by dietary intake (Jordan et al., 2019) and later replenish intestinal macrophages, which ultimately leads to altered gut immunity.

One question remains: How do intestinal macrophages communicate with β-cells? We found that improved β-cell function might occur partially through enhanced glucagon-like peptide-1 (GLP-1) secretion. However, other pathways could also link intestinal macrophages with β-cell function. Intestinal macrophages could directly traffic from the gut to pancreatic islets as a higher migratory potential has been suggested for monocyte-derived $CXCR1^{inter}$ macrophages of the gut (Koscso et al., 2020). Alternatively, cytokines from pro-inflammatory macrophages could disseminate to the pancreas through blood circulation, lymphatic vessels, or even neuronal circuits. One mediator of the neural circuits, the muscarinergic signaling, was ruled out as atropine did not alter improved glycemic control in our macrophage depletion model.

Overall, we identified a causal link between nutritional cues, colonic macrophage subpopulations and glucose homeostasis. Intestinal inflammation upon HFD involved an interferon signature and metabolic shift in intestinal macrophages, potentially via mTOR activation. By colon-specific depletion of macrophages or mTOR inhibition, we demonstrated that modulation of colonic macrophage numbers or activation is directly linked to glycemic control. Targeting colonic macrophages might thus represent a potential therapeutic approach for treating β-cell dysfunction in metabolic disease.

STAR ★ METHODS

Detailed methods are provided in the online version of this paper and include the following:

SUPPLEMENTAL INFORMATION

Supplemental information includes 7 figures and 3 tables and can be found within this article online at….

ACKNOWLEDGMENTS

We thank Marianne Böni-Schnetzler and Marc Donath for their constant support by sharing their laboratory space and expertise; Marc Stawiski, Neena Parayil, Lena Keller, Friederike Schulze, Erez Dror, Anna Steinert and Katarina Radulovic for technical contributions and Romano Schneider for constructive feedback. Danny Labes for his flow cytometry expertise; Sandrine Henri and Anna Baranska for sharing their expertise and isolation protocol in murine intestinal macrophages; Elizabeth Mc Donald in human intestinal macrophages and the members of the Donath, Hess, Recher, Berger and Mehling laboratories at the Department of Biomedicine of the University Hospital of Basel for advice and feedback.

This study was supported by grants from the Swiss National Science Foundation (PZ00P3_161135), the Goldschmidt-Jacobson Foundation, the Jubiläumsstiftung Swiss Life, the Olga Mayenfisch Foundation, the Foundation Basler Diabetesgesellschaft (to CCW), the Nikolaus and Bertha Burckhardt-Bürgin-Stiftung and from the Research Fund for Excellent Junior Researchers of the University of Basel (to TR).

AUTHOR CONTRIBUTIONS

Experimental design: T.R., D.M., C.C.W.. Experimental execution: T.R., S.A.A., A.B., Z.B., S.J.W., D.M., J.W., L.R., C.M., S.G., C.C.W.. Data analyses: T.R., S.A.A., J.R., C.C.W. Figure preparation, manuscript writing: T.R., C.C.W. Editing: T.R., S.J.W., D.M., J.R., E.D., Z.B., S.A.A., S.G., C. M., A.B., J.W., C.C.W.. C.C.W. is the guarantor of this work.

DECLERAION OF INTEREST

The authors declare no conflict of interest.

Figure Titles and Legends

Figure 1

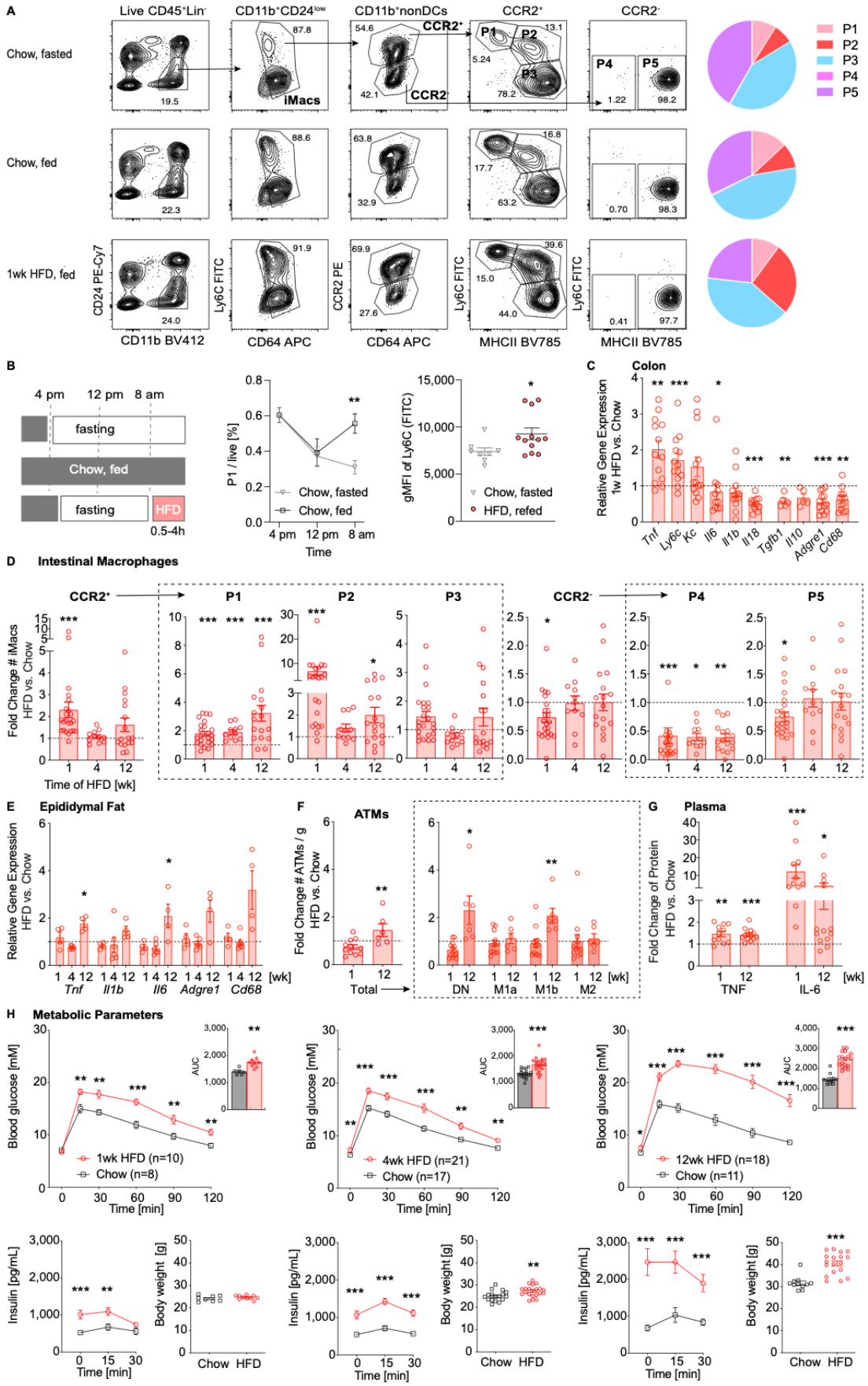

Figure 1. Pro-inflammatory Intestinal Macrophage Subpopulations are Transiently Increased upon Food Intake and Chronically Elevated Following High-Fat Diet Feeding

(**A**) Representative flow cytometry plots and distribution of intestinal macrophage (iMac) subpopulations P1-P5 in wild-type mice (fasted, fed chow diet or coconut-based HFD for 1 week).

(**B**) Experimental design (left); percentage of iMac subpopulation P1 in fasted or fed mice on chow (middle); geometrical mean fluorescent intensity (gMFI) of Ly6C in iMac subpopulation P1 in fasted or HFD refed mice (right).

(**C**) Gene expression in colon of mice fed 1 week of HFD relative to chow fed controls.

(**D**) Fold change of absolute numbers (#) of iMacs ($CCR2^+$ (pro-inflammatory P1, P2, intermediate P3) and $CCR2^-$ (anti-inflammatory/resident P4, P5) subpopulations) in mice fed HFD or chow.

(**E**) Gene expression in adipose tissue of mice fed HFD relative to chow fed controls.

(**F**) Fold change of adipose tissue macrophages per g (ATMs/g) and their subpopulations (double-negative DN, M1a, M1b, M2) in mice fed a HFD compared to controls.

(**G**) Fold change of plasma TNF and IL-6 in mice fed HFD compared to controls.

(**H**) Intraperitoneal Glucose tolerance test (IPGTT), area under the curve (AUC), insulin and body weight in mice fed HFD or chow (n=8-21).

Statistical data are expressed as mean±SEM. Data are representative of 2-6 independent experiments (A-D/F/G) or one experiment (E), each data point representing an individual mouse. *p<0.05, **p<0.01, ***p<0.001, unpaired Mann-Whitney U test with two tailed distribution. See also Figure S1.

Figure 2

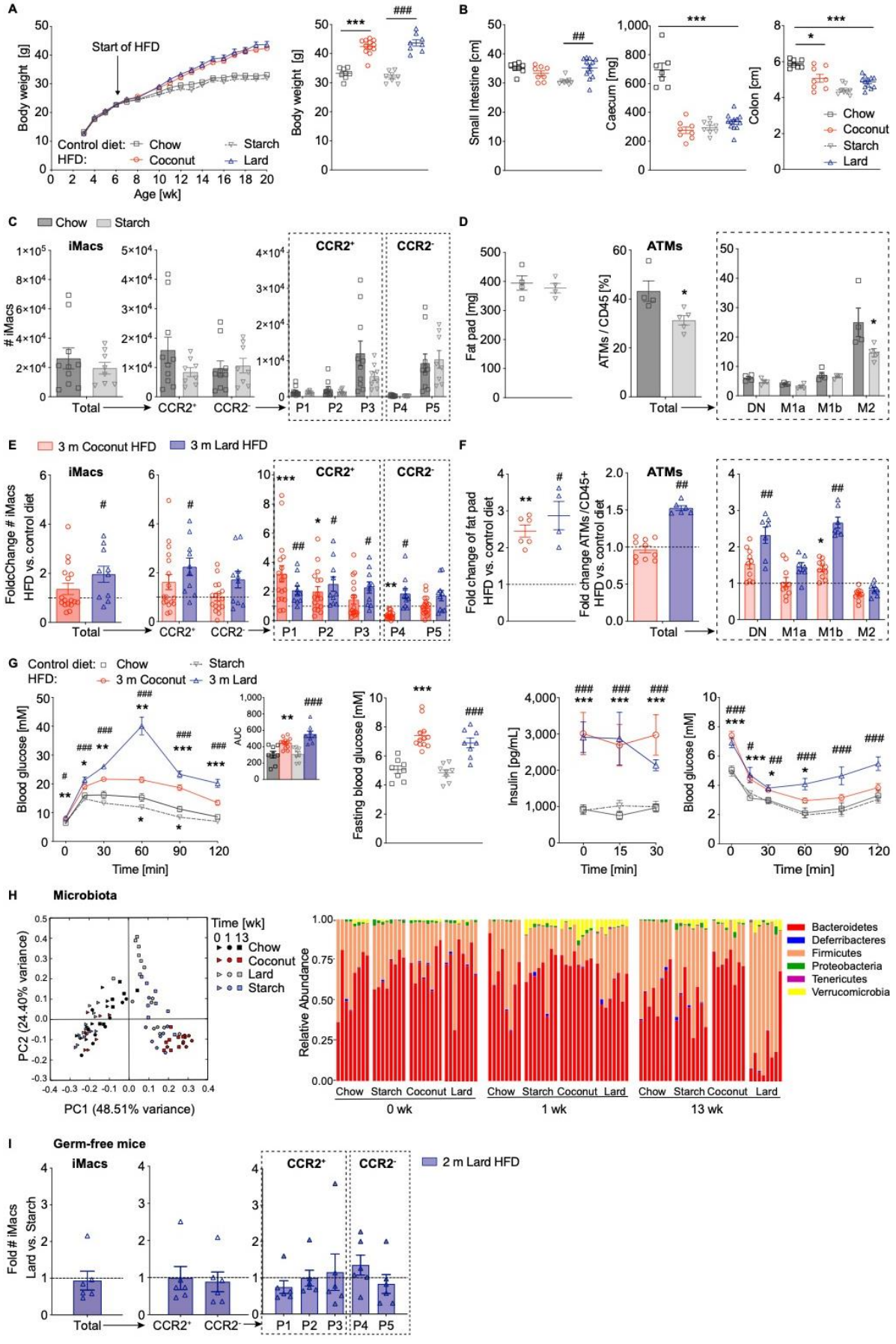
A
Start of HFD
Body weight [g]
Age [wk]
Control diet: Chow Starch
HFD: Coconut Lard
B
Small Intestine [cm]
Caecum [mg]
Colon [cm]
Chow
Coconut
Starch
Lard
C
Chow Starch
iMacs
iMacs
Total
CCR2+
CCR2-
P1 P2 P3 P4 P5
D
Fat pad [mg]
ATMs
ATMs / CD45 [%]
DN M1a M1b M2
E
3 m Coconut HFD
3 m Lard HFD
FoldcChange # iMacs HFD vs. control diet
F
Fold change of fat pad HFD vs. control diet
Fold change ATMs /CD45+ HFD vs. control diet
G
Control diet: Chow Starch
HFD: 3 m Coconut 3 m Lard
Blood glucose [mM]
Time [min]
AUC
Fasting blood glucose [mM]
Insulin [pg/mL]
H
Microbiota
Time [wk]
0 1 13
Chow
Coconut
Lard
Starch
PC2 (24.40% variance)
PC1 (48.51% variance)
Relative Abundance
Bacteroidetes
Deferribacteres
Firmicutes
Proteobacteria
Tenericutes
Verrucomicrobia
0 wk
1 wk
13 wk
I
Germ-free mice
2 m Lard HFD
Fold # iMacs Lard vs. Starch

Figure 2. Gut Microbiota are Essential for the Increase of Pro-inflammatory Intestinal Macrophage Subpopulations upon HFD, while the Fat Source Modulates its Magnitude

(**A-B**) Body weights (**A**) and small intestine, caecum and colon size (**B**) of wild-type mice after 3 months coconut- (red) or lard-based HFD (blue); chow (black) or starch control diet (grey) (n=8-12).

(**C-D**) Absolute numbers (#) of total, $CCR2^{+}/CCR2^{-}$ intestinal macrophages (iMacs) and subpopulations P1-P5 (**C**), fat pad weights and frequency of adipose tissue macrophages (ATMs) and their subpopulations (DN, M1a, M1b, M2) (**D**) in mice fed chow (black) or starch (grey) control diet.

(**E-F**) Fold change of iMacs (total, $CCR2^{+}/CCR2^{-}$ and P1-P5 subpopulations) (**E**), fat pad weights and ATMs (total and DN, M1a, M1b, M2 subpopulations) (**F**) after 3 months of coconut (red) or lard-based (blue) HFDs compared to respective control diets.

(**G**) IPGTT, AUC, fasting blood glucose, insulin and insulin tolerance test (ITT) in mice fed 3 months HFD or control diet (n=8-12).

(**H**) Principal component analysis (PCA; left) and relative phyla abundances (right) of fecal microbiota of mice before and after 1 week and 3 months of HFD compared to controls.

(**I**) Fold change of iMacs in germ-free mice fed lard-based HFD for 2 months compared to starch-fed controls.

Statistical data are expressed as mean±SEM. Data are representative of two independent experiments (C/E/I) or of one experiment (A/B/D/F/G/H). A/E-G: Coconut-based HFD vs. chow: *p<0.05, **p<0.01, ***p<0.001. Lard-based HFD vs. starch: $^{\#}p<0.05$, $^{\#\#}p<0.01$, $^{\#\#\#}p<0.001$, unpaired Mann-Whitney U test with two tailed distribution. See also Figure S2 and Table S1 for diet details.

Figure 3

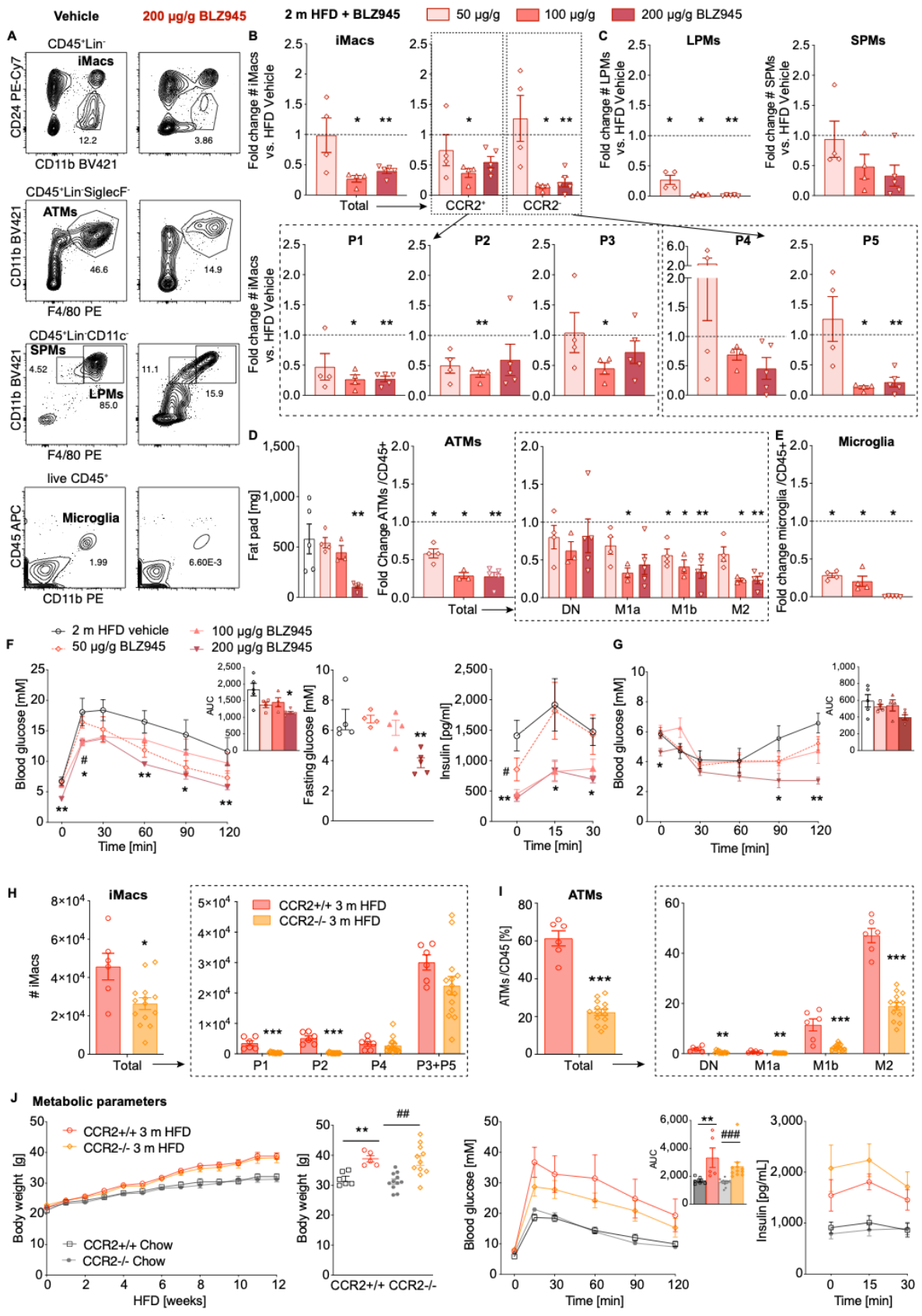
Vehicle
200 µg/g BLZ945
2 m HFD + BLZ945
50 µg/g
100 µg/g
200 µg/g BLZ945
A
CD45+Lin-
iMacs
CD24 PE-Cy7
CD11b BV421
12.2
3.86
CD45+Lin-SiglecF-
ATMs
CD11b BV421
F4/80 PE
46.6
14.9
CD45+Lin-CD11c-
SPMs
LPMs
4.52
85.0
11.1
15.9
live CD45+
Microglia
CD45 APC
CD11b PE
1.99
6.60E-3
B
iMacs
Fold change # iMacs vs. HFD Vehicle
Total
CCR2+
CCR2-
P1
P2
P3
P4
P5
C
LPMs
SPMs
Fold change # LPMs vs. HFD Vehicle
Fold change # SPMs vs. HFD Vehicle
D
Fat pad [mg]
ATMs
Fold Change ATMs /CD45+
DN
M1a
M1b
M2
E
Microglia
Fold change microglia /CD45+
F
2 m HFD vehicle
50 µg/g BLZ945
100 µg/g BLZ945
200 µg/g BLZ945
Blood glucose [mM]
Time [min]
AUC
Fasting glucose [mM]
Insulin [pg/ml]
G
Blood glucose [mM]
Time [min]
AUC
H
iMacs
iMacs
Total
CCR2+/+ 3 m HFD
CCR2-/- 3 m HFD
P1
P2
P4
P3+P5
I
ATMs
ATMs /CD45 [%]
Total
DN
M1a
M1b
M2
J
Metabolic parameters
CCR2+/+ 3 m HFD
CCR2-/- 3 m HFD
CCR2+/+ Chow
CCR2-/- Chow
Body weight [g]
HFD [weeks]
CCR2+/+ CCR2-/-
Blood glucose [mM]
Time [min]
AUC
Insulin [pg/mL]
Time [min]

Figure 3. Macrophage Numbers are Linked to Glycemic Control

(**A**) Representative flow cytometry plots of intestinal macrophages (iMacs), adipose tissue macrophages (ATMs), peritoneal macrophages (small: SPM/ large: LPM) and microglia.

(**B-E**) Fold change of iMacs and their subpopulations P1-P5 (**B**), SPMs and LPMs (**C**), fat pad weights and fold change of ATMs and their subpopulations (DN, M1a, M1b, M2) (**D**) and microglia (**E**) of wild-type mice fed 2 months coconut-based HFD and treated with the CSF1R inhibitor BLZ945 (50, 100, 200 μg/g/d) or vehicle.

(**F-G**) IPGTT, AUC, fasting blood glucose, insulin and ITT of mice after 2 months HFD and BLZ945 treatment (n=4-5).

(**H-I**) Absolute numbers of iMacs and their subpopulations P1-P5 (**H**) and ATMs and their subpopulations (DN, M1a, M1b, M2) (**I**) of CCR2-/- (orange) or CCR2+/+ (red) mice fed 3 months coconut-based HFD.

(**J**) Body weight, IPGTT, AUC and insulin of CCR2-/- or CCR2+/+ mice fed 3 months HFD or chow. (n=5-11).

Statistical data are expressed as mean±SEM. Data are representative of one (A-G) and two independent experiments (H-J), with each data point representing an individual mouse.

*p<0.05, **p<0.01, ***p<0.001, unpaired Mann-Whitney U test with two tailed distribution.

See also Figure S3.

Figure 4

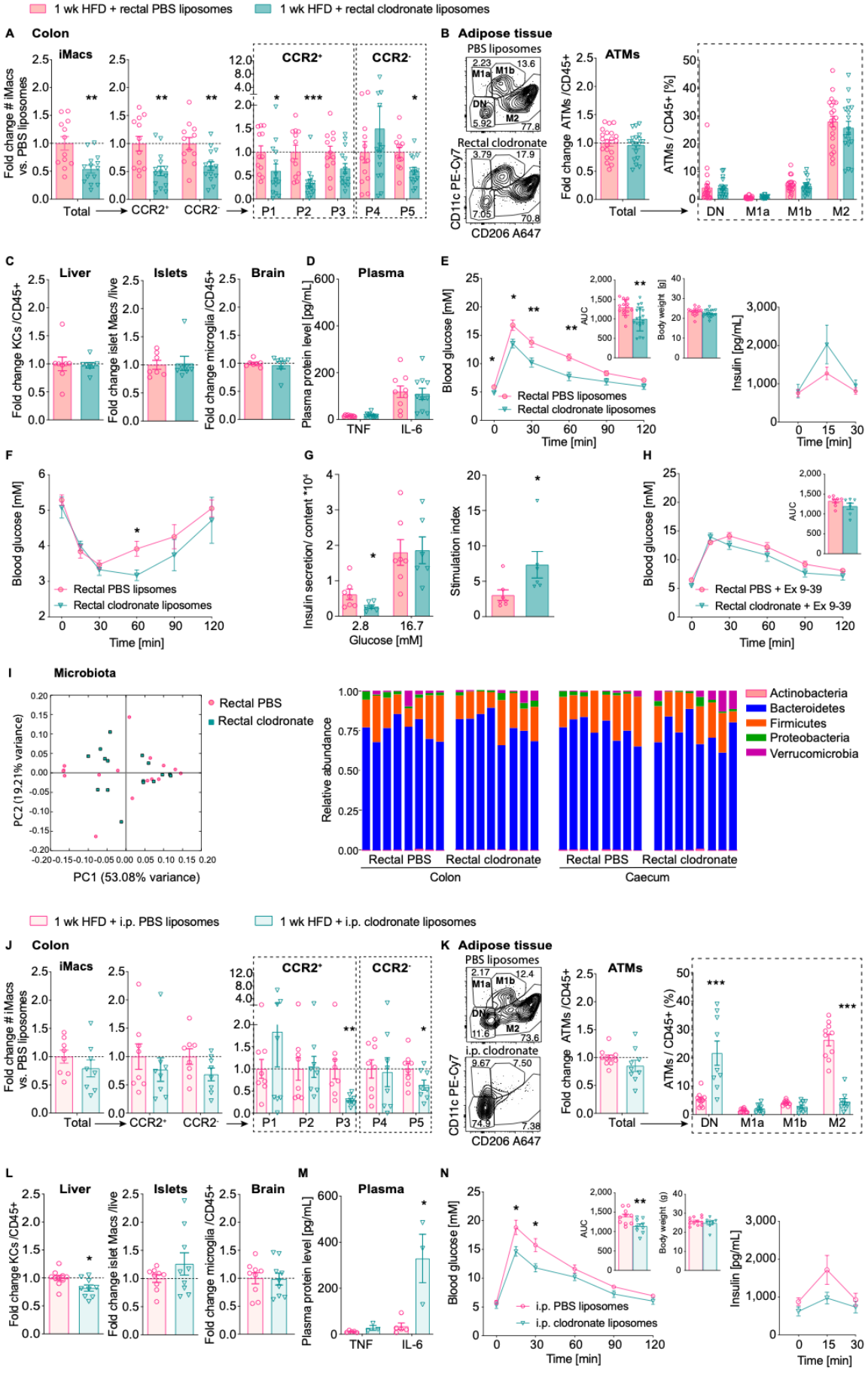
1 wk HFD + rectal PBS liposomes
1 wk HFD + rectal clodronate liposomes
A Colon
iMacs
Fold change # iMacs vs. PBS liposomes
Total
CCR2+
CCR2-
P1
P2
P3
P4
P5
B Adipose tissue
PBS liposomes
Rectal clodronate
CD11c PE-Cy7
CD206 A647
M1a
M1b
M2
DN
ATMs
Fold change ATMs /CD45+
ATMs / CD45+ [%]
C
Liver
Fold change KCs /CD45+
Islets
Fold change islet Macs /live
Brain
Fold change microglia /CD45+
D
Plasma
Plasma protein level [pg/mL]
TNF
IL-6
E
Blood glucose [mM]
Rectal PBS liposomes
Rectal clodronate liposomes
Time [min]
AUC
Body weight [g]
Insulin [pg/mL]
F
Blood glucose [mM]
Rectal PBS lipsomes
Rectal clodronate liposomes
Time [min]
G
Insulin secretion/ content *10⁴
Glucose [mM]
Stimulation index
H
Blood glucose [mM]
Rectal PBS + Ex 9-39
Rectal clodronate + Ex 9-39
Time [min]
AUC
I
Microbiota
Rectal PBS
Rectal clodronate
PC2 (19.21% variance)
PC1 (53.08% variance)
Relative abundance
Actinobacteria
Bacteroidetes
Firmicutes
Proteobacteria
Verrucomicrobia
Colon
Caecum
1 wk HFD + i.p. PBS liposomes
1 wk HFD + i.p. clodronate liposomes
J Colon
K Adipose tissue
i.p. clodronate
L
M
N
i.p. PBS liposomes
i.p. clodronate liposomes

Figure 4. Colon-specific Macrophage Depletion Improves Glucose Metabolism

Wild-type mice fed 1 week with coconut-based HFD and intrarectally treated with clodronate (turquoise) or PBS liposomes (pink) (**A-I**; colon-specific depletion) or intraperitoneally (**J-N**; i.p. systemic depletion):

(**A**/**J**) Fold change of total, $CCR2^{+}$/$CCR2^{-}$ intestinal macrophages (iMacs) and subpopulations P1-P5 in the proximal colon.

(**B**/**K**) Representative flow cytometry plots and fold change of adipose tissue macrophages (ATMs) and their subpopulations (DN, M1a, M1b, M2).

(**C**/**L**) Fold change of Kupffer cells (KCs), islet macrophages and microglia.

(**D**/**M**) Plasma TNF and IL-6.

(**E**/**N**) IPGTT, AUC, body weight and insulin (n=9-18).

(**F**) ITT of mice intrarectally treated with clodronate or PBS liposomes (n=5-9).

(**G**) Basal and glucose stimulated insulin secretion normalized to protein content in islets isolated from mice intrarectally treated with clodronate or PBS liposomes.

(**H**) Oral GTT (OGTT) and AUC after GLP-1 inhibition by Exendin (9-39) injection 30 min before glucose bolus in mice intrarectally treated with clodronate or PBS liposomes (n=7-8).

(**I**) Principal component analysis (PCA; left) and relative phyla abundances (right) of fecal microbiota in HFD mice intrarectally treated with clodronate or PBS liposomes.

Statistical data are expressed as mean±SEM. Data are representative of three (A/B/D), five (E), two (C/I-L/N) independent experiments and one (F-H/M) experiment. *p<0.05, **p<0.01, ***p<0.001, unpaired Mann-Whitney U test with two tailed distribution. Also see Figures S4.

Figure 5

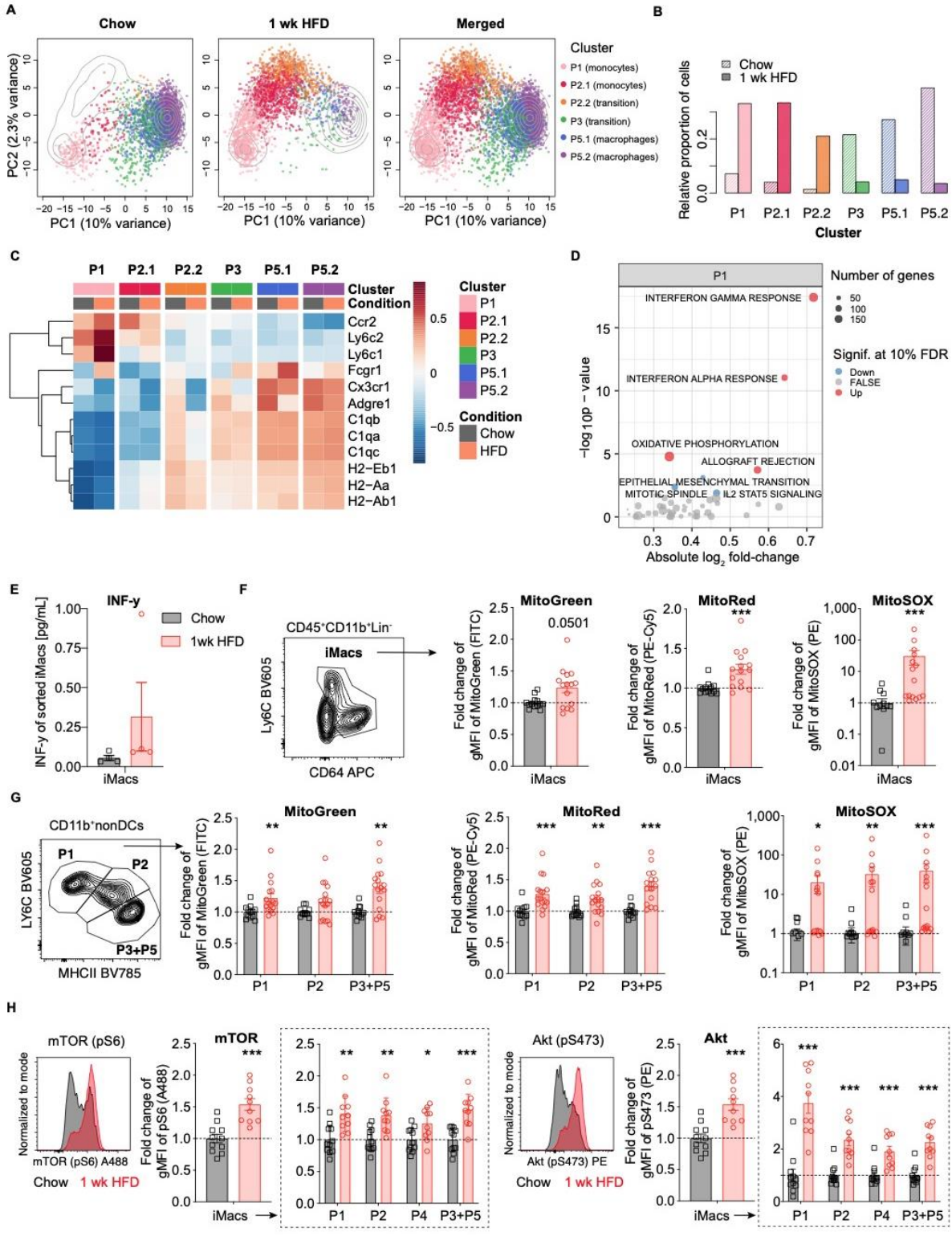
A
Chow
1 wk HFD
Merged
PC2 (2.3% variance)
PC1 (10% variance)
Cluster
P1 (monocytes)
P2.1 (monocytes)
P2.2 (transition)
P3 (transition)
P5.1 (macrophages)
P5.2 (macrophages)
B
Chow
1 wk HFD
Relative proportion of cells
P1 P2.1 P2.2 P3 P5.1 P5.2
Cluster
C
P1 P2.1 P2.2 P3 P5.1 P5.2
Cluster
Condition
Ccr2
Ly6c2
Ly6c1
Fcgr1
Cx3cr1
Adgre1
C1qb
C1qa
C1qc
H2−Eb1
H2−Aa
H2−Ab1
Cluster
P1
P2.1
P2.2
P3
P5.1
P5.2
Condition
Chow
HFD
D
P1
Number of genes
50
100
150
Signif. at 10% FDR
Down
FALSE
Up
INTERFERON GAMMA RESPONSE
INTERFERON ALPHA RESPONSE
OXIDATIVE PHOSPHORYLATION
ALLOGRAFT REJECTION
EPITHELIAL MESENCHYMAL TRANSITION
MITOTIC SPINDLE
IL2 STAT5 SIGNALING
−log10p − value
Absolute log2 fold-change
E
INF-γ
Chow
1wk HFD
INF-γ of sorted iMacs [pg/mL]
iMacs
F
CD45+CD11b+Lin−
iMacs
Ly6C BV605
CD64 APC
MitoGreen
0.0501
MitoRed
MitoSOX
Fold change of gMFI of MitoGreen (FITC)
Fold change of gMFI of MitoRed (PE-Cy5)
Fold change of gMFI of MitoSOX (PE)
G
CD11b+nonDCs
P1
P2
P3+P5
LY6C BV605
MHCII BV785
MitoGreen
MitoRed
MitoSOX
P1 P2 P3+P5
H
mTOR (pS6)
Normalized to mode
mTOR (pS6) A488
Chow 1 wk HFD
mTOR
Fold change of gMFI of pS6 (A488)
iMacs
P1 P2 P4 P3+P5
Akt (pS473)
Akt (pS473) PE
Akt
Fold change of gMFI of pS473 (PE)

Figure 5. Transcriptional Response upon HFD in Intestinal Macrophages Involves an Interferon-Signature and Metabolic Shift, potentially through mTOR-Signaling

(**A-B**) Principal component analysis (PCA) (**A**) and relative proportion of intestinal macrophages (iMacs) (**B**) in wild-type mice fed chow or 1 week coconut-based HFD (mean of two replicates). Colors represent different clusters of iMacs (P1-5).

(**C**) Average gene expression of specific marker genes in iMacs across clusters in mice fed chow or 1 week of HFD.

(**D**) Up- (red) or down-regulated (blue) Molecular Signatures Database (MSigDB) hallmark pathways after 1 week of HFD compared to chow for cluster P1 (FDR<=0.1).

(**E**) IFN-γ protein expression of iMacs in mice fed 1 week of HFD (red) compared to chow fed controls (black).

(**F-G**) Mitochondrial activity indicated by fold change of gMFI of MitoGreen (mitochondrial mass), MitoRed (mitochondrial potential) and MitoSOX (reactive oxygen status) in iMacs (**F**) and subpopulations P1-P5 (**G**) after 1 week of HFD compared to controls .

(H) Fold change of the gMFI of mTOR (pS6) and Akt (pS475) in iMacs and P1-P5 subpopulations after 1 week HFD compared to controls .

Statistical data are expressed as mean±SEM. Data are representative of one (A-E) and two (F-H) experiments, with each data point representing one cell (A) or one individual mouse (E-H). *p<0.05, **p<0.01, ***p<0.001, unpaired Mann-Whitney U test with two tailed distribution. Also see Figures S5 and S6.

Figure 6

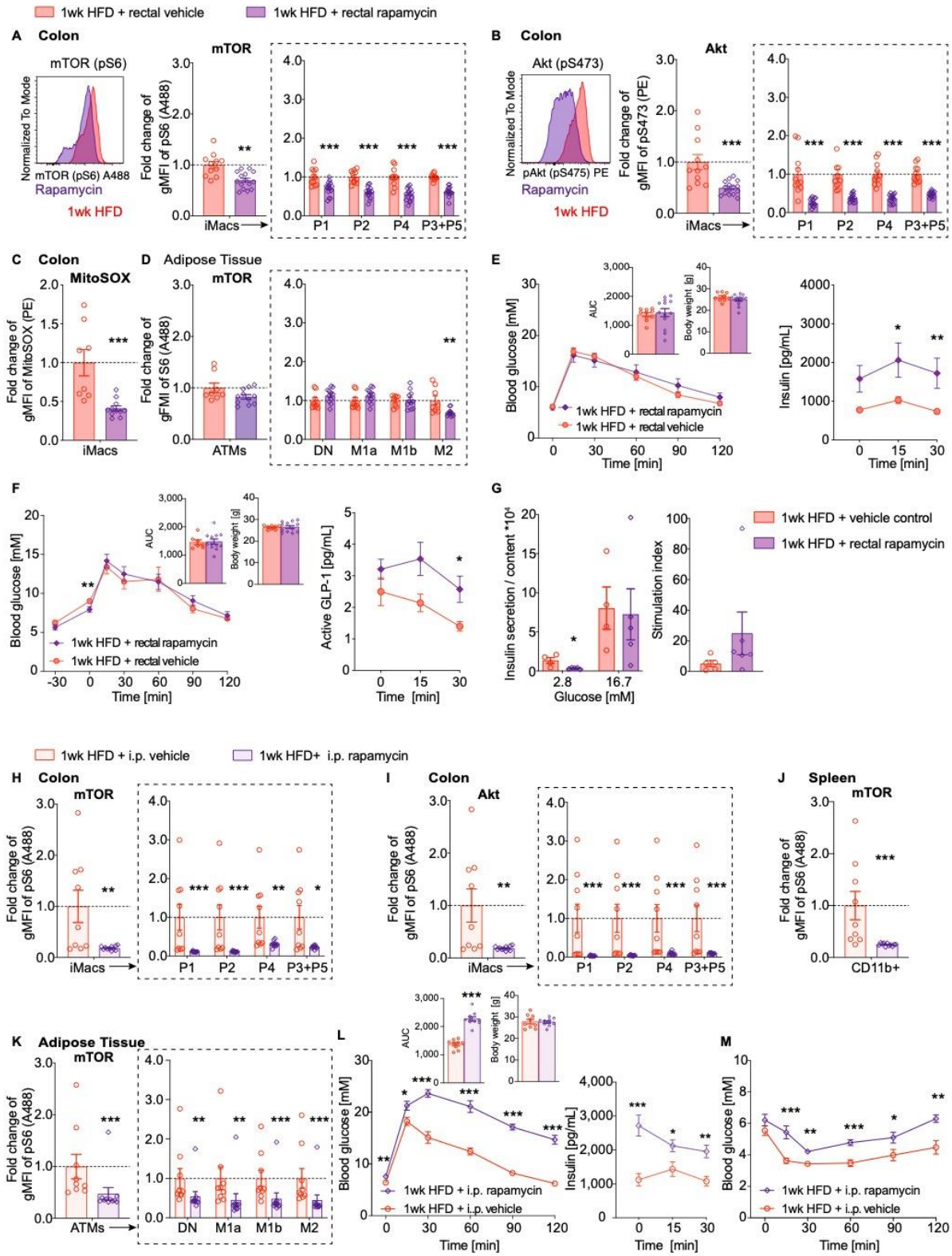
1wk HFD + rectal vehicle
1wk HFD + rectal rapamycin
A Colon
mTOR (pS6)
Normalized To Mode
mTOR (pS6) A488
Rapamycin
1wk HFD
mTOR
Fold change of gMFI of pS6 (A488)
iMacs
P1
P2
P4
P3+P5
B Colon
Akt (pS473)
pAkt (pS475) PE
Akt
Fold change of gMFI of pS473 (PE)
C Colon
MitoSOX
Fold change of gMFI of MitoSOX (PE)
D Adipose Tissue
ATMs
DN
M1a
M1b
M2
Fold change of gFMI of S6 (A488)
E
Blood glucose [mM]
Time [min]
AUC
Body weight [g]
Insulin [pg/mL]
F
Active GLP-1 [pg/mL]
G
Insulin secretion / content *10⁴
Glucose [mM]
Stimulation index
1wk HFD + vehicle control
1wk HFD + i.p. vehicle
1wk HFD+ i.p. rapamycin
H Colon
I Colon
J Spleen
CD11b+
K Adipose Tissue
L
M

Figure 6. Colonic-Specific Inhibition of mTOR Signaling Restores Glycemic Control

Wild-type mice were fed 1 week of coconut-based HFD and intrarectally treated with 3mg/kg rapamycin (purple) or vehicle (red) either intrarectally (**A-G**; colon-specific mTOR inhibition) or intraperitoneally (**H-M**, systemic mTOR inhibition):

(**A-B and H-I**) Fold change of gMFI of phosphorylated S6 (pS6) (**A/H**) and Akt (pS473) (**B/I**) in intestinal macrophages (iMacs) and their subpopulations P1-P5 of mice fed HFD and treated with rapamycin or vehicle.

(C) Fold change of MitoSOX in iMacs isolated from HFD mice intrarectally treated with rapamycin or vehicle.

(**D and J-K**) Fold change of gMFI of pS6 in adipose tissue macrophages (ATMs) and their subpopulations (DN, M1a, M1b, M2) (**D/K**) and splenic monocytes (**J**) in mice fed HFD and treated with rapamycin or vehicle.

(**E/L**) IPGTT, AUC, body weight and insulin in mice fed HFD and treated with rapamycin or vehicle (n=9-13).

(**F**) OGTT, AUC and active GLP-1 (stabilization of GLP-1 by sitagliptin injection 30 min before glucose bolus) in mice fed HFD and intrarectally treated with rapamycin or vehicle (n=7-12).

(**G**) Basal and glucose stimulated insulin secretion normalized to protein content in mice fed HFD and intrarectally treated with rapamycin or vehicle.

(**M**) ITT in mice fed HFD and intraperitoneally treated with rapamycin or vehicle (n=9).

Statistical data are expressed as mean±SEM. Data are representative of two (A/B/D/E) independent experiments and one (C/F-M) experiment. *p<0.05, **p<0.01, ***p<0.001, unpaired Mann-Whitney U test with two tailed distribution.

Figure 7

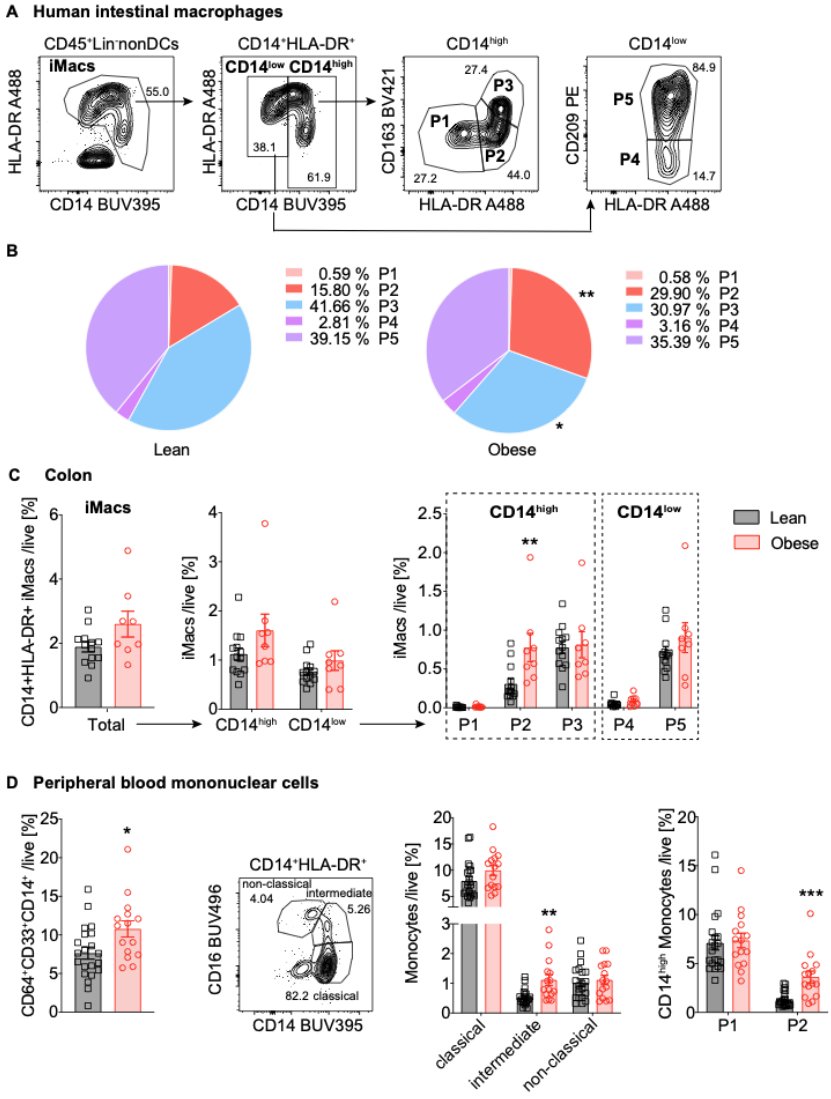
A Human intestinal macrophages
CD45+Lin-nonDCs
iMacs
55.0
HLA-DR A488
CD14 BUV395
CD14+HLA-DR+
CD14low CD14high
38.1
61.9
CD14high
CD163 BV421
27.4
P3
P1
P2
27.2
44.0
HLA-DR A488
CD14low
CD209 PE
84.9
P5
P4
14.7
HLA-DR A488
B
0.59 % P1
15.80 % P2
41.66 % P3
2.81 % P4
39.15 % P5
Lean
**
*
0.58 % P1
29.90 % P2
30.97 % P3
3.16 % P4
35.39 % P5
Obese
C Colon
iMacs
CD14+HLA-DR+ iMacs /live [%]
Total
iMacs /live [%]
CD14high
CD14low
CD14high
CD14low
**
P1
P2
P3
P4
P5
Lean
Obese
D Peripheral blood mononuclear cells
CD64+CD33+CD14+ /live [%]
*
CD14+HLA-DR+
non-classical
4.04
intermediate
5.26
82.2 classical
CD16 BUV496
CD14 BUV395
Monocytes /live [%]
**
classical
intermediate
non-classical
CD14high Monocytes /live [%]
***
P1
P2

Figure 7. Pro-inflammatory Intestinal Macrophages are also Increased in Human Obese Subjects

(**A**) Flow cytometry strategy of human intestinal macrophages (iMacs: $CD14^{high}$ (pro-inflammatory/monocyte-derived P1, P2 and intermediate P3) and $CD14^{low}$ (anti-inflammatory/resident P4, P5) subpopulations).

(**B-C**) Proportional distribution (**B**) and frequencies of human iMacs (total, $CD14^{high}$/$CD14^{low}$ and P1-P5 subpopulations) (**C**) from colon biopsies of lean (BMI < 27 kg/m^2, n=13) or obese subjects (BMI > 32 kg/m^2, n=8).

(**D**) Frequencies of blood monocytes and their subpopulations from lean (n=21) or obese subjects (n=15).

One data point represents one subject. Statistical data are expressed as mean±SEM. *p<0.05. **p<0.01, ***p<0.001, unpaired Mann-Whitney U test with two tailed distribution. Also see Figures S7.

STAR ★ METHODS

KEY RESOURCES TABLE

REAGENT or RESOURCE	SOURCE	IDENTIFIER
Antibodies		
Anti-mouse CD16/CD32	Biolegend	Cat#101310; RRID: AB_2103871
Anti-mouse CD3 (145-2C11) APC-Cy7	Biolegend	Cat#100330; RRID: AB_1877170
Anti-mouse CD19 (6D5) APC-Cy7	Biolegend	Cat#115530; RRID: AB_830707
Anti-mouse NK1.1 (PK136) APC-Cy7	Biolegend	Cat#108723; RRID: AB_830870
Anti-mouse Ly6G (1A8) APC-Cy7	Biolegend	Cat#127624; RRID: AB_10640819
Anti-mouse CD45 (30-F11) PerCP-Cy5.5	Biolegend	Cat#103131; RRID: AB_893344
Anti-mouse CD24 (M1/69) PE-Cy7	Biolegend	Cat#101821; RRID: AB_756047
Anti-mouse CD11b (M1/70) BV421	Biolegend	Cat#101236; RRID: AB_11203704
Anti-mouse CD64 (X54-5/7.1) APC	Biolegend	Cat#139306; RRID: AB_11219391
Anti-mouse Ly6C (HK 1.4) FITC	Biolegend	Cat#128005; RRID: AB_1186134
Anti-mouse I-A/I-E (M5/114.15.2) BV785	Biolegend	Cat#107645; RRID: AB_2565977
Anti-mouse CCR2 (475301) PE	R&D Systems	Cat#FAB5538P-25/100; RRID: AB_10718414
Anti-mouse CD11c (N418) BV650	Biolegend	Cat#117339; RRID: AB_2562414
Anti-mouse CD103 (2E7) PE-Dazzle594	Biolegend	Cat#121430; RRID: AB_2566493
Anti-mouse F4/80 (BM8) PE	Biolegend	Cat#123110; RRID: AB_893486
Anti-mouse CD11c (N418) PE-Cy7	Biolegend	Cat#117318; RRID: AB_493568
Anti-mouse CD206 (C068C2) A647	Biolegend	Cat#141712; RRID: AB_10900420
Anti-mouse Siglec F (E50-2440) BV510	BD Biosciences	Cat#740158; RRID: AB_2739911
Anti-mouse F4/80 (BM8) e660	Thermo Fisher Scientific	Cat#50-4801-80; PRID:AB_11150065
Anti-mouse CD11b (M1/70) A488	Thermo Fisher Scientific	Cat#53-0112-80; PRID:AB_469900
Anti-mouse CD11b (M1/70) e660	Thermo Fisher Scientific	Cat#50-0112-82; PRID:AB_11218507
Anti-mouse CD45 (30-F11) A700	Biolegend	Cat#103128; RRID: AB_493715
Anti-mouse Ly6C (AL-21) BV605	BD Biosciences	Cat#563011; RRID: AB_2737949
Anti-mouse Akt (pS473) PE	BD Biosciences	Cat#560378; RRID: AB_1645328
Anti-mouse S6 (pS235/pS236) (N7-548) A488	BD Biosciences	Cat#560434; RRID: N/A
Anti-human CD19 (HIB19) PE-Cy5	Biolegend	Cat#302209; RRID: AB_314239
Anti-human CD3 (UCHT1) PE-Cy5	Biolegend	Cat#300410; RRID: AB_314064
Anti-human CD56 (5.1H11) PE-Cy5	Biolegend	Cat#362515; RRID: AB_2564088
Anti-human CD20 (2H7) PE-Cy5	Biolegend	Cat#302307; RRID: AB_314255
Anti-human TCRαβ (IP26) PE-Cy5	Biolegend	Cat#306710; RRID: AB_314648
Anti-human CD45 (HI30) PerCP-Cy5.5	Biolegend	Cat#304027; RRID: AB_1236444
Anti-human CD64 (10.1) A647	Biolegend	Cat#305012; RRID: AB_528867
Anti-human HLA-DR (L243) A488	Biolegend	Cat#307619; RRID: AB_493176
Anti-human CD14 (MφP9) BUV395	BD Biosciences	Cat#563562; RRID: AB_2744288
Anti-human CD16 (3G8) BUV496	BD Biosciences	Cat#564654; RRID: AB_2744294
Anti-human CD209 (9E9A) PE	Biolegend	Cat#330105; RRID: AB_1134060
Anti-human CD163 (GH1/61) BV421	Biolegend	Cat#333611; RRID: AB_2562462
Anti-human CCR2 (KO36C2) BV510	Biolegend	Cat#357217; RRID: AB_2566503
Anti-human CD33 (WM53) BV785	Biolegend	Cat#303427; RRID: AB_2650887

CD103 (Ber-ACT8) BV605	Biolegend	Cat#350217 ;RRID: AB_2564282
Biological Samples		
Human colon biopsies	This paper	Cat#1CUSB,# 2CUSB, #10CUSB, #14CUSB, #17CUSB, #19CBDA, #20CUSB, #21CMDP,#22CMDP, #27CUSB, #28CUSB, #29CUSB, #31CMDP, #32CUSB, #34CMDP, #37CMDP, #38CMDP, #47CMDP, #60CMDP, #66CMDP, #68G(B)USB
Human corpus and duodenum biopsies	This paper	Cat#3GUSB, #5GUSB, #6GUSB, #7GUSB, #11GUSB, #12GUSB, #26GUSB, #30GUSB, #36GBMDP, #40GMDP, #41GBUSB, #42G(B)MDP, #44GBMDP/USB, #45GMDP, #46GMDP, #56GUSB, #57GMDP, #59GBMDP, #61GMDP, #67GMDP, #68G(B)USB, #71GBUSB, #72GUSB, #79GMDP
Human Blood	This paper	Cat#5GUSB, #6GUSB, #7GUSB, #10CUSB, #11GUSB, #12GUSB, #14CUSB, #17CUSB, #18GBDA, #19CBDA, #20CUSB, #26GUSB, #27CUSB, #28CUSB, #29CUSB, #30GUSB #31CMDP, #32CUSB, #34CMDP, #36GBMDP, #37CMDP, #38CMDP, #41GBUSB, #42G(B)MDP, #44GBMDP/USB, #45GMDP, #46GMDP, #47CMDP, #52BUSB, #56GUSB, #57GMDP, #59GBMDP, #60CMDP, #66CMDP, #67GMDP #68G(B)USB
Chemicals, Peptides, and Recombinant Proteins		
60% coconut-based HFD	Research Diets	Cat#D12331
60% coconut-based HFD	Sniff	Cat#D12331 (#E15772-3)
Purified control diet (Starch)	Research Diets	Cat#D12450Ji
60% lard-based HFD	Research Diets	Cat#D12492i
Collagenase VIII	Sigma-Aldrich	Cat#C2139
Collagenase IV	Worthington	Cat#LS004189
DNAse I	Roche	Cat#11284932001
Percoll	GE Healthcare	Cat#GE17-0891-01
BLZ945	Novartis	MTA; Cat#BLZ945-AA
Clodronate liposomes	Liposoma	Cat#C-005
Control liposomes (PBS)	Liposoma	Cat#P-005
Rapamycin	MedChemExpress	Cat#HY-10219, CAS: 53123-88-9
Exendin (9-39)	Bachem	Cat#H-8740, CAS: 133514-43-9
Diprotin A	Sigma- Aldrich	Cat#I9759, CAS:90614-48-5
Sitagliptin phosphate monohydrate	Santa Cruz Biotechnology	Cat#sc-364620, CAS: 654671-77-9
Fix Buffer I	BD Biosciences	Cat#557870
Perm Buffer III	BD Biosciences	Cat#558050
MitoTracker. Green FM	Thermo Fisher Scientific	Cat#M7514

MitoTracker. Red CMXRos	Thermo Fisher Scientific	Cat#M7512
MitoSOX™ Red mitochondrial superoxide indicator	Thermo Fisher Scientific	Cat#M36008
DAPI	Biolegend	Cat#422801
Zombie Aqua Fixable Viability Kit	Biolegend	Cat#423102
Zombie NIR Fixable Viability Kit	Biolegend	Cat#423105
Critical Commercial Assays		
Mouse/Rat Insulin Kit	MesoScale Diagnostics	Cat#K152BZC
V-Plex Pro-inflammatory Panel 1 Mouse Kit	MesoScale Diagnostics	Cat#K15048
Active GLP-1 (ver. 2) Kit	MesoScale Diagnostics	Cat#K150JWC
eBioscience Foxp3 Staining Buffer Set	Thermo Fisher Scientific	Cat#00-5523-00
NucleoSpin RNA kit	Macherey Nagel	Cat#740955
RNeasy Plus Universal Mini kit	Qiagen	Cat#73404
GoScript™	Promega	Cat#A5003
GoTaq qPCR Master Mix	Promega	Cat#A4472919
Pierce BCA protein assay kit	Thermo Scientific	Cat#23227
QIAamp FAST DNA Stool Mini Kit	Qiagen	Cat#51604
QIAqick Gel Extraction Kit	Qiagen	Cat#28706
Qubit dsDNA HS Assay Kit	Thermo Fisher Scientific	Cat#Q32854
Deposited Data		
scRNA-seq Data	This paper	GEO: GSE143351
Experimental Models: Organisms/Strains		
Mouse: C57BL/6N	Charles River Laboratories	RRID:IMSR_CRL:027
Mouse: C57BL/6N	University of Basel (originated from Charles River)	RRID:IMSR_CRL:027
Mouse: B6.129S4-Ccr2^{tm1Ifc}/J	The Jackson Laboratory	RRID:IMSR_JAX:004999
Mouse: C57BL/6J	University of Basel and Bern (originated from Jackson Laboratory)	RRID:IMSR_JAX:000664
Oligonucleotides		
Primers for RT-PCR, see Table S2	Microsynth	N/A
Primers for 16S amplicon PCR, see Table S3	Microsynth	N/A
Software and Algorithms		
Prism8	GraphPad Software, LLc.	https://www.graphpad.com
FlowJo (version 10.61)	Becton Dickinson & Company (BD)	https://www.flowjo.com/solutions/flowjo/downloads
BD FACSDiva (version 8.0.1)	Becton Dickinson & Company (BD)	https://www.bdbiosciences.com/en-us/instruments/research-instruments/research-software/flow-cytometry-acquisition/facsdiva-software
R (version 3.6)	The R Foundation	https://www.r-project.org
Bioconductor (version 3.10)	Amezquita, R. A. et al. (2019) Orchestrating single-cell analysis with Bioconductor. Nat Methods.	http://bioconductor.org/

Kallisto (version 0.46.0) and BUStools (version 0.39.2)	Melsted, P. et al. (2019) Modular and efficient pre-processing of single-cell RNA-seq. bioRxiv:673285.	https://pachterlab.github.io/kallisto/ https://www.kallistobus.tools/
QIIME pipeline (version 1.8.0)	Caporaso, J. G. et al., (2010)	http://qiime.org
Usearch61_ref (version 6.1.544)	Edgar, R. C. et al., (2010)	http://qiime.org

LEAD CONTACT AND MATERIALS AVAILABILITY

Further information and requests for resources and reagents should be directed to and will be available by the Lead Contact, Claudia Cavelti-Weder (claudia.cavelti-weder@usb.ch). There are restrictions to the availability of BLZ945 due to Material Availability Statement (MAT) agreements with Novartis. This study did not generate new unique reagents.

EXPERIMENTAL MODEL AND SUBJECT DETAILS

Mice

Male C57BL/6 (B6) mice and CCR2$^{-/-}$ mice were maintained in our SPF-facility at room temperature of 22°C on a 12h light/12h dark cycle. Germ-free B6 mice were bred and maintained in flexible-film isolators or in individually ventilated cages (IVC) at the Clean Mouse Facility, University of Bern, Switzerland. For the high-fat diet (HFD) studies 5-8 week-old weight-matched mice were fed either a coconut-based high-fat diet (HFD: 60 %; #D12331, Research Diets or Sniff) or chow diet up to 3 months. For assessing the influence of different diet compositions and the microbiota the following additional diets were used: a purified control diet without fibers (Starch: 10 %; #D12450Ji; Research Diets) and lard-based HFD (60 %; D12492i; Research Diets). Mice were randomized into different groups according to their starting weights. See diet details in Table S1.

Human Subjects

Colon biopsies were collected from both male and female obese (BMI > 32 kg/m^2, n=8) and lean (BM < 27 kg/m^2, n=13) individuals with an average age of 60±14.89 years. Gastroscopy biopsies of lean (n=12) and obese (n=12) patients were also collected from both genders with an average age of 48.83±16.72 years. In addition, blood was obtained from male and female obese (n=15) and lean (n=21) patients with an average age of 52±17.36 years. Exclusion Criteria: Inability to provide informed consent, intake of corticosteroids, anti-inflammatory/ immunosuppressive drugs potentially altering immune cells, clinical signs of current infection, known anemia (e.g. hemoglobin < 110 g/L for males, < 100 g/L for females) or neutropenia (e.g. leukocyte count < 1.5 × 10^9/L or ANC < 0.5 × 10^9/L), known immunodeficiency (e.g. HIV), vasculitis or collagenosis, inflammatory bowel disease, adrenal insufficiency and/or substitution with glucocorticoids, known clinically significant kidney or liver disease (e.g. creatinine > 1.5 mg/dL, AST/ALT > 2 × ULN, alkaline phosphatase > 2 × ULN, or total bilirubin [tBili] > 1.5 × ULN, liver cirrhosis Child B or C), risky daily alcohol consumption (> 24g/d for males, > 12g for females), known uncontrolled congestive heart failure, known uncontrolled malignant disease or currently pregnant or breastfeeding. Subjects were referred by the Department of Gastroenterology at the University Hospital Basel/Clarunis, University Center for Gastrointestinal and Liver Diseases Basel or the doctor's office MagenDarm Basel for a diagnostic colonoscopy on the basis of symptoms suggestive for irritable bowel syndrome or for colorectal cancer screening (recommended in Switzerland after the age of 50 years). Researchers were blinded during sample-processing and data acquisition. For the statistical analysis between obese and lean patient, researchers were unblinded.

Study Approval

All animal procedures were approved by the local Animal Care and Use Committee and performed in accordance with Swiss Federal regulations. The human material was collected and used with informed consent. Permission for the human study (ID: 2018-00712; full title "Characterization of human intestinal macrophages in metabolic disease- iMAC study" ClinicalTrails.gov) was obtained by the Ethical commission in Basel (Ethikkommission Nordwest- und Zentralschweiz).

METHOD DETAILS

Macrophage Depletion and mTOR inhibition Models

For dose-dependent depletion of macrophages, HFD-fed mice were treated orally with 50, 100 or 200 µg/g CSF1R inhibitor (BLZ945; MTA Novartis, Basel, Switzerland) or its vehicle (20 % Captisol; Ligand, San Diego, US) for up to ten weeks (5 times/week). Treatment started 1 week before HFD feeding.

Depletion by clodronate liposomes: To specifically deplete colonic macrophages, in anesthetized mice clodronate liposomes were injected intrarectally with a flexible gavage needle coated with lubricant. The colon-specific depletion was compared to systemic depletion by intraperitoneal application (i.p.) of clodronate liposomes. The clodronate or control PBS liposomes (Liposoma B.V.) were injected every other day (100 µL/500 µg/injection) starting from day -4 until day 6 after start of HFD feeding.

To inhibit mTOR activation, mice were treated intrarectally or i.p. with 3 mg rapamycin/kg/every other day (Cat#HY-10219, MedChemExpress), according the application of clodronate liposomes.

Isolation of Intestinal Macrophages

Intestinal lamina propria lymphocytes were isolated from the colon of mice or human biopsies. For mouse colon, the length was measured, fat was removed and the tissue was first cut open longitudinally, then cut into 1 cm pieces and washed in ice-cold DPBS or HBSS (without Mg/Ca). To remove the epithelial layer, tissue pieces and biopsies were washed twice in HBSS/2 mM EDTA shaking 20 min at 37 °C. Afterwards washed twice in HBSS and transferred into a gentle MACS C-tube (#130-096-334, Miltenyi Biotec) containing 3 mL Complete IMDM Medium (1x IMDM, 10 % FBS, P/S, Glutamax). Next 3 mL 2x Collagenase

VIII (#C2139, Sigma-Aldrich) digestion solution (Complete IMDM, 2mg/mL Collagenase VIII, 25 µg/mL DNase I) was added to start enzymatic digestion shaking at 37 °C (mouse colon: 25-30 min, human biopsies: 35-40 min). Digested tissue was homogenized using the gentleMACS Octo Dissociator (Militenyi Biotec; program: ms_intestine-01), digestion was stopped by EDTA. Leukocytes were enriched using a percoll gradient (40%/70%, #GE17-0891-01, GE Healthcare) and centrifugated (600 g, 20 min, 22°C, brake and acceleration 0 or 1). The lymphocyte ring was collected from the interphase, washed (550 g, 5 min, 22 °C) with FACS Buffer (1xDPBS, 0.5 % BSA, 5 mM EDTA). Finally, the cells were resuspended in 200 µL FACS Buffer (DPBS/0.5 % BSA/5 mM EDTA) containing Fc Blocking and filtered through a 35 µM strainer FACS tube (#352235, Corning).

Isolation of Macrophages in other Tissues

Adipose and liver tissue were minced with scissors and digested by shaking in a Collagenase IV (#C2139, Worthington) solution (1x HBSS, 10 mM HEPES, 1.5 mg/mL Collagenase IV and 8.25 µg/mL DNAse I) for 20-30 min at 37°C and 400 rpm. Digestion was quenched by adding FACS buffer and suspension was filtered through a cotton gauze. Erythrocytes were removed using Red Cell Lysis Buffer (154 mM NH4Cl, 10 mM KHCO3, 0.1 mM EDTA). Liver lymphocytes were enriched using a 70 %/40 % percoll gradient. Later cells were washed and filtered for FACS staining.

Peritoneal macrophages were isolated by lavage of the peritoneum using 10 mL FACS buffer. Erythrocytes were lysed with Red Cell Lysis Buffer, the remaining cells were washed and filtered for FACS staining.

To isolate microglia whole-brains were excised from the skull and mechanically dissociated in FACS buffer using a Dounce-homogenizer (#D9938-1SET, Merck). Cells were then passed through a 70 µm cell strainer, washed with FACS buffer and enriched by

performing a 70 %/ 37 % percoll gradient (30 min, 750 g, minimal brake). The microglia-containing interphase was subsequently collected and filtered, washed and used for FACS analysis.

Antibodies and Flow Cytometry

To reduce unspecific binding, the Fc receptor was blocked using CD16/32 prior to incubation with monoclonal antibodies (mAbs) for 30 min-1 h on ice. All mAbs used for flow cytometry were listed in Key Resources Table. In case of MitoTracker staining cells were stained with MitoTracker probes (Thermo Fisher Scientific) at 37 °C in the dark (10 nM MitoGreen and 5 n MitoRed for 20 min in 10 % FACS Buffer, 1 µM MitoSOX for 10 min in 1x HBSS (no Mg/Ca)) after the surface staining. For the assessment of mTOR activation cells were fixed with BD Fix I Buffer (10 min, 37 °C) after surface staining. Subsequently cells were washed and permeabilized by adding BD Perm Buffer II (30 min on ice), followed by staining for 1 h at RT with anti-pS6 and anti-pS473. Samples were acquired with a BD LSRIIFortessa (BD) and analyzed with FlowJo software 10.6.1 (BD).

Metabolic Assessments

Metabolic phenotype was assessed by glucose and insulin tolerance tests (GTT/ ITT) performed at 1, 4 and 12 weeks of HFD feeding. For a GTT mice were fasted 6 h. After intraperitoneal (IPGTT) or oral (OGTT) injection of glucose (2 g/ kg bodyweight) blood glucose was monitored from the tail vein after 15, 30, 60, 90 and 120 min using a glucometer (Freestyle, Abbot). For active GLP-1 measurements 25 mg/kg sitagliptin (Cat#sc-364620, Santa Cruz) was injected i.p. 30 min before oral glucose application. To block GLP-1 or parasympaticus action

236 µg/kg Exendin (9-39) (#H-8740, Bachem) or 5 mg/kg atropine (#A0257-5G, Sigma), respectively, were i.p. injected at timepoint -30 min prior glucose application.
ITT was performed after 3 h of fasting by injecting 1-2 U/kg body weight insulin i.p. (Actrapid HM Penfill, Novo Nordisk), glucose levels were measured at 0, 15, 30, 60,90 and 120 minutes after injection.

Plasma insulin, GLP-1, TNF and IL-6 were quantified by electrochemiluminescence (MESO SECTOR S 600) using kits from Meso Scale Diagnostics (MSD, Rockville, MD, USA), according to the manufacturer`s instructions: Mouse/Rat Insulin Kit (#K152BZC),V-PLEX Plus Proinflammatory Panel 1 Mouse Kit (#K15048G), V-PLEX GLP-1 Active Kit vers. 2 (#K15030D).

Quantitative Reverse Transcriptase-Polymerase Chain Reaction (RT-PCR) Analysis

RNA was extracted from distal colon and epididymal adipose tissue using NucleoSpin RNA kit (#740955.250, Macherey-Nagel) or the RNeasy Plus Universal Mini kit (#73404, QIAGEN) according to manufacturer`s instructions. Reverse transcription was performed with GoScript™ Reverse Transcription Mix (#A2801, Promega). For qPCR GoTaq qPCR Master Mix (#A6002, Promega) on a ViiA7 Real-Time PCR System (Thermo Fisher Scientific) was used. Primer sequences (Microsynth, Balgach, Switzerland) are listed in Table S2. The data presented correspond to the mean of $2^{-\Delta\Delta Ct}$ after being normalized to housekeeping genes B2m and Ppia.

Isolation of Pancreatic Islets

Pancreatic mouse islets were isolated by injecting collagenase IV (1.4 mg/mL; Worthington) digestion solution into the pancreas via the common bile duct. The perfused pancreas was digested at 37 °C for 30 min, thereafter quenched (1x HBSS, 1 M HEPES, 0.5 % BSA) and

filtered. Islets were handpicked under a stereoscopic microscope and cultured in RPMI-1640 (containing 11.1 mM glucose, 10 % FBS, 100 U/mL P/S, 2 mM Glutamax, 50 µg/mL Gentamycin, 10 µg/mL Fungison). For flow cytometry analysis islets were washed in PBS/ 0.5 mM EDTA, trypsinized and around 100 islets/tube were collected.

Glucose-Stimulated Insulin Secretion (GSIS) Assay

For GSIS handpicked primary mouse islets were incubated in RPMI-1640 medium overnight. The next day islets were washed and pre-incubated in Krebs-Ringer-bicarbonate buffer (KRB: 115 mM NaCl, 4.7 mM KCl, 2.6 mM $CaCl_2$ $2H_2O$, 1.2 mM KH_2PO_4, 1.2 mM $MgSO_4$ $2H_2O$, 10 mM HEPES, 0.5 % BSA, pH 7.4) containing 2.8 mM glucose. After 1.5 h buffer was replaced to KRB containing low (2.8 mM, basal) or high (16.7 mM, stimulated) glucose and supernatant was collected after 1 h to assess basal and glucose stimulated insulin release. The stimulatory index was defined as the ratio of stimulated insulin secretion at 16.7 mM/h to basal insulin secretion at 2.8 mM/h. To obtain insulin content islets were vortexed in 0.18 mol/l HCl in 70 % ethanol and incubated at least 1 h at -20 °C. Secreted and content insulin were measured by Mouse/Rat Insulin Kit (#K152BZCMeso Scale Discovery).

Microbiota Analysis

gDNA extraction from stool samples: Contents from small intestine, caecum and colon, or feces were frozen in 2 mL tubes and stored at -80 °C until extraction. To extract genomic DNA (gDNA) from feces QIAamp FAST DNA Stool Mini Kit (#51604 Qiagen, Hilden, Germany) was used following the vendor`s instructions with the following adjustment: homogenization of stool particles was performed with 100 mg baked glass beads (Sigma Aldrich) using a tissue

lyser for 3 min, 30 Hz per run (Retsch MM400). DNA concentration was measured by Nanodrop2000 (Thermo Fisher Scientific).

16S amplicon PCR: 100 ng of bacterial DNA were used to amplify the V5/V6 region of the 16S ribosomal gene by PCR using Platinum Taq DNA polymerase (Invitrogen). We used barcoded forward fusion primers 5'- CCATCTCATCCCTGCGTGTCTCCGACTCAG-BARCODE-ATTAGATACCCYGGTAGTCC-3', where core primers have been modified by the addition of a PGM sequencing adaptor, a GT-spacer and unique barcode (see Table S3), that allow pooling of up to 96 different barcodes in combination with the reverse fusion primer 5'-CCTCTCTATGGGCAGTCGGTGATACGAGC-TGACGACARCCATG-3' (Li et al., 2015; Mamantopoulos et al., 2017; Sundquist et al., 2007). All primers were used at a 10 µM working concentration. Cycling conditions were following: initial 5 min denaturation at 94 °C, followed by 35 cycles of 1 minute denaturation at 94 °C, 20 s annealing at 46 °C and 30 s extension at 72 °C. The final extension step took place for 7 min at 72 °C. The PCR product (ca 350 bp) was loaded on a 1 % agarose gel, cut out with a scalpel extracted using the QIAqick Gel Extraction Kit protocol (#28706, Qiagen). The resulting dsDNA concentration was measured by Qubit dsDNA HS Assay Kit (#Q32854, Thermo Fisher Scientific).

16S sequencing: Up to 96 libraries were diluted at 26 pM and were pooled. Libraries were prepared with the OT2 HiQ View 400 kit and emulsion PCR performed on the Ion OneTouch 2 (OT2) instrument (ThermoFischer). The template-positive Ion Sphere Particles containing clonally amplified DNA were enriched using the Ion OneTouch ES instruments (ThermoFisher). Sequencing was carried out using the Ion PGM HiQ View Sequencing 400 kit with the Ion Personal Genome Machine System on an Ion 316 Chip v2 (ThermoFisher) (Whiteley et al., 2012).

Analysis of 16S data: Samples with less than 1000 reads were excluded from the analysis if not stated otherwise. Data analysis was performed using the QIIME pipeline version

1.8.0 (Caporaso et al., 2010). OTUs were picked at a threshold of 97 % similarity using usearch61_ref v.6.1.544 (Edgar, 2010) followed by rarefaction and taxonomy assignment using Greengenes database.

RNA-Sequencing

For single-cell RNA-sequencing (scRNA-seq) (liveCD45^{+}Lin^{-}CD11b^{+}CD24^{-} and CD64^{+} or Ly6C^{+}) CD11b^{+}nonDCs colonic macrophages (see gating strategy (Tamoutounour et al., 2013) and Fig. 1a) were sorted from mice fed 1 week HFD (n=2) or chow diet (n=2) by using FACS Aria III (BD Biosciences). Cell suspensions were loaded into the wells of a 10X Genomics Chromium Single Cell Controller (one well per mouse replicate). Single-cell capture and cDNA and library preparation were performed with a Single Cell 3' v2 Reagent Kit (10X Genomics) according to the manufacturer's instructions. Sequencing was performed on one lane of an Illumina NexSeq 500 machine flow-cell at the ETH Zurich Genomics Facility in Basel, Switzerland.

Data were analyzed by the Bioinformatics Core Facility, Department of Biomedicine, University of Basel, Switzerland. Read quality was assessed with the FastQC tool (version 0.11.5). In brief, sequencing files were processed with Kallisto (version 0.46.0) and BUStools (version 0.39.2) to perform sample and cell demultiplexing, read pseudo-alignment to the mouse transcriptome (Ensembl release 97), and to generate a UMI counts table (Melsted et al., 2019a; Melsted et al., 2019b). Further processing of the UMI counts table was performed by using R 3.6.0 and Bioconductor 3.10 packages (Amezquita et al., 2019), notably DropletUtils (version 1.6.1) (Griffiths et al., 2018; Lun et al., 2019) scran (version 1.14.5) and scater (version 1.14.5) (McCarthy et al., 2017), following mostly the steps illustrated in the simpleSingleCell Bioconductor workflow (Lun et al., 2016).

Based on the distributions observed across cells, cells with library sizes lower than 795, total number of features detected lower than 317, or with a fraction of UMI counts attributed to the mitochondrial genes of 0 % or higher than 7 % were filtered out (Ilicic et al., 2016). Low-abundance genes with average normalized $\log_2$ counts lower than 0.003 were filtered out. This resulted in a filtered matrix including UMI counts for 11,820 genes and 5,797 cells (3,013 from chow-fed mice and 2,784 from HFD-fed mice). UMI counts were normalized with size factors estimated from pools of cells to deal with dominance of zeros in the matrix (Lun et al., 2016; Vallejos et al., 2017). A mean-dependent trend was fitted to the variances of the log expression values of endogenous genes to distinguish between genuine biological variability and technical noise (*trendVar* function of the scran package with loess trend and span of 0.05) (Brennecke et al., 2013). The fitted trend was used to subtract technical noise from the data by using the *denoisePCA* function, retaining the 8 first principal components of the PCA for later analysis.

The package SingleR (version 1.0.0) was used for reference-based annotation of the cells and identification of likely contaminants in our dataset (Aran et al., 2019). We used the Immunological Genome Project (ImmGen) mouse microarray dataset (Heng et al., 2008) as reference, and eliminated 377 cells not annotated to the broad cell types “macrophages” or “monocytes”.

Clustering of cells was done on normalized log-count values by using hierarchical clustering on the Euclidean distances between cells (with Ward’s criterion to minimize the total variance within each cluster; package cluster version 2.1.0). The 6 clusters used for following analyses were identified by applying a dynamic tree cut (package dynamicTreeCut, version 1.63-1).

Differential expression between HFD and chow conditions, stratified by cluster, was performed by using a “pseudo-bulk” approach (Lun and Marioni, 2017): UMI counts of cells from each sample in each cluster were summed. This resulted in 4 samples per cluster,

aggregated from of 29 to 776 cells. Cluster P2.2 was excluded from the analysis because it contained too few chow cells. For each cluster, we only retained genes with CPM (normalized counts per million mapped reads) values above 1 in at least 2 of the 4 pseudo-bulk samples, and detected in at least 5 % of the individual cells.

The package edgeR (version 3.28) (Robinson et al., 2010) was used to perform TMM normalization (Robinson and Oshlack, 2010) and to test for differential expression with the Generalized Linear Model (GLM) framework. Genes with a false discovery rate (FDR) lower than 1 % were considered to be differentially expressed. Gene set enrichment analysis (GSEA) was performed with the function camera (Wu and Smyth, 2012) by using the default parameter value of 0.01 for the correlations of genes within gene sets, on gene sets from the hallmark collectionsupp (Liberzon et al., 2015) of the Molecular Signature Database (MSigDB, version 7.0) (Subramanian et al., 2005), or on DoRothEA v2 regulons (Garcia-Alonso et al., 2019): human TOP10score regulons were downloaded from https://github.com/saezlab/DoRothEA and we obtained the corresponding mouse regulons by considering 1-to-many orthologs of the human genes in each regulon (using Ensembl Compara release 97). We tested only gene sets containing at least 5 genes from the filtered dataset, and considered significant those with a FDR lower than 10 %.

Human Study

Human intestinal macrophages were isolated by enzymatic digestion (see isolation of intestinal macrophages) and identified as live $CD45^{+}Lin^{-}(CD19^{-}CD3^{-}CD56^{-}CD20^{-}TCR\alpha\beta^{-}$ and $nonCD33^{-}CD64^{-}$) and further subdivided by the expression of CD14, HLA-DR, CD163 and CD209. Blood was collected in (2x) EDTA containing tubes. After the dilution with 1x DPBS (1 part blood : 3 parts DPBS), a ficoll density gradient by using Lymphoprep density gradient

medium (#07851, Stemcell technologies) and Leucosep tubes (#871346, OpoPharma) was performed (25 min, 453 g, 22 °C, brake: 1, acceleration: 4). The Lymphoprep layer was washed with FACS Buffer and Red Cell Lysis Buffer was used to remove residual erythrocytes. The remaining cells were used for further flow cytometry staining.

QUANTIFICATION AND STATISTICAL ANALYSIS

Statistical Analysis

The data are presented as mean ± standard error of the mean (SEM) with the numbers of experiments or mice indicated in the figure legends. To test statistical difference between two groups unpaired Mann-Whitney U test with two tailed distribution was used using Prism8 software (GraphPad Software, San Diego, CA). Two-sided P-values of 0.05 or less were considered to be statistically significant.

DATA AND CODE AVAILABILITY

RNA-seq Data

Transcriptome sequencing data of intestinal macrophages have been deposited in the Gene Expression Omnibus (GEO), with the accession number GSE143351.

Go to https://www.ncbi.nlm.nih.gov/geo/query/acc.cgi?acc=GSE143351

Enter token unoveyewbnyzpuj into the box.

Supplemental Information

Targeting Colonic Macrophages Improves Glycemic Control in High-Fat Diet-induced Obesity

Theresa V. Rohm, Shefaa AlAsfoor, Angela J.T. Bosch, Zora Baumann, Sophia J. Wiedemann, Josua Wehner, Elise Dalmas, Leila Rachid, Regula Fuchs, Julien Roux, Catherine Mooser, Stephanie C. Ganal-Vonarburg, Julia B. Pilz, Petr Hruz, Daniel T. Meier, Claudia Cavelti-Weder

Figure S1

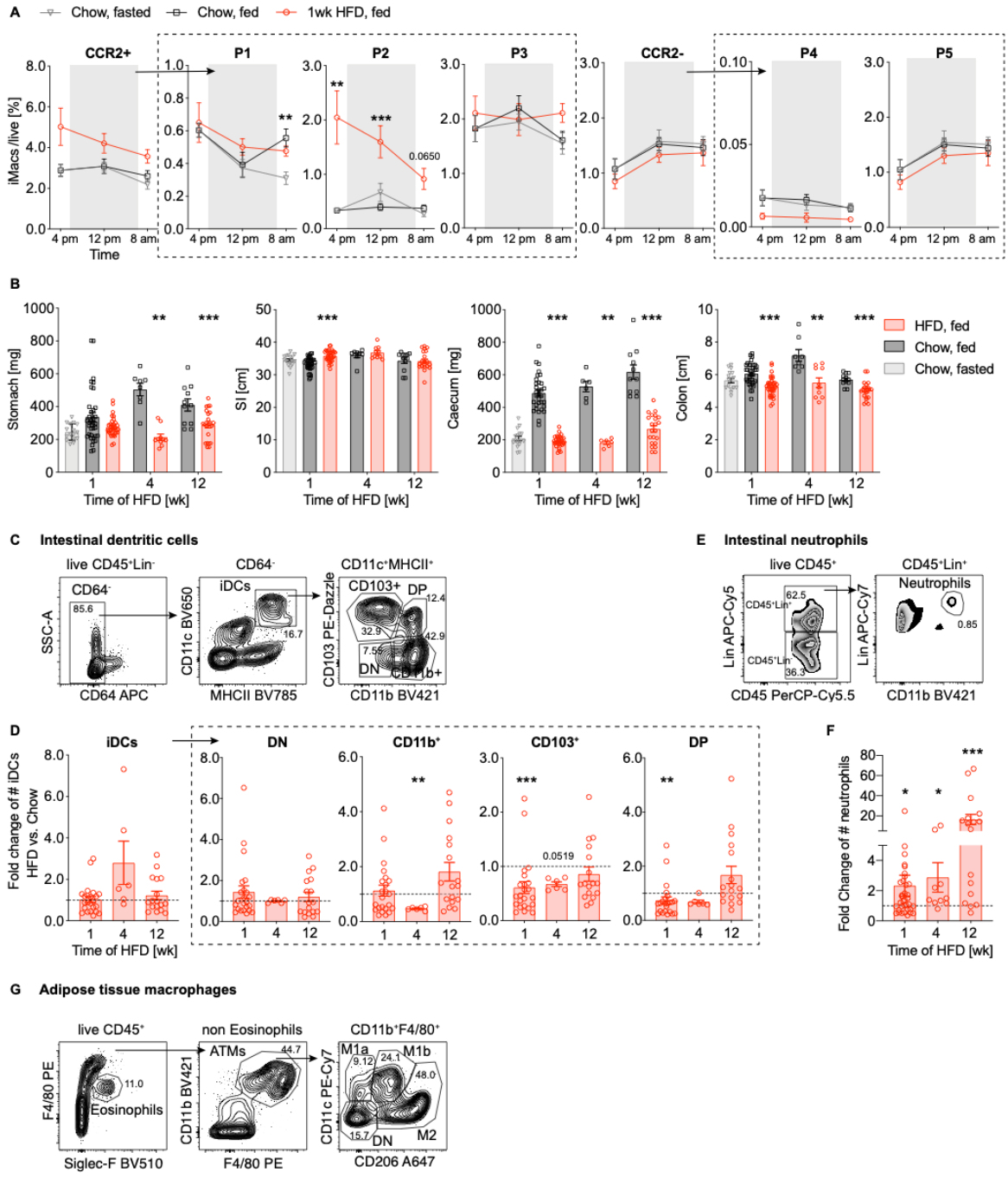
A
Chow, fasted
Chow, fed
1wk HFD, fed
CCR2+
P1
P2
P3
CCR2-
P4
P5
iMacs /live [%]
Time
4 pm 12 pm 8 am
B
Stomach [mg]
SI [cm]
Caecum [mg]
Colon [cm]
Time of HFD [wk]
HFD, fed
Chow, fed
Chow, fasted
C
Intestinal dentritic cells
live CD45+Lin-
CD64-
CD11c+MHCII+
SSC-A
CD64 APC
CD11c BV650
MHCII BV785
CD103 PE-Dazzle
CD11b BV421
iDCs
DP
DN
CD11b+
E
Intestinal neutrophils
live CD45+
CD45+Lin+
Neutrophils
Lin APC-Cy5
Lin APC-Cy7
CD45 PerCP-Cy5.5
D
iDCs
DN
CD11b+
CD103+
DP
Fold change of # iDCs HFD vs. Chow
F
Fold Change of # neutrophils
G
Adipose tissue macrophages
live CD45+
non Eosinophils
CD11b+F4/80+
Eosinophils
ATMs
M1a
M1b
M2
F4/80 PE
Siglec-F BV510
CD206 A647
CD11c PE-Cy7

Supplemental Figure 1 (related to Figure 1). The Effect of Food Intake and HFD on Intestinal Immunity

(**A**) Frequencies of intestinal macrophages (iMacs) ($CCR2^+$ (pro-inflammatory P1, P2, intermediate P3) and $CCR2^-$ (anti-inflammatory/resident P4, P5) subpopulations) in wild-type mice fasted (grey), fed chow diet (black) or 1 week of HFD (red) at timepoints 4 pm, 12 pm and 8 am.

(**B**) Macroscopic measurements of the stomach, small intestine, caecum and colon in wild-type mice fasted (grey), fed chow diet (black) or HFD (red).

(**C**) Flow cytometry gating strategy of intestinal dendritic cells (iDCs) and their subpopulations (DN, $CD11b^+$, $CD103^+$ DP).

(**D**) Fold change of absolute numbers (#) of iDCs and their subpopulations (DN, $CD11b^+$, $CD103^+$ DP) after HFD compared to chow controls.

(**E-F**) Flow cytometry gating strategy (**E**) and absolute numbers of intestinal neutrophils (**F**) with HFD compared to chow controls.

(**G**) Flow cytometry gating strategy of adipose tissue macrophages (ATMs) and their subpopulations (DN, M1a, M1b, M2).

Statistical data are expressed as mean±SEM. Data are a representative of 2-6 independent experiments (A/B/D/F) , with each data point representing one individual mouse. *$p<0.05$, **$p<0.01$, ***$p<0.001$, unpaired Mann-Whitney U test with two tailed distribution.

Figure S2

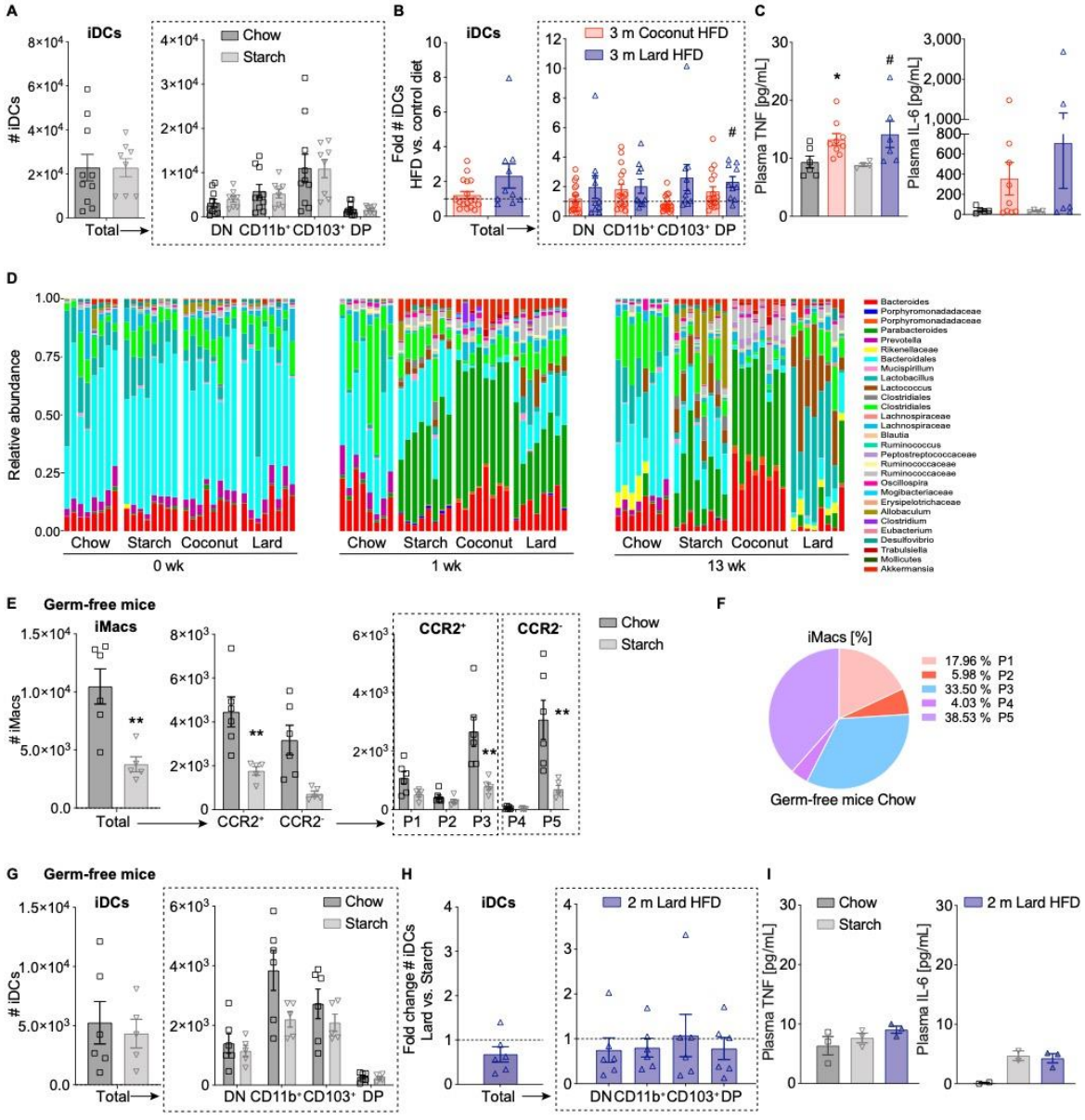
A
iDCs
iDCs
Chow
Starch
Total
DN CD11b+ CD103+ DP
B
iDCs
Fold # iDCs HFD vs. control diet
3 m Coconut HFD
3 m Lard HFD
Total
DN CD11b+ CD103+ DP
C
Plasma TNF [pg/mL]
Plasma IL-6 [pg/mL]
D
Relative abundance
Chow Starch Coconut Lard
0 wk
1 wk
13 wk
Bacteroides
Porphyromonadadaceae
Porphyromonadadaceae
Parabacteroides
Prevotella
Rikenellaceae
Bacteroidales
Mucispirillum
Lactobacillus
Lactococcus
Clostridiales
Clostridiales
Lachnospiraceae
Lachnospiraceae
Blautia
Ruminococcus
Peptostreptococcaceae
Ruminococcaceae
Ruminococcaceae
Oscillospira
Mogibacteriaceae
Erysipelotrichaceae
Allobaculum
Clostridium
Eubacterium
Desulfovibrio
Trabulsiella
Mollicutes
Akkermansia
E
Germ-free mice
iMacs
iMacs
Total
CCR2+
CCR2-
P1 P2 P3 P4 P5
Chow
Starch
F
iMacs [%]
17.96 % P1
5.98 % P2
33.50 % P3
4.03 % P4
38.53 % P5
Germ-free mice Chow
G
Germ-free mice
iDCs
iDCs
Total
Chow
Starch
DN CD11b+ CD103+ DP
H
iDCs
Fold change # iDCs Lard vs. Starch
Total
2 m Lard HFD
DN CD11b+ CD103+ DP
I
Chow
Starch
2 m Lard HFD
Plasma TNF [pg/mL]
Plasma IL-6 [pg/mL]

Supplemental Figure 2 (Related to Figure 2). Changes in Intestinal Immunity in Relation to Fibers Content, Fat Source and Gut Microbiota

(**A**) Absolute numbers (#) of intestinal dendritic cells (iDCs) and their subpopulations (DN, $CD11b^+$, $CD103^+$ DP) in wild-type mice fed chow (black) or starch (grey) control diet.

(**B**) Fold change of absolute numbers of iDCs their subpopulations (DN, $CD11b^+$, $CD103^+$ DP) after 3 months of coconut- (red) or lard-based (blue) HFDs compared to respective control diets.

(**C**) Plasma TNF and IL-6 in mice fed 3 months HFD or control diet.

(**D**) Relative genus abundances of fecal microbiota before and after 1 week and 3 months of HFD compared to controls.

(**E-F**) Absolute numbers of intestinal macrophages (iMacs) (**E**) and the distribution of their subpopulations P1-P5 (**F**) in germ-free mice fed chow (black) or starch (grey) control diet.

(**G**) Absolute numbers of iDCs in germ-free mice fed chow or starch control diet.

(**H**) Fold change of absolute numbers of iDCs their subpopulations (DN, $CD11b^+$, $CD103^+$ DP) in germ-free mice fed 2 months of lard-based HFD compared to starch-fed controls.

(**I**) Plasma TNF and IL-6 in germ-free mice after 2 months of HFD.

Statistical data are expressed as mean±SEM. Data are a representative of two independent experiments, with each data point representing one individual mouse. Chow vs. starch or coconut-based HFD vs. chow: *$p<0.05$, **$p<0.01$. Lard-based HFD vs. starch: $^{\#}p<0.05$, unpaired Mann-Whitney U test with two tailed distribution. Also see Table S1 for diet details.

Figure S3

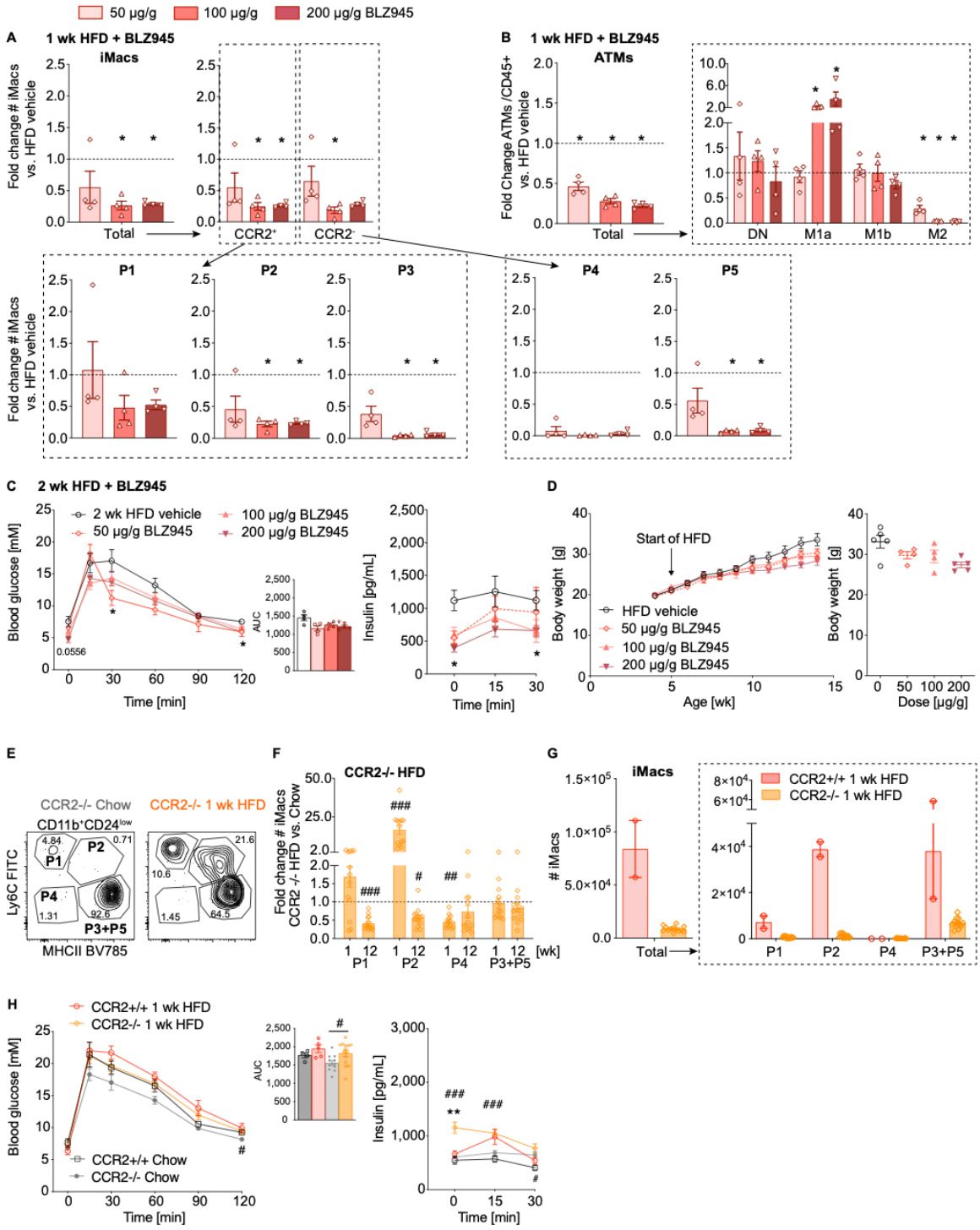
50 µg/g
100 µg/g
200 µg/g BLZ945
A
1 wk HFD + BLZ945
iMacs
Fold change # iMacs vs. HFD vehicle
Total
CCR2+
CCR2-
P1
P2
P3
P4
P5
B
1 wk HFD + BLZ945
ATMs
Fold Change ATMs /CD45+ vs. HFD vehicle
DN
M1a
M1b
M2
C
2 wk HFD + BLZ945
2 wk HFD vehicle
50 µg/g BLZ945
100 µg/g BLZ945
200 µg/g BLZ945
Blood glucose [mM]
Time [min]
AUC
Insulin [pg/mL]
D
Start of HFD
HFD vehicle
Body weight [g]
Age [wk]
Dose [µg/g]
E
CCR2-/- Chow
CCR2-/- 1 wk HFD
CD11b+CD24low
Ly6C FITC
MHCII BV785
F
CCR2-/- HFD
Fold change # iMacs CCR2 -/- HFD vs. Chow
[wk]
G
iMacs
iMacs
CCR2+/+ 1 wk HFD
CCR2-/- 1 wk HFD
H
CCR2+/+ Chow
CCR2-/- Chow

Supplemental Figure 3 (Related to Figure 3). Systemic Pharmacological and Genetic Depletion of Macrophages improves Glycemic Control

(**A**-**B**) Fold change of intestinal macrophages (iMacs) (**A**) and adipose tissue macrophages (ATMs) (**B**) and their subpopulations in wild-type mice after 1 week of HFD and 2 weeks oral BLZ945 treatment (50, 100, 200 μg/g/d) compared to vehicle treated mice.

(**C**) IPGTT, AUC, insulin after 2 weeks of HFD and 3 weeks BLZ945 treatment (n=4-5).

(**D**) Body weight over 2 months HFD and BLZ945 treatment.

(**E**) Representative flow cytometry plots of iMac subpopulations P1-P5 in CCR2-/- mice fed chow (grey) or 1 week of HFD (orange).

(F) Fold change of iMacs and their subpopulations P1-P5 in CCR2-/- mice fed 1 or 12 weeks HFD compared to CCR2-/- chow controls.

(**G**) Absolute numbers of iMacs and their subpopulations P1-P5 in CCR2+/+ (red) or CCR2-/- mice (orange) fed 1 week of HFD.

(**H**) IPGTT, AUC, insulin in CCR2+/+ or CCR2-/- mice fed 1 week of HFD compared to controls fed chow (n=5-14).

Statistical data are expressed as mean±SEM. Data are representative of (A-D) one and two independent experiments (E-H), with each data point representing one individual mouse. *p<0.05, **p<0.01. CCR2-/- HFD vs. CCR2-/- chow: $^{\#}$p<0.05, $^{\#\#}$p<0.01, $^{\#\#\#}$p<0.001, unpaired Mann-Whitney U test with two tailed distribution.

Figure S4

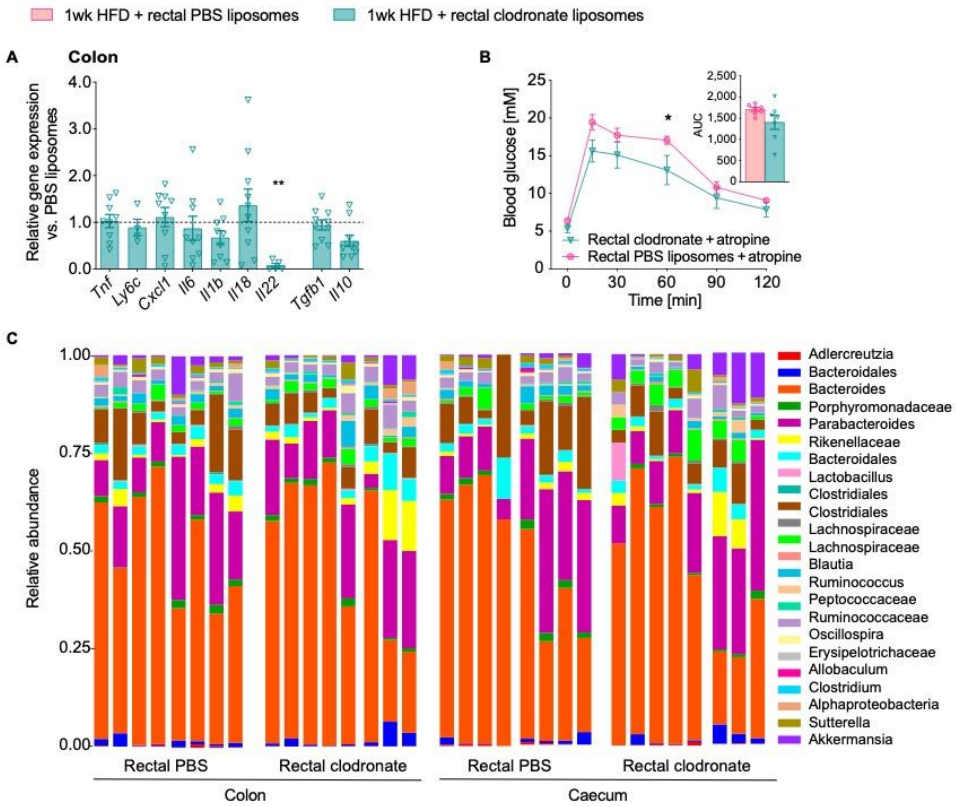

Supplemental Figure 4 (Related to Figure 4). The Effect of Intrarectal Clodronate Liposomes under HFD

(**A**) Colon gene expression in mice fed 1 week of coconut-based HFD and treated intrarectally with clodronate liposomes relative to controls.

(**B**) OGTT and AUC of mice fed 1 week of HFD and treated intrarectally with clodronate or PBS liposomes after atropine injection 30 min before glucose bolus (n=7).

(**C**) Relative genus abundances of fecal microbiota in mice fed 1 week of HFD and treated intrarectally with clodronate or PBS liposomes.

Statistical data are expressed as mean±SEM. Data are a representative of two (A/C) independent experiments and one (B) experiment, with each data point representing one individual mouse. *p<0.05, **p<0.01, unpaired Mann-Whitney U test with two tailed distribution.

Figure S5

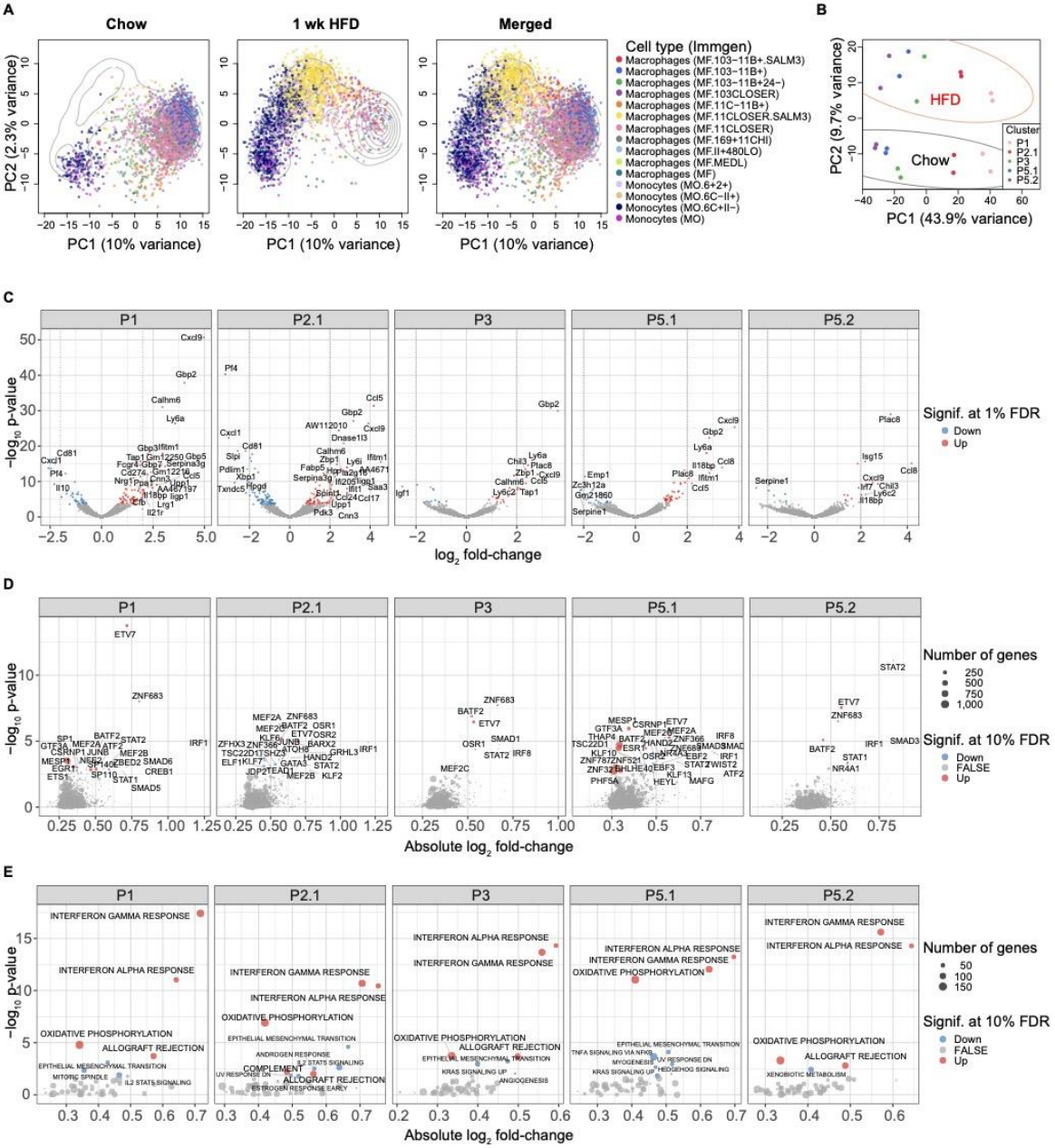
A
Chow
1 wk HFD
Merged
PC2 (2.3% variance)
PC1 (10% variance)
Cell type (Immgen)
Macrophages (MF.103−11B+.SALM3)
Macrophages (MF.103−11B+)
Macrophages (MF.103−11B+24−)
Macrophages (MF.103CLOSER)
Macrophages (MF.11C−11B+)
Macrophages (MF.11CLOSER.SALM3)
Macrophages (MF.11CLOSER)
Macrophages (MF.169+11CHI)
Macrophages (MF.II+480LO)
Macrophages (MF.MEDL)
Macrophages (MF)
Monocytes (MO.6+2+)
Monocytes (MO.6C−II+)
Monocytes (MO.6C+II−)
Monocytes (MO)
B
HFD
Chow
Cluster
P1
P2.1
P3
P5.1
P5.2
PC2 (9.7% variance)
PC1 (43.9% variance)
C
P1
P2.1
P3
P5.1
P5.2
−log10 p-value
log2 fold-change
Signif. at 1% FDR
Down
Up
D
Absolute log2 fold-change
Number of genes
Signif. at 10% FDR
FALSE
E
INTERFERON GAMMA RESPONSE
INTERFERON ALPHA RESPONSE
OXIDATIVE PHOSPHORYLATION
ALLOGRAFT REJECTION
EPITHELIAL MESENCHYMAL TRANSITION
COMPLEMENT
ESTROGEN RESPONSE EARLY
KRAS SIGNALING UP
HEDGEHOG SIGNALING
XENOBIOTIC METABOLISM

Supplemental Figure 5 (Related to Figure 5). Transcriptional Profiling of Intestinal Macrophages after HFD

(**A**) PCA of sorted intestinal macrophages (iMacs) from mice fed chow or 1 week of HFD. One point represents one cell, colored by the annotated cell type using the ImmGen microarray reference (cell types with at least 10 cells annotated are shown).

(**B**) PCA of pseudo-bulk RNA-seq samples used for differential expression analysis between chow and 1 week of HFD. One point represents one macrophage cluster per mouse.

(**C**) Volcano plots showing the differential expression between 1 week of HFD and chow for each cluster. Up- (red) or down-regulated (blue) genes are shown when significant at 1% FDR threshold and absolute $\log_2$ fold-change above 2.

(**D**) Up- (red) or down-regulated (blue) regulons after 1 week of HFD compared to chow for each cluster (10% FDR threshold).

(**E**) Up- (red) or down-regulated (blue) MSigDB hallmark pathways after 1 week of HFD compared to chow for each cluster (10% FDR threshold).

Data are representative of two replicates (n=2 per group) (A-E) and point sizes reflect the number of genes included in each annotated pathway (D/E).

Figure S6

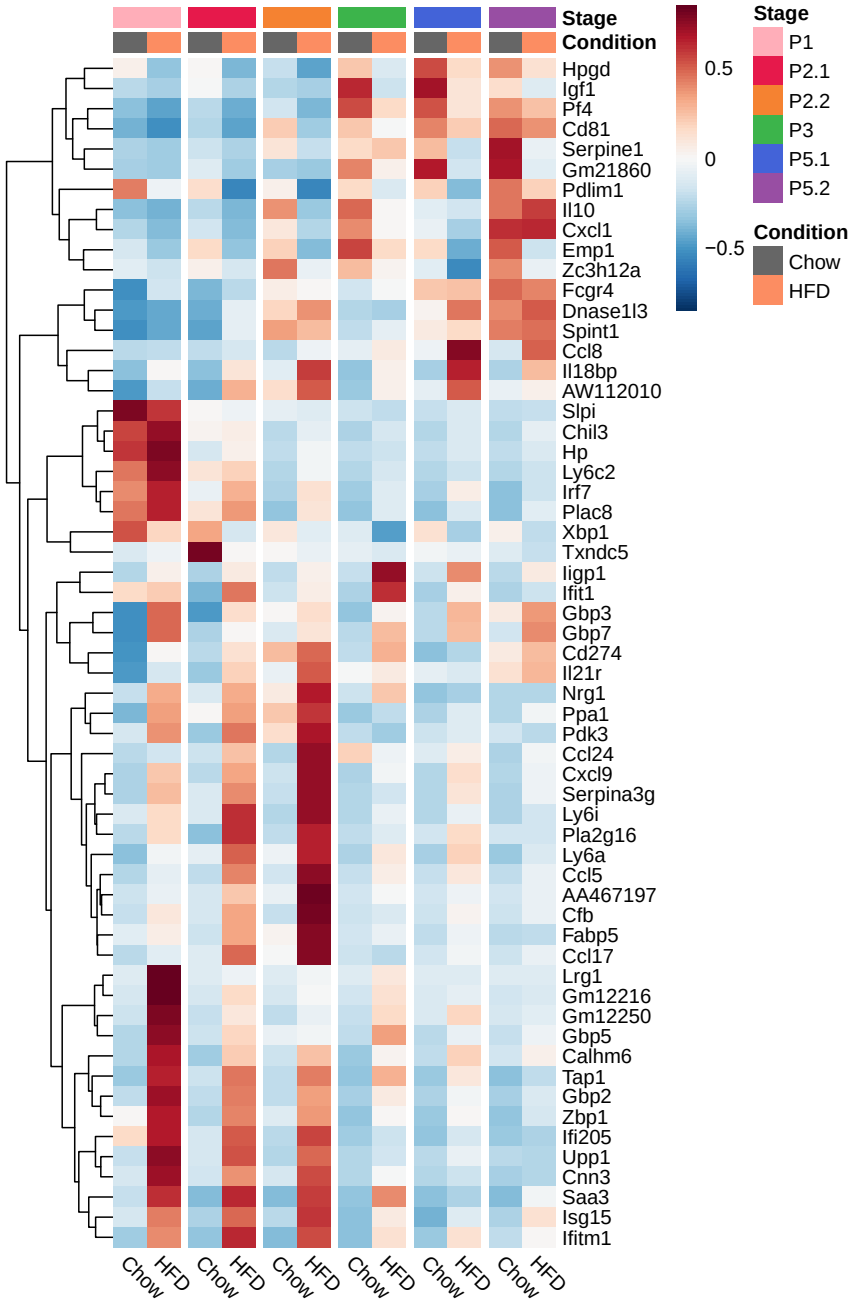

Supplemental Figure 6 (Related to Figure 5). Differential Gene Expression of Intestinal Macrophages after HFD

Average expression of genes differentially expressed in intestinal macrophages of mice fed 1 week HFD vs. chow (n=2 per group). Differential expression testing was done per cluster (P1, P2.1, P3, P5.1 and P5.2), significant at a 1% FDR threshold and with absolute $\log_2$ fold-change above 2.

Figure S7

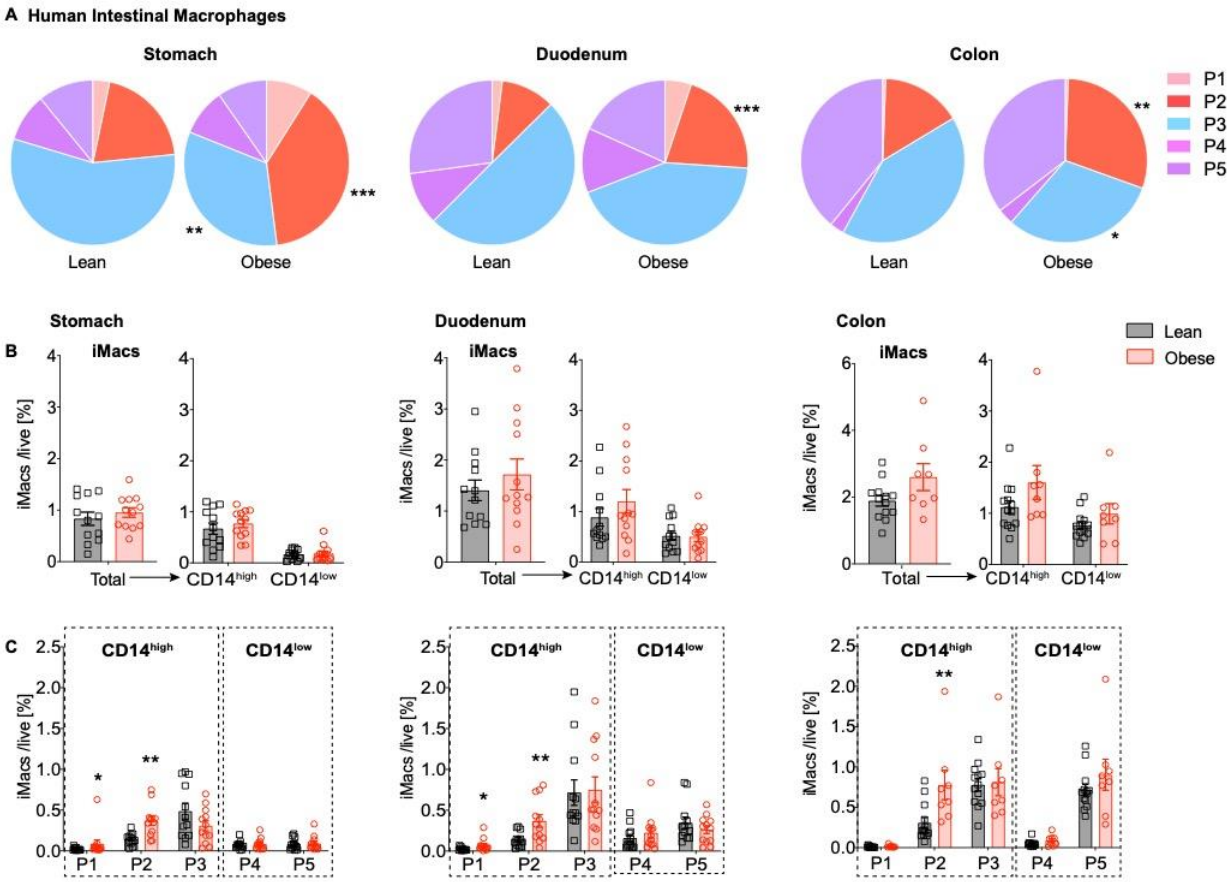

Supplemental Figure 7 (Related to Figure 7). Pro-inflammatory Intestinal Macrophages also Increase in Stomach, Duodenum and Colon of Obese Subjects

(**A**) Proportional distribution of human intestinal macrophages (iMacs) in stomach, duodenum and colon isolated from lean (black, BMI <27 kg/m^2) and obese subjects (red, BMI >32 kg/m^2) (n=8-13).

(**B-C**) Frequencies of human iMacs: total, CD14^{high}/CD14^{low} (**B**), and P1-P5 subpopulations (**C**) isolated from lean (black) or obese subjects (red) from the stomach, duodenum and colon transversum (n=8-13).

Each point represents one subject. Statistical data are expressed as mean±SEM. *p<0.05. **p<0.01, unpaired Mann-Whitney U test with two tailed distribution.

Supplemental Tables with Titles and Legends

Table S1 (Related to Figures 2 and S2). Diet composition of control diets and HFD

Diet	Fat	Protein	Carbohydrates	Fibers
Chow diet	4.5 % Crude fat	18.5 %	35 % Starch	4.5 %
Coconut HFD	58 % Coconut fat (Soybean and Coconut Oil)	16.4 %	25.5 % (Maltodextrin 10, Sucrose)	0.5 %
Starch	10 % Lard fat (Soybean Oil and Lard)	20 %	70 % Starch (Maltodextrin 10, Sucrose)	0 %
Lard HFD	60 % Lard fat (Soybean Oil and Lard)	20 %	20 % (Maltodextrin 10, Sucrose)	0 %

Units in kcal%.

Table S2 (Related to STAR Methods). Primers sequences used for quantitative RT-PCR

Gene	Forward Primer	Reverse Primer
Housekeeping genes		
B2m	5′ TTCTGGTGCTTGTCTCACTGA	5′ CAGTATGTTCGGCTTCCCATTC
Ppia	5′ GAGCTGTTTGCAGACAAAGTTC	5′ CCCTGGCACATGAATCCTGG
Inflammation markers		
Tnf	5′ ACTGAACTTCGGGGTGATCG	5′ TGAGGGTCTGGGCCATAGAA
Il6	5′ GGATACCACTCCCAACAGACCT	5′ GCCATTGCACAACTCTTTTCTC
Il1b	5′ GCAACTGTTCCTGAACTCAACT	5′ ATCTTTTGGGGTCCGTCAACT
Kc	5′ CTGGGATTCACCTCAAGAACATC	5′ CAGGGTCAAGGCAAGCCTC
Il10	5′ AGGCGCTGTCATCGATTTCTC	5′ GCCTTGTAGACACCTTGGTCTT
Il18	5′TCTTGCGTCAACTTCAAGGA	5′GTGAAGTCGGCCAAAGTTGT
Il22	5′TTG AGG TGT CCA ACT TCC AGC A	5′AGC CGG ACG TCT GTG TTG TTA
Tgfb1	5′CTCTCCACCTGCAAGACCAT	5′CGAGCCTTAGTTTGGACAGG
Immune cells		
Ly6c	5′ GCAGTGCTACGAGTGCTATGG	5′ ACTGACGGGTCTTTAGTTTCCTT
Cd68	5′ GCAGCACAGTGGACATTCAT	5′ AGAGAAACATGGCCC GAAGT
Emr1	5′ GCC CAG GAGTGGAATGTCAA	5′ CAGACACTCATCAACATCTGCG

Table S3 (Related to STAR Methods). Primers sequences used for 16S amplicon PCR

1	CTAAGGTAAC	**33**	TTCTCATTGAAC	**65**	TCCTGGCACATC
2	TAAGGAGAAC	**34**	TCGCATCGTTC	**66**	CCGCAATCATC
3	AAGAGGATTC	**35**	TAAGCCATTGTC	**67**	TTCCTACCAGTC
4	TACCAAGATC	**36**	AAGGAATCGTC	**68**	TCAAGAAGTTC
5	CAGAAGGAAC	**37**	CTTGAGAATGTC	**69**	TTCAATTGGC
6	CTGCAAGTTC	**38**	TGGAGGACGGAC	**70**	CCTACTGGTC
7	TTCGTGATTC	**39**	TAACAATCGGC	**71**	TGAGGCTCCGAC
8	TTCCGATAAC	**40**	CTGACATAATC	**72**	CGAAGGCCACAC
9	TGAGCGGAAC	**41**	TTCCACTTCGC	**73**	TCTGCCTGTC
10	CTGACCGAAC	**42**	AGCACGAATC	**74**	CGATCGGTTC
11	TCCTCGAATC	**43**	CTTGACACCGC	**75**	TCAGGAATAC
12	TAGGTGGTTC	**44**	TTGGAGGCCAGC	**76**	CGGAAGAACCTC
13	TCTAACGGAC	**45**	TGGAGCTTCCTC	**77**	CGAAGCGATTC
14	TTGGAGTGTC	**46**	TCAGTCCGAAC	**78**	CAGCCAATTCTC
15	TCTAGAGGTC	**47**	TAAGGCAACCAC	**79**	CCTGGTTGTC
16	TCTGGATGAC	**48**	TTCTAAGAGAC	**80**	TCGAAGGCAGGC
17	TCTATTCGTC	**49**	TCCTAACATAAC	**81**	CCTGCCATTCGC
18	AGGCAATTGC	**50**	CGGACAATGGC	**82**	TTGGCATCTC
19	TTAGTCGGAC	**51**	TTGAGCCTATTC	**83**	CTAGGACATTC
20	CAGATCCATC	**52**	CCGCATGGAAC	**84**	CTTCCATAAC
21	TCGCAATTAC	**53**	CTGGCAATCCTC	**85**	CCAGCCTCAAC
22	TTCGAGACGC	**54**	CCGGAGAATCGC	**86**	CTTGGTTATTC
23	TGCCACGAAC	**55**	TCCACCTCCTC	**87**	TTGGCTGGAC
24	AACCTCATTC	**56**	CAGCATTAATTC	**88**	CCGAACACTTC
25	CCTGAGATAC	**57**	TCTGGCAACGGC	**89**	TCCTGAATCTC
26	TTACAACCTC	**58**	TCCTAGAACAC	**90**	CTAACCACGGC
27	AACCATCCGC	**59**	TCCTTGATGTTC	**91**	CGGAAGGATGC
28	ATCCGGAATC	**60**	TCTAGCTCTTC	**92**	CTAGGAACCGC
29	TCGACCACTC	**61**	TCACTCGGATC	**93**	CTTGTCCAATC
30	CGAGGTTATC	**62**	TTCCTGCTTCAC	**94**	TCCGACAAGC
31	TCCAAGCTGC	**63**	CCTTAGAGTTC	**95**	CGGACAGATC
32	TCTTACACAC	**64**	CTGAGTTCCGAC	**96**	TTAAGCGGTC

REFERENCES

Amezquita, R.A., Lun, A.T.L., Becht, E., Carey, V.J., Carpp, L.N., Geistlinger, L., Martini, F., Rue-Albrecht, K., Risso, D., Soneson, C., et al. (2019). Orchestrating single-cell analysis with Bioconductor. Nature methods.

Aran, D., Looney, A.P., Liu, L., Wu, E., Fong, V., Hsu, A., Chak, S., Naikawadi, R.P., Wolters, P.J., Abate, A.R., et al. (2019). Reference-based analysis of lung single-cell sequencing reveals a transitional profibrotic macrophage. Nat Immunol *20*, 163-172.

Backhed, F., Ding, H., Wang, T., Hooper, L.V., Koh, G.Y., Nagy, A., Semenkovich, C.F., and Gordon, J.I. (2004). The gut microbiota as an environmental factor that regulates fat storage. Proc Natl Acad Sci U S A *101*, 15718-15723.

Bain, C.C., Bravo-Blas, A., Scott, C.L., Perdiguero, E.G., Geissmann, F., Henri, S., Malissen, B., Osborne, L.C., Artis, D., and Mowat, A.M. (2014). Constant replenishment from circulating monocytes maintains the macrophage pool in the intestine of adult mice. Nat Immunol *15*, 929-937.

Bain, C.C., Scott, C.L., Uronen-Hansson, H., Gudjonsson, S., Jansson, O., Grip, O., Guilliams, M., Malissen, B., Agace, W.W., and Mowat, A.M. (2013). Resident and pro-inflammatory macrophages in the colon represent alternative context-dependent fates of the same Ly6Chi monocyte precursors. Mucosal Immunol *6*, 498-510.

Brennecke, P., Anders, S., Kim, J.K., Kolodziejczyk, A.A., Zhang, X., Proserpio, V., Baying, B., Benes, V., Teichmann, S.A., Marioni, J.C., et al. (2013). Accounting for technical noise in single-cell RNA-seq experiments. Nature methods *10*, 1093-1095.

Bujko, A., Atlasy, N., Landsverk, O.J.B., Richter, L., Yaqub, S., Horneland, R., Oyen, O., Aandahl, E.M., Aabakken, L., Stunnenberg, H.G., et al. (2018). Transcriptional and functional profiling defines human small intestinal macrophage subsets. J Exp Med *215*, 441-458.

Cao, W., Manicassamy, S., Tang, H., Kasturi, S.P., Pirani, A., Murthy, N., and Pulendran, B. (2008). Toll-like receptor-mediated induction of type I interferon in plasmacytoid dendritic cells requires the rapamycin-sensitive PI(3)K-mTOR-p70S6K pathway. Nat Immunol *9*, 1157-1164.

Caporaso, J.G., Kuczynski, J., Stombaugh, J., Bittinger, K., Bushman, F.D., Costello, E.K., Fierer, N., Pena, A.G., Goodrich, J.K., Gordon, J.I., et al. (2010). QIIME allows analysis of high-throughput community sequencing data. Nat Methods *7*, 335-336.

de La Serre, C.B., Ellis, C.L., Lee, J., Hartman, A.L., Rutledge, J.C., and Raybould, H.E. (2010). Propensity to high-fat diet-induced obesity in rats is associated with changes in the gut microbiota and gut inflammation. American journal of physiology. Gastrointestinal and liver physiology *299*, G440-448.

Ding, S., Chi, M.M., Scull, B.P., Rigby, R., Schwerbrock, N.M., Magness, S., Jobin, C., and Lund, P.K. (2010). High-fat diet: bacteria interactions promote intestinal inflammation which precedes and correlates with obesity and insulin resistance in mouse. PLoS One *5*, e12191.

Dror, E., Dalmas, E., Meier, D.T., Wueest, S., Thevenet, J., Thienel, C., Timper, K., Nordmann, T.M., Traub, S., Schulze, F., et al. (2017). Postprandial macrophage-derived IL-1beta stimulates insulin, and both synergistically promote glucose disposal and inflammation. Nat Immunol *18*, 283-292.

Edgar, R.C. (2010). Search and clustering orders of magnitude faster than BLAST. Bioinformatics *26*, 2460-2461.

Garcia-Alonso, L., Holland, C.H., Ibrahim, M.M., Turei, D., and Saez-Rodriguez, J. (2019). Benchmark and integration of resources for the estimation of human transcription factor activities. Genome Res *29*, 1363-1375.

Griffiths, J.A., Richard, A.C., Bach, K., Lun, A.T.L., and Marioni, J.C. (2018). Detection and removal of barcode swapping in single-cell RNA-seq data. Nat Commun *9*, 2667.

Harwood, F.C., Klein Geltink, R.I., O'Hara, B.P., Cardone, M., Janke, L., Finkelstein, D., Entin, I., Paul, L., Houghton, P.J., and Grosveld, G.C. (2018). ETV7 is an essential component of a rapamycin-insensitive mTOR complex in cancer. Sci Adv *4*, eaar3938.

Heng, T.S., Painter, M.W., and Immunological Genome Project, C. (2008). The Immunological Genome Project: networks of gene expression in immune cells. Nat Immunol *9*, 1091-1094.

Ilicic, T., Kim, J.K., Kolodziejczyk, A.A., Bagger, F.O., McCarthy, D.J., Marioni, J.C., and Teichmann, S.A. (2016). Classification of low quality cells from single-cell RNA-seq data. Genome Biol *17*, 29.

Jordan, S., Tung, N., Casanova-Acebes, M., Chang, C., Cantoni, C., Zhang, D., Wirtz, T.H., Naik, S., Rose, S.A., Brocker, C.N., et al. (2019). Dietary Intake Regulates the Circulating Inflammatory Monocyte Pool. Cell *178*, 1102-1114 e1117.

Kawano, Y., Nakae, J., Watanabe, N., Kikuchi, T., Tateya, S., Tamori, Y., Kaneko, M., Abe, T., Onodera, M., and Itoh, H. (2016). Colonic Pro-inflammatory Macrophages Cause Insulin Resistance in an Intestinal Ccl2/Ccr2-Dependent Manner. Cell Metab *24*, 295-310.

Kinnebrew, M.A., Buffie, C.G., Diehl, G.E., Zenewicz, L.A., Leiner, I., Hohl, T.M., Flavell, R.A., Littman, D.R., and Pamer, E.G. (2012). Interleukin 23 production by intestinal CD103(+)CD11b(+) dendritic cells in response to bacterial flagellin enhances mucosal innate immune defense. Immunity *36*, 276-287.

Koscso, B., Kurapati, S., Rodrigues, R.R., Nedjic, J., Gowda, K., Shin, C., Soni, C., Ashraf, A.Z., Purushothaman, I., Palisoc, M., et al. (2020). Gut-resident CX3CR1(hi) macrophages induce tertiary lymphoid structures and IgA response in situ. Sci Immunol *5*.

Lamming, D.W., Ye, L., Katajisto, P., Goncalves, M.D., Saitoh, M., Stevens, D.M., Davis, J.G., Salmon, A.B., Richardson, A., Ahima, R.S., et al. (2012). Rapamycin-induced insulin resistance is mediated by mTORC2 loss and uncoupled from longevity. Science *335*, 1638-1643.

Li, H., Limenitakis, J.P., Fuhrer, T., Geuking, M.B., Lawson, M.A., Wyss, M., Brugiroux, S., Keller, I., Macpherson, J.A., Rupp, S., et al. (2015). The outer mucus layer hosts a distinct intestinal microbial niche. Nature communications *6*, 8292.

Li, Y., Lee, P.Y., Kellner, E.S., Paulus, M., Switanek, J., Xu, Y., Zhuang, H., Sobel, E.S., Segal, M.S., Satoh, M., et al. (2010). Monocyte surface expression of Fcgamma receptor RI (CD64), a biomarker reflecting type-I interferon levels in systemic lupus erythematosus. Arthritis Res Ther *12*, R90.

Liberzon, A., Birger, C., Thorvaldsdottir, H., Ghandi, M., Mesirov, J.P., and Tamayo, P. (2015). The Molecular Signatures Database (MSigDB) hallmark gene set collection. Cell Syst *1*, 417-425.

Linke, M., Fritsch, S.D., Sukhbaatar, N., Hengstschlager, M., and Weichhart, T. (2017). mTORC1 and mTORC2 as regulators of cell metabolism in immunity. FEBS Lett *591*, 3089-3103.

Luck, H., Tsai, S., Chung, J., Clemente-Casares, X., Ghazarian, M., Revelo, X.S., Lei, H., Luk, C.T., Shi, S.Y., Surendra, A., et al. (2015). Regulation of obesity-related insulin resistance with gut anti-inflammatory agents. Cell Metab *21*, 527-542.

Lun, A.T., McCarthy, D.J., and Marioni, J.C. (2016). A step-by-step workflow for low-level analysis of single-cell RNA-seq data with Bioconductor. F1000Res *5*, 2122.

Lun, A.T.L., and Marioni, J.C. (2017). Overcoming confounding plate effects in differential expression analyses of single-cell RNA-seq data. Biostatistics *18*, 451-464.

Lun, A.T.L., Riesenfeld, S., Andrews, T., Dao, T.P., Gomes, T., participants in the 1st Human Cell Atlas, J., and Marioni, J.C. (2019). EmptyDrops: distinguishing cells from empty droplets in droplet-based single-cell RNA sequencing data. Genome Biol *20*, 63.

Mamantopoulos, M., Ronchi, F., Van Hauwermeiren, F., Vieira-Silva, S., Yilmaz, B., Martens, L., Saeys, Y., Drexler, S.K., Yazdi, A.S., Raes, J., et al. (2017). Nlrp6- and ASC-Dependent Inflammasomes Do Not Shape the Commensal Gut Microbiota Composition. Immunity *47*, 339-348 e334.

McCarthy, D.J., Campbell, K.R., Lun, A.T., and Wills, Q.F. (2017). Scater: pre-processing, quality control, normalization and visualization of single-cell RNA-seq data in R. Bioinformatics *33*, 1179-1186.

Melsted, P., Booeshaghi, A.S., Gao, F., Beltrame, E., Lu, L., Hjorleifsson, K.E., Gehring, J., and Pachter, L. (2019a). Modular and efficient pre-processing of single-cell RNA-seq. bioRxiv, 673285.

Melsted, P., Ntranos, V., and Pachter, L. (2019b). The barcode, UMI, set format and BUStools. Bioinformatics *35*, 4472-4473.

Mowat, A.M., and Agace, W.W. (2014). Regional specialization within the intestinal immune system. Nat Rev Immunol *14*, 667-685.

Ogino, T., Nishimura, J., Barman, S., Kayama, H., Uematsu, S., Okuzaki, D., Osawa, H., Haraguchi, N., Uemura, M., Hata, T., et al. (2013). Increased Th17-inducing activity of CD14+ CD163 low myeloid cells in intestinal lamina propria of patients with Crohn's disease. Gastroenterology *145*, 1380-1391 e1381.

Pixley, F.J., and Stanley, E.R. (2004). CSF-1 regulation of the wandering macrophage: complexity in action. Trends Cell Biol *14*, 628-638.
Platt, A.M., Bain, C.C., Bordon, Y., Sester, D.P., and Mowat, A.M. (2010). An independent subset of TLR expressing CCR2-dependent macrophages promotes colonic inflammation. J Immunol *184*, 6843-6854.

Poitou, C., Dalmas, E., Renovato, M., Benhamo, V., Hajduch, F., Abdennour, M., Kahn, J.F., Veyrie, N., Rizkalla, S., Fridman, W.H., et al. (2011). CD14dimCD16+ and CD14+CD16+ monocytes in obesity and during weight loss: relationships with fat mass and subclinical atherosclerosis. Arterioscler Thromb Vasc Biol *31*, 2322-2330.

Qualls, J.E., Kaplan, A.M., van Rooijen, N., and Cohen, D.A. (2006). Suppression of experimental colitis by intestinal mononuclear phagocytes. J Leukoc Biol *80*, 802-815.

Robinson, M.D., McCarthy, D.J., and Smyth, G.K. (2010). edgeR: a Bioconductor package for differential expression analysis of digital gene expression data. Bioinformatics *26*, 139-140.

Robinson, M.D., and Oshlack, A. (2010). A scaling normalization method for differential expression analysis of RNA-seq data. Genome Biol *11*, R25.

Rogacev, K.S., Cremers, B., Zawada, A.M., Seiler, S., Binder, N., Ege, P., Grosse-Dunker, G., Heisel, I., Hornof, F., Jeken, J., et al. (2012). CD14++CD16+ monocytes independently predict cardiovascular events: a cohort study of 951 patients referred for elective coronary angiography. J Am Coll Cardiol *60*, 1512-1520.

Rossol, M., Kraus, S., Pierer, M., Baerwald, C., and Wagner, U. (2012). The CD14(bright) CD16+ monocyte subset is expanded in rheumatoid arthritis and promotes expansion of the Th17 cell population. Arthritis Rheum *64*, 671-677.

Schmitz, F., Heit, A., Dreher, S., Eisenacher, K., Mages, J., Haas, T., Krug, A., Janssen, K.P., Kirschning, C.J., and Wagner, H. (2008). Mammalian target of rapamycin (mTOR) orchestrates the defense program of innate immune cells. Eur J Immunol *38*, 2981-2992.

Smythies, L.E., Sellers, M., Clements, R.H., Mosteller-Barnum, M., Meng, G., Benjamin, W.H., Orenstein, J.M., and Smith, P.D. (2005). Human intestinal macrophages display profound inflammatory anergy despite avid phagocytic and bacteriocidal activity. J Clin Invest *115*, 66-75.

Subramanian, A., Tamayo, P., Mootha, V.K., Mukherjee, S., Ebert, B.L., Gillette, M.A., Paulovich, A., Pomeroy, S.L., Golub, T.R., Lander, E.S., et al. (2005). Gene set enrichment analysis: A knowledge-based approach for interpreting genome-wide expression profiles. Proc Natl Acad Sci U S A *102*, 15545-15550.

Sundquist, A., Bigdeli, S., Jalili, R., Druzin, M.L., Waller, S., Pullen, K.M., El-Sayed, Y.Y., Taslimi, M.M., Batzoglou, S., and Ronaghi, M. (2007). Bacterial flora-typing with targeted, chip-based Pyrosequencing. BMC Microbiol *7*, 108.

Tamoutounour, S., Guilliams, M., Montanana Sanchis, F., Liu, H., Terhorst, D., Malosse, C., Pollet, E., Ardouin, L., Luche, H., Sanchez, C., et al. (2013). Origins and functional specialization of macrophages and of conventional and monocyte-derived dendritic cells in mouse skin. Immunity *39*, 925-938.

Tamoutounour, S., Henri, S., Lelouard, H., de Bovis, B., de Haar, C., van der Woude, C.J., Woltman, A.M., Reyal, Y., Bonnet, D., Sichien, D., et al. (2012). CD64 distinguishes macrophages from dendritic cells in the gut and reveals the Th1-inducing role of mesenteric lymph node macrophages during colitis. Eur J Immunol *42*, 3150-3166.

Um, S.H., Frigerio, F., Watanabe, M., Picard, F., Joaquin, M., Sticker, M., Fumagalli, S., Allegrini, P.R., Kozma, S.C., Auwerx, J., et al. (2004). Absence of S6K1 protects against age- and diet-induced obesity while enhancing insulin sensitivity. Nature *431*, 200-205.

Utzschneider, K.M., Kratz, M., Damman, C.J., and Hullar, M. (2016). Mechanisms Linking the Gut Microbiome and Glucose Metabolism. J Clin Endocrinol Metab *101*, 1445-1454.

Vallejos, C.A., Risso, D., Scialdone, A., Dudoit, S., and Marioni, J.C. (2017). Normalizing single-cell RNA sequencing data: challenges and opportunities. Nat Methods *14*, 565-571.

Waise, T.M.Z., Rasti, M., Duca, F.A., Zhang, S.Y., Bauer, P.V., Rhodes, C.J., and Lam, T.K.T. (2019). Inhibition of upper small intestinal mTOR lowers plasma glucose levels by inhibiting glucose production. Nature communications *10*, 714.

Whiteley, A.S., Jenkins, S., Waite, I., Kresoje, N., Payne, H., Mullan, B., Allcock, R., and O'Donnell, A. (2012). Microbial 16S rRNA Ion Tag and community metagenome sequencing using the Ion Torrent (PGM) Platform. J Microbiol Methods *91*, 80-88.

Winer, D.A., Luck, H., Tsai, S., and Winer, S. (2016). The Intestinal Immune System in Obesity and Insulin Resistance. Cell Metab *23*, 413-426.

Wu, D., and Smyth, G.K. (2012). Camera: a competitive gene set test accounting for inter-gene correlation. Nucleic Acids Res *40*, e133.
Ziegler-Heitbrock, L., Ancuta, P., Crowe, S., Dalod, M., Grau, V., Hart, D.N., Leenen, P.J., Liu, Y.J., MacPherson, G., Randolph, G.J., et al. (2010). Nomenclature of monocytes and dendritic cells in blood. Blood *116*, e74-80.

Zoncu, R., Efeyan, A., and Sabatini, D.M. (2011). mTOR: from growth signal integration to cancer, diabetes and ageing. Nat Rev Mol Cell Biol *12*, 21-35.

5 Discussion

So far, intestinal macrophage subpopulations have been mainly studied in the context of inflammatory gastrointestinal tract disorders such as colitis and inflammatory bowel disease[137,138,142]. In terms of metabolic disease, evidence points towards pro-inflammatory macrophages that "remote control" insulin resistance and adipose tissue inflammation in an intestinal CCL2/CCR2-dependent manner[135,136]. Intestinal macrophages are not a homogenous cell population and can be classified into five subpopulations (P1-P5) along a differentiation trajectory. However, the role of these intestinal macrophage subpopulations has not yet been studied in obesity. Our study provides a detailed characterization of intestinal macrophage subpopulations in obesity both in mice and humans. We found that HFD-induced intestinal macrophage activation is directly linked to impaired glucose metabolism, potentially in a mTOR-dependent manner. A deepened understanding of the (patho-)physiological role of intestinal innate immunity could help to develop novel therapeutic targets for obesity-related glucose intolerance.

5.1 Pro-inflammatory Intestinal Macrophage Subpopulations are Transiently Increased upon Food Intake and Chronically Elevated Following High-Fat Diet Feeding

We found that pro-inflammatory/monocyte-derived intestinal macrophage subpopulations respond to nutritional signals, as subpopulation P1 transiently increases upon food intake compared to the fasted state. With chronic HFD, P1 and P2 intestinal macrophage subpopulations become chronically elevated. Intestinal inflammation appears in mice already after 1 week of HFD and persists up to 3 months of HFD, however, less pronounced at the later time points. This could be explained by a smaller stomach weight after 1 and 3 months of HFD, indicating reduced HFD consumption at later time points. This is in agreement with previously reported transient hyperphagia at the start of HFD[121,185,186]. In addition, adaptation processes to dietary fat might explain why we see the highest effect on intestinal macrophages so early.

Intestinal inflammation characterized by increased pro-inflammatory macrophages (P1/P2) is associated with impaired glucose tolerance and elevated insulin secretion. However, differences in body weight and adipose tissue inflammation occur later. Hence, intestinal inflammation precedes adipose tissue alterations, suggestive for a potent role in the initiation of glucose dysregulation. As it has been shown that macrophages play a physiological role in supporting postprandial insulin secretion[101], it appears likely that intestinal macrophages are altered in phenotype and function in a state of overnutrition and impact on glucose homeostasis.

5.2 Gut Microbiota are essential for the Increase in Pro-Inflammatory Intestinal Macrophage Subpopulations, while the Fat Source Modulates its Magnitude

In our study we took great care in assessing the influence of different dietary compositions regarding fiber content (fiber-rich chow and fiber-deficient purified starch control diet) and fat source (lard- and coconut-based HFD) on intestinal macrophage subpopulations and glycemic control. Such a detailed assessment is of importance as the classical "chow" diet contains fibers and differs depending on seasonal harvests unlike purified/ standardized HFDs. Therefore, we used an additional control diet, named starch, that is purified/ standardized and identical to the lard-based HFD except for its fat content.

The observed phenotypical switch to pro-inflammatory intestinal macrophages (P1/P2) associated with impaired glycemic control is independent of fiber content (chow and starch) and fat source (lard or coconut) of the diet. However, the fat source seems to modulate the magnitude of the effect as lard-based HFD induces more detrimental changes with regards to glycemic control as well as macrophage activation. This indicates that the inflammatory innate immune response might correlate with the magnitude of metabolic consequences. Macroscopically, we observed larger caecum and colon sizes under fiber-rich control diet, potentially caused by an increased osmotic load. Therefore, colon shortening under HFD might be not caused by inflammation as other studies suggested when comparing to a chow diet with fibers[135,187].

Last, we also assessed how gut microbiota are changed with the different diets and how these changes correlate with glycemic control. Both HFDs induced different microbial changes, but both caused glucose intolerance. The occurrence of a shift in microbiota composition to a non-specific "dysbiotic" state, rather than a shift to a defined microbial composition could be related to macrophage recruitment under HFD condition. This suggests that microbial dysbiosis per se rather than a specific microbial composition at phylum and genus level[112,119,120] is related to obesity-associated glucose dysregulation. This is in agreement with another study showing that short-term HFD-induced insulin resistance is not causally related to the microbiota composition[121]. Hence, the presence or an as of yet unidentified factor of microbiota seems to determine glycemic control. This notion is supported by the fact that GF mice are protected from metabolic disease, which show lower recruitment of immune cells into the gut[188]. In line with that, we found low numbers of intestinal macrophages in GF mice and no increase in its pro-inflammatory subpopulations upon HFD feeding. These findings thus led us to propose that the number of macrophages in the gut is interlinked with glucose metabolism.

5.3 Macrophage Numbers are Linked to Glycemic Control

To test whether the number of macrophages are linked to glycemic control, we dose-dependently depleted macrophages by increasing doses of the colony stimulating factor-1 receptor (CSF1R) inhibitor BLZ945. CSF1R is important for macrophage development and survival[189]. Indeed, CSF1R blockage demonstrated gradual macrophage depletion linked with improvements in glycemic control such as lower fasting blood glucose, improved glucose tolerance and insulin sensitivity.

To further address the specific role of pro-inflammatory intestinal macrophage subpopulations, we also examined the metabolic and macrophage phenotype of CCR2-/- mice. CCR2-/- mice are known in the context of obesity to have reduced food intake and improved insulin resistance[135,190]. Unexpectedly, CCR2-/- mice showed a reappearance of pro-inflammatory Ly6C^{high} macrophages in the colon after 1 week of HFD, however, in much lower absolute numbers. This suggests an additional CCR2-independent monocyte recruitment process into the gut during short-term HFD. After 2 months, we confirmed previous literature showing that CCR2-/- mice are lacking predominantly the pro-inflammatory intestinal macrophages (P1/P2)[138]. Also, they exhibit reduced macrophage infiltration into the adipose tissue, consistent with what is already known[190]. In addition, glycemic control is modestly improved in CCR2-/- under HFD, however, less pronounced than in previous studies[135,190]. Altogether, these data provide evidence that not only the number of intestinal macrophages plays a role in the regulation of glucose homeostasis, but also pro-inflammatory subpopulations.

5.4 Colon-specific Macrophage Depletion Improves Glucose Metabolism

To establish a direct causal link between intestinal macrophages and glucose metabolism, we established an *in vivo* colon-specific macrophage depletion model. Colon-specific macrophage depletion leads to improved glucose tolerance, insulin secretion and sensitivity as well as islet cell function, independently of the microbiota. So far, there is no other mouse model available in which intestinal macrophages are specifically targeted. Mechanistically, the metabolic improvements may be partially attributed to GLP-1 as glucose tolerance was not improved under GLP-1 inhibition. GLP-1 has been shown to induce M2 polarization of human macrophages via STAT3 activation as a possible protective effect against diabetes[191].

To compare colon-specific macrophage depletion to systemic macrophage depletion, we also injected clodronate liposomes intraperitoneally. Here, intraperitoneal clodronate liposomes primarily improved insulin resistance, mostly driven by adipose tissue macrophage

depletion. Hence, in comparison to systemic depletion, our intrarectal macrophage depletion model clearly highlights intestinal macrophages as an important initiator of metabolic disease.

5.5 Transcriptional Response upon HFD in Intestinal Macrophages Involves an Interferon-Signature and Metabolic Shift, potentially through mTOR-Signaling

To identify potential mechanisms that control intestinal macrophage activation in obesity, we investigated the transcriptional response of intestinal macrophages to HFD. The most pronounced effects we observed in our RNA-seq data concern interferon IFN-γ and IFN-α, suggesting that interferons play a key role in intestinal innate response induced by HFD. We found interferon regulators *Irf1/Irf7/Irf8* and *Stat1/Stat2* up-regulated by HFD, which potentially represent the transcription factors involved in interferon signaling[192]. Another study also suggests a connection between IFN in intestinal immunity and glycemic control as the gut-specific anti-inflammatory agent, 5-aminosalicylic acid, reduced colonic IFN-γ levels and improved glucose tolerance[193]. Consistent with a link between IFN, intestinal macrophages an glycemic control, GF mice, who are protected from metabolic disease, show also lower IFN-γ production as well no IFN-I response in the gut[194]. The first pathway shown to be activated by interferons is the JAK (Janus activated kinase)-STAT (signal transducer and activator of transcription) pathway[195–197]. However, other pathways also regulate interferon signaling such as the mitogen-activated protein kinase (MAPK) p38 and the phosphatidylinositol 3-kinase (PI3K) signaling pathway[198].

In addition to IFN-γ and IFN-α signaling, we found that obesity-associated intestinal inflammation is strongly linked to oxidative phosphorylation. Increased transcript abundance of genes relating oxidative phosphorylation was consistent with enhanced mitochondrial activity in all intestinal macrophage subpopulations under HFD.

Moreover, interferon-signaling and energy metabolism have been extensively described in conjunction with the mTOR-pathway[199–204]. It was shown that mTOR is required by innate immune cells for their defense program involving type-I interferons [199,205]. As both interferon signaling and energy metabolism is transcriptionally regulated by HFD in our RNA-seq data, we postulated that mTOR might govern the transcriptional changes in intestinal macrophages observed upon HFD. Indeed, mTOR is activated in all intestinal macrophages, similar to their enhanced mitochondrial activity. These findings indicate an enhanced anabolic state of intestinal macrophages induced by HFD[206–208]. Interestingly, mTOR activation occurs in response to different nutrients and is exaggerated in a nutrient-overabundant state such as

obesity[209]. Thus, intestinal inflammation upon HFD might be initiated by mTOR activation, potentially promoting the interferon-response and metabolic alterations.

5.6 Colon-specific mTOR Inhibition Restores Glycemic Control

We next assessed the role of mTOR inhibition on intestinal macrophages and glycemic control. Although activation of mTOR signaling has previously been associated with a state of overnutrition[210], one of its best known inhibitors – rapamycin – has been described to induce insulin resistance[211,212]. Accordingly, we found that systemic mTOR inhibition is associated with glucose intolerance and insulin resistance as previously described[211–215].

However, colon-specific inhibition of mTOR *in vivo* by intrarectal administration of rapamycin led to increased insulin secretion via enhanced GLP-1 secretion and hence improved islet cell function, reminiscent of the effect of colon-specific macrophage depletion. A previous study assessing mTOR inhibition in the small intestine also found improved glycemic control and suggested reduced glucose production as mechanism of action[216]. Therefore, mTOR seems to be a key signaling pathway in intestinal macrophages that impacts their transcriptional response upon HFD.

5.7 Pro-inflammatory Intestinal Macrophages are also Increased in Human Obese Subjects

To validate our mouse data in human disease, we characterized human intestinal macrophages in obese versus lean individuals. We found that pro-inflammatory macrophages (P2) are also increased in obese human subjects. So far, an increase in pro-inflammatory intestinal macrophages in humans has only been documented in the context of celiac disease[217] or Crohn`s disease[218,219].

Similar to mice, human intestinal macrophages comprise a continuum of cells derived from blood monocytes[158]. In the present study, we observed higher $CD33^{+}CD64^{+}CD14^{+}$ monocytes. After further distinction into monocyte subpopulations (classical, intermediate and non-classical monocytes), mainly intermediate monocytes were seen to be upregulated. Other studies have shown that increased non-classical and intermediate monocytes are linked with WHO obesity classification and fat mass[220–225]. However, we did not find increased non-classical monocytes as in[222,226]. $CD64^{+}$ expression on monocytes is associated with inflammatory responses including sepsis and infection[227,228] as well as involving interferon signaling[229]. The literature has shown that not only obesity and diabetes [230,231] but also dietary intake is linked to higher circulating inflammatory monocytes[232]. Thus, it is plausible that overnutrition increases bone marrow-derived blood monocytes that are recruited to the gut wall,

where they accumulate and influence glucose dysregulation by their pro-inflammatory phenotype.

5.8 Strengths and Limitations of the Study

The major strength of our work is our pharmacological approach of colon-specific macrophage depletion, highlighting intestinal macrophages as key drivers of glucose dysregulation in obesity. Although predominantly pro-inflammatory subpopulation P2 was depleted by our approach, currently there is no way to specifically target this subgroup of intestinal macrophages. However, as the vast majority of *in vivo* approaches only achieve systemic depletion of tissue macrophages[233], at least we found a strategy to dissect *in vivo* colon-specific effects. Effects because of increased local apoptosis cannot completely be ruled out, however we could not detect any increase in pro-/anti-inflammatory cytokines in the colon or circulation.

We found that improved β-cell function might be partially mediated through glucagon-like peptide-1 (GLP-1) secretion. However, also other pathways could link intestinal macrophages with β-cell function. The question remains whether intestinal macrophages directly traffic from the gut to pancreatic islets as a higher migratory potential has been suggested for monocyte-derived CXCR1^{inter} macrophages of the gut[234]. Alternatively, cytokines from pro-inflammatory macrophages could disseminate to the pancreas through the blood circulation, lymphatic vessels or even neuronal circuits. One mediator of the neural circuits, the muscarinergic signaling, was ruled out as atropine did not alter improved glycemic control in our macrophage depletion model.

The tissue-specific effects of mTOR on glucose homeostasis underline the importance of targeting macrophage activity in a specific cellular compartment. However, it might be also possible that additional mediators contribute to the metabolic phenotype of intestinal macrophages in obesity, independent of mTOR. Hence, it would be also of interest to elucidate other potential actors involved in interferon-signaling such Irf7 or JAK-STAT signaling.

The validation of our results in human tissue is a major advance, as there is considerable heterogeneity in human data compared to mice in terms of differences in sex, age, diets and microbiota. However, monocyte transfer studies would be needed to understand the process of enhanced recruitment and their impact in changing the differentiation and phenotype of intestinal macrophages. Finally, single-cell techniques and targeted manipulations of human intestinal macrophages in obese or patients with T2D would be of high interest.

5.9 Clinical Relevance

Our data point towards an interaction between HFD, the inflammatory response of intestinal macrophages – involving interferon signaling via mTOR – and impaired glycemic control. A deepened understanding of the pathophysiological role of intestinal macrophages and the underlying mechanisms might spur the development of therapeutic strategies to modulate glycemic response. Our colon-specific approaches clearly highlight that future therapies might benefit more from a tissue- or even cell-specific rather than systemic manipulation. Such targeted therapies that moderate intestinal macrophage activation could be achieved by suppositories for instance via IFN-γ and mTOR inhibition. In sum, targeted approaches by specifically impacting intestinal inflammation might represent a novel avenue in treating β-cell dysfunction in the onset of metabolic disease.

6 Conclusion

Overall, our findings reveal a direct cross-talk between nutritional cues, intestinal macrophage subpopulations and insulin-producing β-cells. We identified that intestinal macrophage activation upon HFD involves an interferon signature and metabolic shift, potentially via mTOR activation. By colon-specific depletion of macrophages as well as inhibition of their activation, we highlighted that colonic macrophages are directly linked to glycemic control. Translational data of human gut tissue confirm the switch to pro-inflammatory intestinal macrophages in obese subjects, potentially by enhanced monocyte influx. The present study demonstrates that not only adipose tissue inflammation, but also intestinal innate immunity contributes to glycemic dysfunction in obesity via pro-inflammatory macrophages. Understanding the underlying mechanism of intestinal macrophage activity may have important implications for the development of therapies modulating metabolic and inflammatory consequences of metabolic disease.

References

1. WHO. Obesity-and-Overweight @ Www.Who.Int. (2017).
2. Elabbassi, W. N. & Haddad, H. A. The epidemic of the metabolic syndrome. *Saudi Med. J.* **26**, 373–375 (2005).
3. Chadt, A., Scherneck, S., Joost, H.-G. & Al-Hasani, H. Molecular links between Obesity and Diabetes: "Diabesity." in *Endotext* (eds. Feingold, K. R. et al.) (2000).
4. Gregor, M. F. & Hotamisligil, G. S. Inflammatory Mechanisms in Obesity. *Annu. Rev. Immunol.* **29**, 415–445 (2011).
5. Weisberg, S. P. *et al.* Obesity is associated with macrophage accumulation in adipose tissue. *J. Clin. Invest.* **112**, 1796–1808 (2003).
6. Monteiro, R. & Azevedo, I. Chronic inflammation in obesity and the metabolic syndrome. *Mediators Inflamm.* **2010**, (2010).
7. de la Iglesia, R. *et al.* Dietary strategies implicated in the prevention and treatment of metabolic syndrome. *Int. J. Mol. Sci.* **17**, 1–21 (2016).
8. Soares, R. & Costa, C. *Oxidative stress, inflammation, and angiogenesis in the metabolic syndrome*. (2009). doi:10.1007/978-1-4020-9701-0.
9. Mottillo, S. *et al.* The metabolic syndrome and cardiovascular risk: A systematic review and meta-analysis. *J. Am. Coll. Cardiol.* **56**, 1113–1132 (2010).
10. World Health Organization. DALY estimates, 2000-2016. (2018).
11. WHO, K. facts of diabetes mellitus. Diabetes @ Www.Who.Int. 2 (2017).
12. Chadt, A., Scherneck, S., Joost, H.-G. & Al-Hasani, H. Molecular links between Obesity and Diabetes: "Diabesity." *Endotext* (2000).
13. Roche, A. F., Sievogel, R. M., Chumlea, W. C. & Webb, P. Grading body fatness from limited anthropometric data. *Am. J. Clin. Nutr.* **34**, 2831–2838 (1981).
14. Clinical guidelines on the identification, evaluation, and treatment of overweight and obesity in adults: executive summary. Expert Panel on the Identification, Evaluation, and Treatment of Overweight in Adults. *Am. J. Clin. Nutr.* **68**, 899–917 (1998).
15. Alegría Ezquerra, E., Castellano Vázquez, J. M. & Barrero, A. A. Obesity, metabolic syndrome and diabetes: Cardiovascular implications and therapy. *Rev. Esp. Cardiol.* **61**, 752–764 (2008).
16. Al-Goblan, A. S., Al-Alfi, M. A. & Khan, M. Z. Mechanism linking diabetes mellitus and obesity. *Diabetes, Metab. Syndr. Obes. Targets Ther.* **7**, 587–591 (2014).
17. Association American Diabetes. Diagnosis and classification of diabetes mellitus. *Diabetes Care* **33**, S62–S69 (2010).
18. Kharroubi, A. T. Diabetes mellitus: The epidemic of the century. *World J. Diabetes* **6**, 850 (2015).
19. American Diabetes Association. Diagnosis and classification of diabetes mellitus. *Diabetes Care* **32**, S62-7 (2009).
20. Stone, M. A. *et al.* Incorrect and incomplete coding and classification of diabetes: A systematic review. *Diabet. Med.* **27**, 491–497 (2010).
21. Datei:Diabetes_mellitus_Typ_1 @ medlexi.de.
22. Maahs, D. M., West, N. A., Lawrence, J. M. & Mayer-Davis, E. J. Epidemiology of type 1 diabetes. *Endocrinol. Metab. Clin. North Am.* **39**, 481–497 (2010).
23. Devendra, D., Liu, E. & Eisenbarth, G. S. Type 1 diabetes: recent developments. *BMJ* **328**, 750–754 (2004).
24. Skyler, J. S. *et al.* Differentiation of diabetes by pathophysiology, natural history, and prognosis. *Diabetes* **66**, 241–255 (2017).
25. Daneman, D. Type 1 diabetes. *Lancet* **367**, 847–858 (2006).
26. Chen, L., Magliano, D. J. & Zimmet, P. Z. The worldwide epidemiology of type 2 diabetes mellitus - Present and future perspectives. *Nat. Rev. Endocrinol.* **8**, 228–236 (2012).
27. Halban, P. A. *et al.* β-Cell failure in type 2 diabetes: Postulated mechanisms and prospects for prevention and treatment. *J. Clin. Endocrinol. Metab.* **99**, 1983–1992 (2014).
28. Butler, A. E. *et al.* β-cell deficit and increased β-cell apoptosis in humans with type 2 diabetes. *Diabetes* **52**, 102–110 (2003).
29. Nolan, C. J., Ruderman, N. B., Kahn, S. E., Pedersen, O. & Prentki, M. Insulin resistance as a physiological defense against metabolic stress: Implications for the management of subsets of type 2 diabetes. *Diabetes* **64**, 673–686 (2015).
30. Watve, M. G. & Yajnik, C. S. Evolutionary origins of insulin resistance: A behavioral switch hypothesis. *BMC Evol. Biol.* **7**, 1–13 (2007).
31. Mergenthaler, P., Lindauer, U., Dienel, G. A. & Meisel, A. Sugar for the brain: the role of glucose in

physiological and pathological brain function. *Trends Neurosci.* **36**, 587–597 (2013).
32. Gerich, J. E. Control of glycaemia. *Baillieres. Clin. Endocrinol. Metab.* **7**, 551–586 (1993).
33. Aronoff, S. L., Berkowitz, K., Shreiner, B. & Want, L. Glucose Metabolism and Regulation: Beyond Insulin and Glucagon. *Diabetes Spectr.* **17**, 183–190 (2004).
34. Kaloyianni, M. & Freedland, R. A. Contribution of several amino acids and lactate to gluconeogenesis in hepatocytes isolated from rats fed various diets. *J. Nutr.* **120**, 116–122 (1990).
35. Vecchio, I., Tornali, C., Bragazzi, N. L. & Martini, M. The discovery of insulin: An important milestone in the history of medicine. *Front. Endocrinol.* **9**, 1–8 (2018).
36. Pfeifer, M. A., Halter, J. B. & Porte, D. Insulin secretion in diabetes mellitus. *Am. J. Med.* **70**, 579–588 (1981).
37. Clough, H. D., Allen, R. S. & Murlin, J. R. Aqueous Extracts of Pancreas. *Am. J. Physiol. Content* **68**, 213–238 (1924).
38. Bromer, W. W., Sinn, L. G., Staub, A. & Behrens, O. K. The amino acid sequence of glucagon. *Diabetes* **6**, 234–238 (1957).
39. Gerich, J. E. *et al.* Characterization of the glucagon response to hypoglycemia in man. *J. Clin. Endocrinol. Metab.* **38**, 77–82 (1974).
40. Moore, C. X. & Cooper, G. J. S. Co-secretion of amylin and insulin from cultured islet β-cells: Modulation by nutrient secretagogues, islet hormones and hypoglycemic agents. *Biochem. Biophys. Res. Commun.* **179**, 1–9 (1991).
41. Kieffer, T. J. & Habener, J. F. The glucagon-like peptides. *Endocr. Rev.* **20**, 876–913 (1999).
42. Drucker, D. J. The biology of incretin hormones. *Cell Metab.* **3**, 153–165 (2006).
43. Nadkarni, P., Chepurny, O. G. & Holz, G. G. Regulation of glucose homeostasis by GLP-1. *Prog. Mol. Biol. Transl. Sci.* **121**, 23–65 (2014).
44. Röder, P. V, Wu, B., Liu, Y. & Han, W. Pancreatic regulation of glucose homeostasis. *Exp. Mol. Med.* **48**, e219 (2016).
45. Dolenšek, J., Rupnik, M. S. & Stožer, A. Structural similarities and differences between the human and the mouse pancreas. *Islets* **7**, e1024405–e1024405 (2015).
46. Islam, M. S. *The islets of Langerhans*. *Adv. Exp. Med. and Biol.* vol. 654 (2010).
47. Brissova, M. *et al.* Assessment of human pancreatic islet architecture and composition by laser scanning confocal microscopy. *J. Histochem. Cytochem.* **53**, 1087–1097 (2005).
48. Goke, B. Islet cell function: alpha and beta cells--partners towards normoglycaemia. *Int. J. Clin. Pract.* 2–7 (2008) doi:10.1111/j.1742-1241.2007.01686.x.
49. Katsuura, G., Asakawa, A. & Inui, A. Roles of pancreatic polypeptide in regulation of food intake. *Peptides* **23**, 323–329 (2002).
50. Wierup, N., Svensson, H., Mulder, H. & Sundler, F. The ghrelin cell: a novel developmentally regulated islet cell in the human pancreas. *Regul. Pept.* **107**, 63–69 (2002).
51. Hauge-Evans, A. C. *et al.* Somatostatin secreted by islet delta-cells fulfills multiple roles as a paracrine regulator of islet function. *Diabetes* **58**, 403–411 (2009).
52. Amidei, C. & Trese, S. *Neuroanatomy and physiology*. *Management of Adult Glioma in Nursing Practice* (2019). doi:10.1007/978-3-319-76747-5_1.
53. Mühlemann, M. Intestinal stem cells and the Na\(^+\)-D-Glucose Transporter SGLT1: potential targets regarding future therapeutic strategies for diabetes. (2018).
54. Henquin, J. C., Ravier, M. A., Nenquin, M., Jonas, J. C. & Gilon, P. Hierarchy of the beta-cell signals controlling insulin secretion. *Eur. J. Clin. Invest.* **33**, 742–750 (2003).
55. Rorsman, P. & Braun, M. Regulation of insulin secretion in human pancreatic islets. *Annu. Rev. Physiol.* **75**, 155–179 (2013).
56. Maechler, P. & Wollheim, C. B. Mitochondrial glutamate acts as a messenger in glucose-induced insulin exocytosis. *Nature* **402**, 685–689 (1999).
57. Meda, P. & Schuit, F. Glucose-stimulated insulin secretion: The hierarchy of its multiple cellular and subcellular mechanisms. *Diabetologia* **56**, 2552–2555 (2013).
58. Henquin, J. C. Triggering and amplifying pathways of regulation of insulin secretion by glucose. *Diabetes* **49**, 1751–1760 (2000).
59. Reaven, G. M. The insulin resistance syndrome: definition and dietary approaches to treatment. *Annu. Rev. Nutr.* **25**, 391–406 (2005).
60. Mokdad, A. H. *et al.* Prevalence of obesity, diabetes, and obesity-related health risk factors, 2001. *JAMA* **289**, 76–79 (2003).
61. Wellen, K. E. & Hotamisligil, G. S. Inflammation, stress, and diabetes. *J. Clin. Invest.* **115**, 1111–1119 (2005).
62. Schenk, S., Saberi, M. & Olefsky, J. M. Personal perspective Insulin sensitivity : modulation by nutrients and inflammation. *Department Med. Div. Endocrinol. Metab.* **118**, 2992–3002 (2008).
63. Xu, H. *et al.* Chronic inflammation in fat plays a crucial role in the development of obesity-related

insulin resistance. *J. Clin. Invest.* **112**, 1821–1830 (2003).
64. Weisberg, S. P. *et al.* Obesity is associated with macrophage accumulation. *J. Clin. Invest.* **112**, (2003).
65. Hotamisligil, G. S., Arner, P., Caro, J. F., Atkinson, R. L. & Spiegelman, B. M. Increased adipose tissue expression of tumor necrosis factor-alpha in human obesity and insulin resistance. *J. Clin. Invest.* **95**, 2409–2415 (1995).
66. Cai, D. *et al.* Local and systemic insulin resistance resulting from hepatic activation of IKK-beta and NF-kappaB. *Nat. Med.* **11**, 183–190 (2005).
67. Roytblat, L. *et al.* Raised interleukin-6 levels in obese patients. *Obes. Res.* **8**, 673–675 (2000).
68. Shemesh, T. *et al.* Differential association of C-reactive protein with adiposity in men and women in an Aboriginal community in northeast Arnhem Land of Australia. *Int. J. Obes.* **31**, 103–108 (2007).
69. Bochud, M. *et al.* Association between C-reactive protein and adiposity in women. *J. Clin. Endocrinol. Metab.* **94**, 3969–3977 (2009).
70. Boni-Schnetzler, M. *et al.* Free fatty acids induce a proinflammatory response in islets via the abundantly expressed interleukin-1 receptor I. *Endocrinology* **150**, 5218–5229 (2009).
71. Menu, P. *et al.* ER stress activates the NLRP3 inflammasome via an UPR-independent pathway. *Cell Death Dis.* **3**, e261 (2012).
72. Back, S. H. & Kaufman, R. J. Endoplasmic reticulum stress and type 2 diabetes. *Annu. Rev. Biochem.* **81**, 767–793 (2012).
73. Brownlee, M. Biochemistry and Molecular Cell Biology of Diabetic Complications. *Nature* **414**, 813–820 (2001).
74. Olefsky, J. M. & Glass, C. K. Macrophages, Inflammation, and Insulin Resistance. *Annu. Rev. Physiol.* **72**, 219–246 (2010).
75. Chawla, A., Nguyen, K. D. & Goh, Y. P. S. Macrophage-mediated inflammation in metabolic disease. *Nat. Rev. Immunol.* **11**, 738–749 (2011).
76. Cole, J., Aberdein, J., Jubrail, J. & Dockrell, D. H. The Role of Macrophages in the Innate Immune Response to Streptococcus pneumoniae and Staphylococcus aureus. Mechanisms and Contrasts. *Adv. Microb. Physiol.* **65**, 125–202 (2014).
77. Janeway, C. A. J. & Medzhitov, R. Innate immune recognition. *Annu. Rev. Immunol.* **20**, 197–216 (2002).
78. Gordon, S. Phagocytosis: The Legacy of Metchnikoff. *Cell* **166**, 1065–1068 (2016).
79. Ginhoux, F. & Guilliams, M. Tissue-Resident Macrophage Ontogeny and Homeostasis. *Immunity* **44**, 439–449 (2016).
80. Sieweke, M. H. & Allen, J. E. Beyond Stem Cells: Self-Renewal of Differentiated Macrophages. *Science* **342**, 1242974 (2013).
81. Shepard, J. L. & Zon, L. I. Developmental derivation of embryonic and adult macrophages. *Curr. Opin. Hematol.* **7**, 3–8 (2000).
82. Lichanska, A. M. & Hume, D. A. Origins and functions of phagocytes in the embryo. *Exp. Hematol.* **28**, 601–611 (2000).
83. Geissmann, F. *et al.* Development of monocytes, macrophages, and dendritic cells. *Science* **327**, 656–661 (2010).
84. Gordon, S. & Taylor, P. R. Monocyte and macrophage heterogeneity. *Nat. Rev. Immunol.* **5**, 953–964 (2005).
85. Hamilton, J. A. & Achuthan, A. Colony stimulating factors and myeloid cell biology in health and disease. *Trends Immunol.* **34**, 81–89 (2013).
86. Yeung, Y. G., Jubinsky, P. T., Sengupta, A., Yeung, D. C. & Stanley, E. R. Purification of the colony-stimulating factor 1 receptor and demonstration of its tyrosine kinase activity. *Proc. Natl. Acad. Sci. U. S. A.* **84**, 1268–1271 (1987).
87. Stanley, E. R. & Chitu, V. CSF-1 receptor signaling in myeloid cells. *Cold Spring Harb. Perspect. Biol.* **6**, 1–21 (2014).
88. Gordon, S. & Martinez-Pomares, L. Physiological roles of macrophages. *Pflugers Arch. Eur. J. Physiol.* **469**, 365–374 (2017).
89. Rubartelli, A., Lotze, M. T., Latz, E. & Manfredi, A. Mechanisms of sterile inflammation. *Front. Immunol.* **4**, 2012–2013 (2013).
90. Boutens, L. & Stienstra, R. Adipose tissue macrophages: going off track during obesity. *Diabetologia* **59**, 879–894 (2016).
91. Kraakman, M. J., Murphy, A. J., Jandeleit-Dahm, K. & Kammoun, H. L. Macrophage polarization in obesity and type 2 diabetes: Weighing down our understanding of macrophage function? *Front. Immunol.* **5**, 1–6 (2014).
92. Sica, A. & Mantovani, A. Macrophage plasticity and polarization: in vivo veritas. *J. Clin. Invest.* **122**, 787–795 (2012).
93. Lawrence, T. & Natoli, G. Transcriptional regulation of macrophage polarization: enabling diversity

with identity. *Nat. Rev. Immunol.* **11**, 750–761 (2011).
94. Gordon, S. Alternative activation of macrophages. *Nat. Rev. Immunol.* **3**, 23–35 (2003).
95. Martinez, F. O. & Gordon, S. The M1 and M2 paradigm of macrophage activation: time for reassessment. *F1000Prime Rep.* **6**, 1–13 (2014).
96. Drareni, K., Gautier, J. F., Venteclef, N. & Alzaid, F. Transcriptional control of macrophage polarisation in type 2 diabetes. *Semin. Immunopathol.* **41**, 515–529 (2019).
97. Wentworth, J. M. *et al.* Macrophages Are Associated With Insulin Resistance in. *Diabetes* **59**, (2010).
98. Galván-Peña, S. & O'Neill, L. A. J. Metabolic reprogramming in macrophage polarization. *Front. Immunol.* **5**, 1–6 (2014).
99. Gao, D. *et al.* Interleukin-1β mediates macrophage-induced impairment of insulin signaling in human primary adipocytes. *Am. J. Physiol. Endocrinol. Metab.* **307**, E289–E304 (2014).
100. Donath, M. Y., Dalmas, É., Sauter, N. S. & Böni-Schnetzler, M. Inflammation in obesity and diabetes: Islet dysfunction and therapeutic opportunity. *Cell Metab.* **17**, 860–872 (2013).
101. Dror, E. *et al.* Postprandial macrophage-derived IL-1b stimulates insulin , and both synergistically promote glucose disposal and inflammation. *Nat. Immunol.* **18**, 283–292 (2017).
102. de La Serre, C. B. *et al.* Propensity to high-fat diet-induced obesity in rats is associated with changes in the gut microbiota and gut inflammation. *Am. J. Physiol. - Gastrointest. Liver Physiol.* **299**, G440–G448 (2010).
103. Cani, P. D. *et al.* Metabolic Endotoxemia Initiates Obesity and Insulin Resistance. *Diabetes* **56**, 1761–1772 (2007).
104. Caesar, R. *et al.* Gut-derived lipopolysaccharide augments adipose macrophage accumulation but is not essential for impaired glucose or insulin tolerance in mice. *Gut* **61**, 1701–1707 (2012).
105. Cani, P. D. *et al.* Metabolic Endotoxemia Initiates Obesity and Insulin Resistance. *Diabetes* **56**, 1761–1772 (2007).
106. Gérard, C. & Vidal, H. Impact of gut microbiota on host glycemic control. *Front. Endocrinol.* **10**, 1–13 (2019).
107. Utzschneider, K. M., Kratz, M., Damman, C. J. & Hullar, M. Mechanisms Linking the Gut Microbiome and Glucose Metabolism. *J. Clin. Endocrinol. Metab.* **101**, 1445–1454 (2016).
108. Kumar, K. A., Pai, N. G., Baburajan, N. P. & Jayakumar, R. P. Development of twin bellow pump for space application. *J. Spacecr. Technol.* **27**, 25–30 (2016).
109. Cotillard, A. *et al.* Dietary intervention impact on gut microbial gene richness. *Nature* **500**, 585–588 (2013).
110. Le Chatelier, E. *et al.* Richness of human gut microbiome correlates with metabolic markers. *Nature* **500**, 541–546 (2013).
111. Schwiertz, A. *et al.* Microbiota and SCFA in lean and overweight healthy subjects. *Obesity (Silver Spring).* **18**, 190–195 (2010).
112. Zhang, H. *et al.* Human gut microbiota in obesity and after gastric bypass. *Proc. Natl. Acad. Sci. U. S. A.* **106**, 2365–2370 (2009).
113. Duncan, S. H. *et al.* Human colonic microbiota associated with diet, obesity and weight loss. *Int. J. Obes.* **32**, 1720–1724 (2008).
114. Bäckhed, F., Manchester, J. K., Semenkovich, C. F. & Gordon, J. I. Mechanisms underlying the resistance to diet-induced obesity in germ-free mice. *Proc. Natl. Acad. Sci. U. S. A.* **104**, 979–984 (2007).
115. Vrieze, A. *et al.* Transfer of intestinal microbiota from lean donors increases insulin sensitivity in individuals with metabolic syndrome. *Gastroenterology* **143**, 913-916.e7 (2012).
116. Koutnikova, H. *et al.* Impact of bacterial probiotics on obesity, diabetes and non-alcoholic fatty liver disease related variables: A systematic review and meta-analysis of randomised controlled trials. *BMJ Open* **9**, 1–12 (2019).
117. Tremaroli, V. *et al.* Roux-en-Y Gastric Bypass and Vertical Banded Gastroplasty Induce Long-Term Changes on the Human Gut Microbiome Contributing to Fat Mass Regulation. *Cell Metab.* **22**, 228–238 (2015).
118. Turnbaugh, P. J. *et al.* An obesity-associated gut microbiome with increased capacity for energy harvest. *Nature* **444**, 1027–1031 (2006).
119. Wang, J. *et al.* A metagenome-wide association study of gut microbiota in type 2 diabetes. *Nature* **490**, 55–60 (2012).
120. Karlsson, F. H. *et al.* Gut metagenome in European women with normal, impaired and diabetic glucose control. *Nature* **498**, 99–103 (2013).
121. Foley, K. P. *et al.* Long term but not short term exposure to obesity related microbiota promotes host insulin resistance. *Nat. Commun.* **9**, 1–15 (2018).
122. Swann, J. R. *et al.* Systemic gut microbial modulation of bile acid metabolism in host tissue compartments. *Proc. Natl. Acad. Sci. U. S. A.* **108**, 4523–4530 (2011).

123. Thomas, C. *et al.* TGR5-Mediated Bile Acid Sensing Controls Glucose Homeostasis. *Cell Metab.* **10**, 167–177 (2009).
124. Deacon, C. F. Peptide degradation and the role of DPP-4 inhibitors in the treatment of type 2 diabetes. *Peptides* **100**, 150–157 (2018).
125. Faerch, K. *et al.* GLP-1 response to oral glucose is reduced in prediabetes, screen-detected type 2 diabetes, and obesity and influenced by sex: The ADDITION-PRO Study. *Diabetes* **64**, 2513–2525 (2015).
126. Larsen, M. P. & Torekov, S. S. Glucagon-Like Peptide 1: A Predictor of Type 2 Diabetes? *J. Diabetes Res.* **2017**, (2017).
127. Forslund, K. *et al.* Disentangling type 2 diabetes and metformin treatment signatures in the human gut microbiota. *Nature* **528**, 262–266 (2015).
128. Ding, S. *et al.* High-fat diet: Bacteria interactions promote intestinal inflammation which precedes and correlates with obesity and insulin resistance in mouse. *PLoS One* **5**, (2010).
129. Li, H. *et al.* Intestinal, adipose, and liver inflammation in diet-induced obese mice. *Metabolism* **57**, 1704–1710 (2008).
130. Luck, H. *et al.* Regulation of obesity-related insulin resistance with gut anti-inflammatory agents. *Cell Metab.* **21**, 527–542 (2015).
131. Monteiro-Sepulveda, M. *et al.* Jejunal T Cell Inflammation in Human Obesity Correlates with Decreased Enterocyte Insulin Signaling. *Cell Metab.* **22**, 113–124 (2015).
132. Garidou, L. *et al.* The Gut Microbiota Regulates Intestinal CD4 T Cells Expressing RORγt and Controls Metabolic Disease. *Cell Metab.* **22**, 100–112 (2015).
133. Wang, X. *et al.* Interleukin-22 alleviates metabolic disorders and restores mucosal immunity in diabetes. *Nature* **514**, 237–241 (2014).
134. Johnson, A. M. F. *et al.* High fat diet causes depletion of intestinal eosinophils associated with intestinal permeability. *PLoS One* **10**, 1–15 (2015).
135. Kawano, Y. *et al.* Colonic Pro-inflammatory Macrophages Cause Colonic Pro-inflammatory Macrophages Cause Insulin Resistance in an Intestinal. *Cell Metab.* **24**, 295–310 (2016).
136. Biswas, S. K. & Bonecchi, R. Previews Colonic Macrophages ‘“ Remote Control ”’ Adipose Tissue Inflammation and Insulin Resistance. *Cell Metab.* **24**, 196–198 (2016).
137. Tamoutounour, S. *et al.* CD64 distinguishes macrophages from dendritic cells in the gut and reveals the Th1-inducing role of mesenteric lymph node macrophages during colitis. *Eur. J. Immunol.* **42**, 3150–3166 (2012).
138. Bain, C. C. *et al.* Resident and pro-inflammatory macrophages in the colon represent alternative context-dependent fates of the same Ly6C hi monocyte precursors. *Mucosal Immunol.* **6**, (2013).
139. Sanchis, M. *et al.* Origins and Functional Specialization of Macrophages and of Conventional and Monocyte-Derived Dendritic Cells in Mouse Skin. *Immunity* **39**, 925–938 (2013).
140. Sheng, J., Ruedl, C. & Karjalainen, K. Most Tissue-Resident Macrophages Except Microglia Are Derived from Fetal Hematopoietic Stem Cells. *Immunity* **43**, 382–393 (2015).
141. Smythies, L. E. *et al.* Human intestinal macrophages display profound inflammatory anergy despite avid phagocytic and bacteriocidal activity. *J. Clin. Invest.* **115**, 66–75 (2005).
142. Hausmann, M. *et al.* Toll-like receptors 2 and 4 are up-regulated during intestinal inflammation. *Gastroenterology* **122**, 1987–2000 (2002).
143. Platt, A. M., Bain, C. C., Bordon, Y., Sester, D. P. & Mowat, A. M. An Independent Subset of TLR Expressing CCR2-Dependent Macrophages Promotes Colonic Inflammation. *J. Immunol.* **184**, 6843–6854 (2010).
144. Kamada, N. *et al.* Unique CD14+ intestinal macrophages contribute to the pathogenesis of Crohn disease via IL-23/IFN-γ axis. *J. Clin. Investig.* **118**, (2008).
145. Rivollier, A., He, J., Kole, A., Valatas, V. & Kelsall, B. L. Inflammation switches the differentiation program of Ly6chi monocytes from antiinflammatory macrophages to inflammatory dendritic cells in the colon. *J. Exp. Med.* **209**, 139–155 (2012).
146. van Rooijen, N. & Hendrikx, E. Liposomes for specific depletion of macrophages from organs and tissues. *Methods Mol. Biol.* **605**, 189–203 (2010).
147. Qualls, J. E. Suppression of experimental colitis by intestinal mononuclear phagocytes. *J. Leukoc. Biol.* **80**, 802–815 (2006).
148. Tamoutounour, S. *et al.* Origins and functional specialization of macrophages and of conventional and monocyte-derived dendritic cells in mouse skin. *Immunity* **39**, 925–938 (2013).
149. Guilliams, M. *et al.* Skin-draining lymph nodes contain dermis-derived CD103- dendritic cells that constitutively produce retinoic acid and induce Foxp3+ regulatory T cells. *Immunobiology* **115**, 1–3 (2016).
150. Bapat, S. P., Suh, J. M., Fang, S., Liu, S. & Zhang, Y. Depletion of Fat Tregs prevents age associated insulin resistance. *Nature* **528**, 137–141 (2016).

151. Morris, D. L. *et al.* Adipose tissue macrophages: phenotypic plasticity and diversity in lean and obese states. *Curr. Opin. Clin. Nutr. Metab. Care* **14**, 341–346 (2015).
152. Lumeng, C. N. *et al.* Aging is associated with an increase in T cells and inflammatory macrophages in visceral adipose tissue. *J. Immunol.* **187**, 6208–6216 (2012).
153. AlAsfoor, S. *et al.* Imatinib reduces non-alcoholic fatty liver disease in obese mice by targeting inflammatory and lipogenic pathways in macrophages and liver. *Sci. Rep.* **8**, 1–13 (2018).
154. Ghosn, E. E. B. *et al.* Two physically, functionally, and developmentally distinct peritoneal macrophage subsets. *Proc. Natl. Acad. Sci.* **107**, 2568–2573 (2010).
155. Krenkel, O. & Tacke, F. Liver macrophages in tissue homeostasis and disease. *Nat. Rev. Immunol.* **17**, 306 (2017).
156. David, B. A. *et al.* Combination of Mass Cytometry and Imaging Analysis Reveals Origin, Location, and Functional Repopulation of Liver Myeloid Cells in Mice. *Gastroenterology* **151**, 1176–1191 (2016).
157. Morinaga, H. *et al.* Characterization of distinct subpopulations of hepatic macrophages in HFD/obese mice. *Diabetes* **64**, 1120–1130 (2015).
158. Bujko, A. *et al.* Transcriptional and functional profiling defines human small intestinal macrophage subsets. *J. Exp. Med.* **215**, 441–458 (2017).
159. Ziegler-Heitbrock, L. *et al.* Nomenclature of monocytes and dendritic cells in blood. *Blood* **116**, 5–7 (2010).
160. Li, H. *et al.* The outer mucus layer hosts a distinct intestinal microbial niche. *Nat. Commun.* **6**, (2015).
161. Mamantopoulos, M. *et al.* Nlrp6- and ASC-Dependent Inflammasomes Do Not Shape the Commensal Gut Microbiota Composition. *Immunity* **47**, 339-348.e4 (2017).
162. Sundquist, A. *et al.* Bacterial flora-typing with targeted, chip-based Pyrosequencing. *BMC Microbiol.* **7**, 1–11 (2007).
163. Whiteley, A. S. *et al.* Microbial 16S rRNA Ion Tag and community metagenome sequencing using the Ion Torrent (PGM) Platform. *J. Microbiol. Methods* **91**, 80–88 (2012).
164. Caporaso, J. G. *et al.* QIIME allows analysis of high-throughput community sequencing data. *Nat. Methods* **7**, 335–336 (2010).
165. Edgar, R. C. Search and clustering orders of magnitude faster than BLAST. *Bioinformatics* **26**, 2460–2461 (2010).
166. Melsted, P., Ntranos, V. & Pachter, L. The barcode, UMI, set format and BUStools. *Bioinformatics* **35**, 4472–4473 (2019).
167. Melsted, P. *et al.* Modular and efficient pre-processing of single-cell RNA-seq. *BioRxiv* 673285 (2019) doi:10.1101/673285.
168. Amezquita, R. A. *et al.* Orchestrating single-cell analysis with Bioconductor. *Nat. Methods* **17**, 137–145 (2019).
169. Griffiths, J. A., Richard, A. C., Bach, K., Lun, A. T. L. & Marioni, J. C. Detection and removal of barcode swapping in single-cell RNA-seq data. *Nat. Commun.* **9**, 2667 (2018).
170. Lun, A. T. L. *et al.* EmptyDrops: distinguishing cells from empty droplets in droplet-based single-cell RNA sequencing data. *Genome Biol.* **20**, 63 (2019).
171. McCarthy, D. J., Campbell, K. R., Lun, A. T. L. & Wills, Q. F. Scater: pre-processing, quality control, normalization and visualization of single-cell RNA-seq data in R. *Bioinformatics* **33**, 1179–1186 (2017).
172. Lun, A. T. L., McCarthy, D. J. & Marioni, J. C. A step-by-step workflow for low-level analysis of single-cell RNA-seq data with Bioconductor. *F1000Research* **5**, 2122 (2016).
173. Ilicic, T. *et al.* Classification of low quality cells from single-cell RNA-seq data. *Genome Biol.* **17**, 29 (2016).
174. Vallejos, C. A., Risso, D., Scialdone, A., Dudoit, S. & Marioni, J. C. Normalizing single-cell RNA sequencing data: challenges and opportunities. *Nat. Methods* **14**, 565–571 (2017).
175. Brennecke, P. *et al.* Accounting for technical noise in single-cell RNA-seq experiments. *Nat. Methods* **10**, 1093–1095 (2013).
176. Aran, D. *et al.* Reference-based analysis of lung single-cell sequencing reveals a transitional profibrotic macrophage. *Nat. Immunol.* **20**, 163–172 (2019).
177. Heng, T. S. P. & Painter, M. W. The Immunological Genome Project: networks of gene expression in immune cells. *Nat. Immunol.* **9**, 1091–1094 (2008).
178. Lun, A. T. L. & Marioni, J. C. Overcoming confounding plate effects in differential expression analyses of single-cell RNA-seq data. *Biostatistics* **18**, 451–464 (2017).
179. Robinson, M. D., McCarthy, D. J. & Smyth, G. K. edgeR: a Bioconductor package for differential expression analysis of digital gene expression data. *Bioinformatics* **26**, 139–140 (2010).
180. Robinson, M. D. & Oshlack, A. A scaling normalization method for differential expression analysis of RNA-seq data. *Genome Biol.* **11**, R25 (2010).
181. Wu, D. & Smyth, G. K. Camera: a competitive gene set test accounting for inter-gene correlation. *Nucleic Acids Res.* **40**, e133 (2012).

182. Liberzon, A. *et al.* The Molecular Signatures Database (MSigDB) hallmark gene set collection. *Cell Syst.* **1**, 417–425 (2015).
183. Subramanian, A. *et al.* Gene set enrichment analysis: a knowledge-based approach for interpreting genome-wide expression profiles. *Proc. Natl. Acad. Sci. U. S. A.* **102**, 15545–15550 (2005).
184. Garcia-Alonso, L., Holland, C. H., Ibrahim, M. M., Turei, D. & Saez-Rodriguez, J. Benchmark and integration of resources for the estimation of human transcription factor activities. *Genome Res.* **29**, 1363–1375 (2019).
185. Heymsfield, S. B. *et al.* Hyperphagia: Current concepts and future directions proceedings of the 2nd international conference on hyperphagia. *Obesity* **22**, S1–S17 (2014).
186. Licholai, J. A. *et al.* Why Do Mice Overeat High-Fat Diets? How High-Fat Diet Alters the Regulation of Daily Caloric Intake in Mice. *Obesity* **26**, 1026–1033 (2018).
187. Kim, K.-A., Gu, W., Lee, I.-A., Joh, E.-H. & Kim, D.-H. High fat diet-induced gut microbiota exacerbates inflammation and obesity in mice via the TLR4 signaling pathway. *PLoS One* **7**, e47713–e47713 (2012).
188. Larsson, E. *et al.* Analysis of gut microbial regulation of host gene expression along the length of the gut and regulation of gut microbial ecology through MyD88. *Gut* **61**, 1124–1131 (2012).
189. Jones, C. V. & Ricardo, S. D. Macrophages and CSF-1: Implications for development and beyond. *Organogenesis* **9**, 249–260 (2013).
190. Weisberg, S. P. *et al.* CCR2 modulates inflammatory and metabolic effects of high-fat feeding. *J. Clin. Invest.* **116**, (2006).
191. Shiraishi, D., Fujiwara, Y., Komohara, Y., Mizuta, H. & Takeya, M. Glucagon-like peptide-1 (GLP-1) induces M2 polarization of human macrophages via STAT3 activation. *Biochem. Biophys. Res. Commun.* **425**, 304–308 (2012).
192. Davison, K. K. & Birch, L. L. Regulation of type I interferon responses. *Nat Rev Immunol* **64**, 2391–2404 (2008).
193. Luck, H. *et al.* Regulation of Obesity-Related Insulin Resistance with Gut Anti-inflammatory Agents Article Regulation of Obesity-Related Insulin Resistance with Gut Anti-inflammatory Agents. *Cell Metab.* **21**, 527–542 (2015).
194. Ganal, S. C. *et al.* Priming of Natural Killer Cells by Nonmucosal Mononuclear Phagocytes Requires Instructive Signals from Commensal Microbiota. *Immunity* **37**, 171–186 (2012).
195. Shuai, K., Schindler, C., Prezioso, V. & Darnell, J. Activation of Transcription by IFN-γ: Tyrosine Phosphorylation of a 91-kD DNA Binding Protein. *Science* **258**, 1808–1812 (1993).
196. Schindler, C., Shuai, K., Prezioso, V. R. & Darnell, J. E. J. Interferon-dependent tyrosine phosphorylation of a latent cytoplasmic transcription factor. *Science* **257**, 809–813 (1992).
197. Fu, X. Y., Schindler, C., Improta, T., Aebersold, R. & Darnell Jr, J. E. The proteins of ISGF-3, the interferon alpha-induced transcriptional activator, define a gene family involved in signal transduction. *Proc. Natl. Acad. Sci. U. S. A.* **89**, 7840–7843 (1992).
198. Platanias, L. C. Mechanisms of type-I- and type-II-interferon-mediated signalling. *Nat. Rev. Immunol.* **5**, 375–386 (2005).
199. Schmitz, F. *et al.* Mammalian target of rapamycin (mTOR) orchestrates the defense program of innate immune cells. *Eur. J. Immunol.* **38**, 2981–2992 (2008).
200. Kroczynska, B. *et al.* Interferon γ (IFNγ) signaling via mechanistic target of rapamycin complex 2 (mTORC2) and regulatory effects in the generation of type II interferon biological responses. *J. Biol. Chem.* **291**, 2389–2396 (2016).
201. Livingstone, M. *et al.* Assessment of mTOR-Dependent translational regulation of interferon stimulated genes. *PLoS One* **10**, 1–20 (2015).
202. Mao, Z. & Zhang, W. Role of mTOR in Glucose and Lipid Metabolism. *Mol. Sci.* **19**, E2043 (2018).
203. Haissaguerre, M., Saucisse, N. & Cota, D. Influence of mTOR in energy and metabolic homeostasis. *Mol. Cell. Endocrinol.* **397**, 67–77 (2014).
204. Linke, M., Fritsch, S. D., Sukhbaatar, N., Hengstschläger, M. & Weichhart, T. mTORC1 and mTORC2 as regulators of cell metabolism in immunity. *FEBS Lett.* **591**, 3089–3103 (2017).
205. John R.Giudicessi, BA.Michael J.Ackerman., 2013. Toll-like receptor–mediated induction of type I interferon in plasmacytoid dendritic cells requires the rapamycin-sensitive PI(3)K-mTOR-p70S6K pathway. *Nat. Immunol.* **23**, 1–7 (2008).
206. Zacksenhaus, E. *et al.* Mitochondrial OXPHOS Induced by RB1 Deficiency in Breast Cancer: Implications for Anabolic Metabolism, Stemness, and Metastasis. *Trends in Cancer* **3**, 768–779 (2017).
207. Weichhart, T., Hengstschläger, M. & Linke, M. Regulation of innate immune cell function by mTOR. *Nat Rev Immunol* **15**, 599–614 (2018).
208. Düvel, K. *et al.* Activation of a metabolic gene regulatory network downstream of mTOR complex 1. *Mol. Cell.* **39**, 171–183 (2011).
209. Zoncu, R., Sabatini, D. M. & Efeyan, A. mTOR: from growth signal integration to cancer, diabetes and

aging. *Nat Rev Mol Cell Biol* **12**, 21–35 (2011).
210. Pulakat, L. *et al.* Adaptive mechanisms to compensate for overnutrition-induced cardiovascular abnormalities. *Am. J. Physiol. - Regul. Integr. Comp. Physiol.* **301**, 885–895 (2011).
211. Lamming, D. W. *et al.* Rapamycin-induced insulin resistance is mediated by mTORC2 loss and uncoupled from longevity. *Science* **335**, 1638–1643 (2012).
212. Kleinert, M. *et al.* Acute mTOR inhibition induces insulin resistance and alters substrate utilization in vivo. *Mol. Metab.* **3**, 630–641 (2014).
213. Deblon, N. *et al.* Chronic mTOR inhibition by rapamycin induces muscle insulin resistance despite weight loss in rats. *Br. J. Pharmacol.* **165**, 2325–2340 (2012).
214. Kevin Range, and D. M. Y. A. M. Rapamycin-induced insulin resistance is mediated by mTORC2 loss and uncoupled from longevity. *Science* **23**, 1–7 (2012).
215. Johnston, O., Rose, C. L., Webster, A. C. & Gill, J. S. Sirolimus is associated with new-onset diabetes in kidney transplant recipients. *J. Am. Soc. Nephrol.* **19**, 1411–1418 (2008).
216. Waise, T. M. Z. *et al.* Inhibition of upper small intestinal mTOR lowers plasma glucose levels by inhibiting glucose production. *Nat. Commun.* **10**, 1–10 (2019).
217. Beitnes, A. C. R. *et al.* Rapid accumulation of CD14 +CD11c + dendritic cells in gut mucosa of celiac disease after in vivo gluten challenge. *PLoS One* **7**, 1–9 (2012).
218. Bain, C. C. *et al.* Resident and pro-inflammatory macrophages in the colon represent alternative context-dependent fates of the same Ly6Chi monocyte precursors. *Mucosal Immunol.* **6**, 498–510 (2013).
219. Ogino, T. *et al.* Increased Th17-inducing activity of CD14+CD163lowmyeloid cells in intestinal lamina propria of patients with Crohn's disease. *Gastroenterology* **145**, 1380-1391.e1 (2013).
220. Zawada, A. M. *et al.* Monocyte heterogeneity in human cardiovascular disease. *Immunobiology* **217**, 1273–1284 (2012).
221. Rogacev, K. S. *et al.* Monocyte heterogeneity in obesity and subclinical atherosclerosis. *Eur. Heart J.* **31**, 369–376 (2010).
222. Poitou, C. *et al.* CD14dimCD16+ and CD14+CD16+ monocytes in obesity and during weight loss: Relationships with fat mass and subclinical atherosclerosis. *Arterioscler. Thromb. Vasc. Biol.* **31**, 2322–2330 (2011).
223. Cottam, D. R., Schaefer, P. A., Shaftan, G. W., Velcu, L. & Angus, L. D. G. Effect of surgically-induced weight loss on leukocyte indicators of chronic inflammation in morbid obesity. *Obes. Surg.* **12**, 335–342 (2002).
224. Cottam, D. R., Schaefer, P. A., Fahmy, D., Shaftan, G. W. & Angus, L. D. G. The effect of obesity on neutrophil Fc receptors and adhesion molecules (CD16, CD11b, CD62L). *Obes. Surg.* **12**, 230–235 (2002).
225. Stansfield, B. K. & Ingram, D. A. Clinical significance of monocyte heterogeneity. *Clin. Transl. Med.* **4**, (2015).
226. Rothe, G. *et al.* Peripheral blood mononuclear phagocyte subpopulations as cellular markers in hypercholesterolemia. *Arterioscler. Thromb. Vasc. Biol.* **16**, 1437–1447 (1996).
227. Grey, D. *et al.* Increased CD64 expression on polymorphonuclear neutrophils indicates infectious complications following solid organ transplantation. *Cytom. Part A* **79**, 446–460 (2011).
228. Groselj-Grenc, M., Ihan, A. & Derganc, M. Neutrophil and monocyte CD64 and CD163 expression in critically ill neonates and children with sepsis: comparison of fluorescence intensities and calculated indexes. *Mediators Inflamm.* **2000**, 202646 (2008).
229. Li, Y. *et al.* Monocyte surface expression of Fcgamma receptor RI (CD64), a biomarker reflecting type-I interferon levels in systemic lupus erythematosus. *Arthritis Res. Ther.* **12**, R90–R90 (2010).
230. Nagareddy, P. R. *et al.* Adipose tissue macrophages promote myelopoiesis and monocytosis in obesity. *Cell Metab.* **19**, 821–835 (2014).
231. Nagareddy, P. R. *et al.* Hyperglycemia promotes myelopoiesis and impairs the resolution of atherosclerosis. *Cell Metab.* **17**, 695–708 (2013).
232. Pool, I. M. *et al.* Dietary Intake Regulates the Circulating Inflammatory Monocyte Pool. *Cell* **178**, 1102-1114.e17 (2019).
233. Neels, J. G. Ablation of CD11c-positive cells normalizes insulin sensitivity in obese insulin resistant animals. *Cell Metab.* **8**, 301–309 (2009).
234. Koscsó, B. *et al.* Gut-resident CX3CR1hi macrophages induce tertiary lymphoid structures and IgA response in situ. *Sci. Immunol.* **5**, (2020).
235. Calisto, J. De, Villablanca, E. J. & Mora, J. R. FcγRI (CD64): an identity card for intestinal macrophages Jaime. *Eur. J. Immunol.* **42**, 3136–3140 (2013).

Acknowledgments

Zunächst bedanke ich mich bei Herrn Prof. Dr. Marc Donath und Prof. Dr. Christoph Hess für die exzellente Betreuung, ihren steten Optimismus und ihre brillanten Ideen, die mir das Absolvieren meiner Doktorarbeit erst ermöglichte. Weiterhin richtet sich mein Dank an Herrn Prof. Dr. Gerhard Christofori für die freundliche Übernahme des Koreferats und das sehr hilfreiche Feedback in meinem PhD Komitee.

Für die Zuteilung meines Projekts, diverse Denkanregungen sowie für ihre konstruktive Kritik und stete Unterstützung in meine weitere Entwicklung fühle ich mich bei PD Dr. Claudia Cavelti-Weder zum außerordentlichen Dank verpflichtet.

Ein besonderer Dankesgruß geht an PD Dr. Marianne Böni-Schnetzler und Dr. Daniel Zeman. Ich möchte mich für die erstklassigen Begleitung durch meinen PhD bedanken. Ihre stete Unterstützung erleichterte mir die praktische Arbeit, insbesondere durch das Vermitteln ihrer Laborerfahrung und ihrem technischen Knowhow, sehr.

Zudem danke ich besonders Zora Baumann, Dr. Shefaa Alasfoor, Dr. Angela, Bosch, Dr. Romano Schneider, Neena Parayil, Marc Stawiski unseres *Translational Diabetes* Teams, sowie der gesamten *Diabetes Research* Gruppe, vor allem Sophia Wiedemann, Josua Wehner und Leila Rachid für ihre praktische Unterstützung sowie eine abwechslungsreiche und ausgesprochen angenehme Arbeitsatmosphäre sowie für die schönen Erinnerungen. Ebenso danke ich Dr. Elise Dalmas und Dr. Erez Dror für ihre Tipps zu Flow cytometry und Makrophagen sowieso Dr. Friederike Schulze für das Heranführen an die Maushandhabung in meiner Anfangsphase.

Das Labor 312 mit der Arbeitsgruppe *Clinical Immunology* (Claudia Donat, Pascal Rabatscher, Denise Dubler, Joel Leonardi, Dr. Eylül Tuncer, Dr. Kinga Csorba, Dr. Andrea Kieninger-Gräfitsch, Dr. Sophia Thanei, Dr. Lucia Schirmbeck, Dr. Robert Kölm und weiteren Klinikern Dr. Stephan Moser, Severin Vogt) zu teilen, war toll und ihre stete Bereitschaft zu Teilen nicht nur Utensilien und Reagenzien, sondern auch die witzigen Stunden zusammen werde ich sehr vermissen.

Ebenfalls möchte ich den Arbeitsgruppen von Prof. Dr. Christoph Hess (bes. Dr. Gleen Bantug), Prof. Dr. Mike Recher (bes. Annaise Jauch, Benedikt Meyer), PD Dr. Christoph Berger (bes. Julia Hirsiger), und PD Dr. Matthias Mehling (bes. Corina Frick, Mali Cristina Coray) für den tollen wissenschaftlichen Austausch, die Zusammenarbeit und schönen Momente danken.

Ich möchte mich ganz herzlich bei dem gesamten Team des Tierstalles des Departements Biomedizin bedanken. Danke an Ueli Schneider, Nicole Meier, Dominik Viscardi sowie allen Tierpflegern für die tolle Versorgung und lustige Atmosphäre.

Vielen Dank für die finanzielle Unterstützung durch die Unigrants der Universität Basel, sowie einen enormen Dank an alle unsere Kollaborationspartner. Besonderen Dank für die Zusammenarbeit bei den *Germ-free* Mäusen an Dr. Stephanie Ganal-Vonarburg und Dr. Catherine Mooser vom Inselspital in Bern.

Für die stete motivierende Unterstützung und die allzeit bereite Durchsicht meiner Arbeit möchte ich meinen Dank besonders an Sophia Wiedemann und Zora Baumann ausdrücken. Ebenfalls richtet sich mein Dank für das spontane Korrekturlesen in der Endphase an Dr. Jasmin Grählert.

Ebenso möchte ich mich neben meinem unersetzlichen Mitbewohner und Mitstreiter Valerio Sabatino auch besonders bei Gerlinde Offenmüller sowie meinen engsten Freunden in Basel Sabine Winkler, Sophia Wiedemann, Josua Wehner, Nicole Kirchhammer, Michal Stanczak, Celeste Manfredonia, Selin Gogacz und auch ausserordentlich bei meiner besten Freundin aus der Heimat Jutta Unkelbach für die stete Unterstützung, Motivation und Ermutigung in jeder Lebenslage danken.

Schließlich danke ich vor allem meiner Familie von ganzen Herzen für die grenzenlose Unterstützung während meiner gesamten Laufbahn. Meinen Eltern Bernd und Eva sowie meinen älteren Brüdern Andreas und Friedrich und meinem Zwillingsbruder Julius möchte ich für die Kraft und Fürsorge während dieser Zeit danken. Ich bin sehr stolz euch als Eltern und Brüder zu haben.